AD-A051 221 ECOLOGICAL ENTERPRISES INC BEDFORD MA F/G 4/2
THEORETICAL STUDY OF THREE-DIMENSIONAL SLOPE AND VALLEY WIND SY--ETC(U)
DEC 77 W TANG, L PENG DAAG29-76-C-0007
UNCLASSIFIED NL

1 OF 2
AD A051221

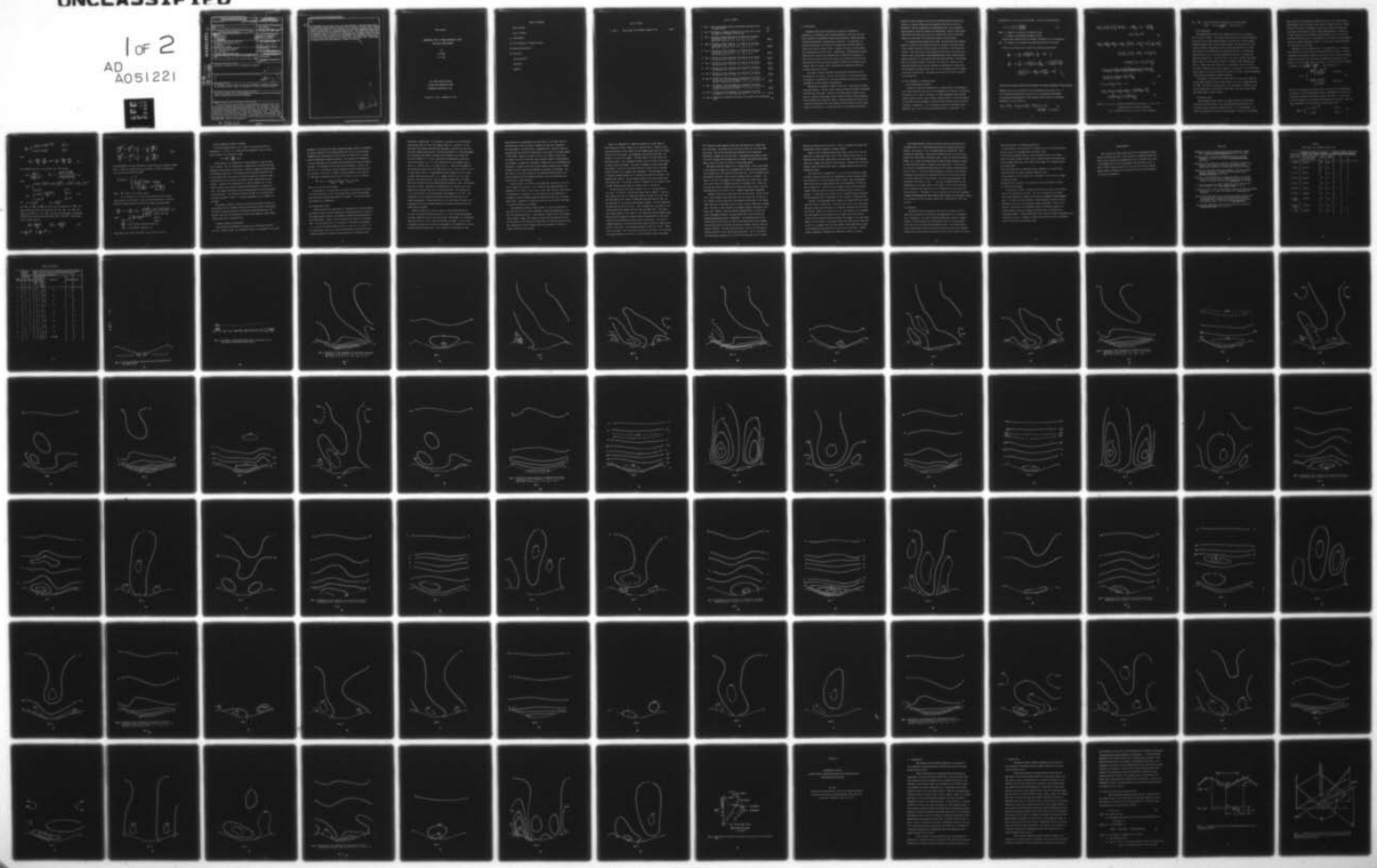

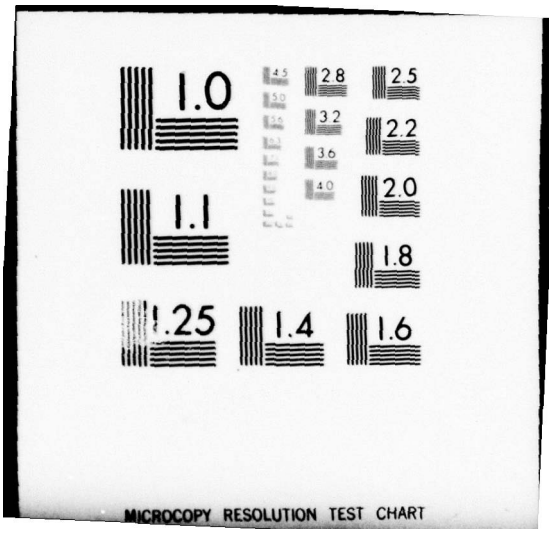
1.0
1.1
1.25
1.4
1.6
1.8
2.0
2.2
2.5
2.8
3.2
3.6
4.0
4.5
5.0
5.6
MICROCOPY RESOLUTION TEST CHART

AD A051221

SECURITY CLASSIFICATION OF THIS PAGE (When Data Entered)

REPORT DOCUMENTATION PAGE

READ INSTRUCTIONS BEFORE COMPLETING FORM

1. REPORT NUMBER

2. GOVT ACCESSION NO.

3. RECIPIENT'S CATALOG NUMBER

4. TITLE (and Subtitle)

Theoretical Study of Three-Dimensional Slope and Valley Wind Systems.

5. TYPE OF REPORT & PERIOD COVERED

Final Report
Oct. 21, 1975- Dec. 15, 1977

6. PERFORMING ORG. REPORT NUMBER

7. AUTHOR(s)

Dr. Wen Tang
Dr. Li Peng

8. CONTRACT OR GRANT NUMBER(s)

DAAG29-76-C-0007

9. PERFORMING ORGANIZATION NAME AND ADDRESS

Ecological Enterprises, Inc.
54 Loomis St.
Bedford, MA 01730

10. PROGRAM ELEMENT, PROJECT, TASK AREA & WORK UNIT NUMBERS

11. CONTROLLING OFFICE NAME AND ADDRESS

U.S. Army Research Office
P.O. Box 12211
Research Triangle Park, N.C.

12. REPORT DATE

12 Dec 77

Dec. 12, 1977

13. NUMBER OF PAGES

12 116 P.

14. MONITORING AGENCY NAME & ADDRESS (if different from Controlling Office)

Final rept. 21 Oct 75-15 Dec 77,

15. SECURITY CLASS. (of this report)

Unclassified.

15a. DECLASSIFICATION/DOWNGRADING SCHEDULE

NA

16. DISTRIBUTION STATEMENT (of this Report)

Approved for public release; distribution unlimited.

DDC
RECEIVED
MAR 16 1978
B
A

17. DISTRIBUTION STATEMENT (of the abstract entered in Block 20, if different from Report)

NA

18. SUPPLEMENTARY NOTES

The findings in this report are not to be construed as official Department of the Army position, unless so designated by other authorized documents.

19. KEY WORDS (Continue on reverse side if necessary and identify by block number)

Slope wind, valley wind, mountain-valley wind system, meso-scale circulation, surface temperature, meso-scale modelling.

20. ABSTRACT (Continue on reverse side if necessary and identify by block number)

A numerical model for studying a three-dimensional mountain-valley wind system over a typical mountain-valley terrain has been developed. This model is non-hydrostatic with Boussinesq approximation. The non-linear interaction between the thermally induced motion in the valley and the wind in the upper troposphere is investigated in a truly three-dimensional sense. The interplay between the slope wind and valley plain wind is examined. Computational results for different surface thermal conditions, geometrical factors of terrain, and

next page

DD FORM 1 JAN 73 1473 EDITION OF 1 NOV 65 IS OBSOLETE

SECURITY CLASSIFICATION OF THIS PAGE (When Data Entered)

20.

cont.

meteorological and physical inputs have been obtained. Available observations and analytical theory appear to support several findings in this study. Another important contribution is the development of a method of computing surface temperature and heat flux in a typical valley terrain. This method has taken into consideration both the effect of the shadow cast by the ridge opposite the slope for different times of the day for the incoming solar radiation, and the effect of elevated mountain surface in the calculation of the effective long-wave radiation at given positions from the valley slope and valley floor. This method has checked well with observations in valleys in Vermont.

Final Report

THEORETICAL STUDY OF THREE-DIMENSIONAL SLOPE AND VALLEY WIND SYSTEMS

By

Wen Tang

Li Peng

U.S. Army Research Office

Contract No. DAAG29-76-C-0007

Ecological Enterprises, Inc.

October 21, 1975 - December 15, 1977

Table of Contents

List of Tables

List of Figures

I. Introduction

Mountain-valley wind circulation has long been of interest to inhabitants in mountainous areas and meteorologists. Yet it has not been fully explored and understood. Various daily operations require much more detailed meteorological knowledge than in the past. In particular, an accurate short-range small meso-scale 3-dimensional prediction model is needed over mountain-valley terrain. Aiming at this goal we shall divide the investigation into three tasks: 1) to develop a 3-dimensional numerical model with the initial value approach and to study the basic physics in this particular kind of local wind system, 2) to compare results from the numerical model with some simple analytical solutions and available observations, and 3) to build a short range meso-scale prediction model for mountain-valley wind systems.

This report discusses problems associated with the first task and partially with the second. The last task and part of the second one shall be studied as a continuation of the tasks presently undertaken and will be completed in the next phase of investigation.

Theoretical and numerical studies of flow over a small mountain ridge have been numerous. The most recent studies by Mahrer and Pielke (1975,1977) and Clark are interesting. However, the boundary layer problem, such as flow in a typical valley region, needs further attention and investigation. Both theoretical and numerical sutdies of mountain-valley wind systems for a typical 3-dimensional meso-scale mountain-valley terrain have been seldom found in the literature. Few intrigue linear or non-linear interactions

between the free atmospheric flow and the thermally induced flow near the surface in a typical valley have been reported except for the work by Tang(1976), Tang and Peng(1974) for 2-dimensional ones, and over general mountain-basin situation by Mahrer and Pielke(1977), Studies on the interplay between the slope wind or the cross-valley flow and the valley wind (along the valley axis) are completely lacking in the literature.

In studying mountain-valley wind systems the non-hydrostatic approximation is believed to be important because of the basic convective nature of the problem, especially when horizontal and vertical scales become comparable. Since this investigation emphasizes the study of the flow in the boundary layer, computations with parameterizations under various meteorological conditions for the present model have been performed. The development of the numerical model is presented in Section II. Results of the numerical modeling under various conditions are presented in Section III. Some available observational data will be used for comparison and discussed at the end of Section III. Discussion of the study and future study will be in Section IV.

II. The development of numerical model

1) The differential equations

In order to simulate circulation over a valley terrain, the configuration of the relief and the slope of the topography are believed to be critical. In contrast to the study of lee waves for which linearized lower boundary surface condition may be used to obtain a general picture of the wave pattern in the middle of the atmosphere, non-linear lower boundary conditon should be used here. Furthermore, a set of equations should have coordinates transformed so that it can be used for arbitrary terrain. A generalized σ -

coordinates in z is thus used in the model. The basic transformation is

$$z' = H \frac{z - h(x,y)}{H - h(x,y)} \qquad (1)$$

where z = height in rectangular coordinate system,

z'= height in transformed coordinate system,

h(x,y)=terrain height profile in regular rectangular (x,y,z) coordinates,

and H = height of top boundary over horizontal ground for the model.

With this transformation we obtain the following relationships:

$$\frac{\partial}{\partial x} \rightarrow \frac{\partial}{\partial x'} - \left(\frac{H-z'}{H-h}\right) h_{x'} \frac{\partial}{\partial z'} \equiv [\quad]_{x'}$$

$$\frac{\partial^2}{\partial x^2} \rightarrow \frac{\partial^2}{\partial x'^2} - 2\left(\frac{H-z'}{H-h}\right) h_{x'} \frac{\partial^2}{\partial z' \partial x'} + \left(\frac{H-z'}{H-h}\right)^2 h_{x'}^2 \frac{\partial^2}{\partial z'^2}$$

$$- \frac{H-z'}{(H-h)^2}\left[(H-h) h_{x'x'} + 2h_{x'}^2\right] \frac{\partial}{\partial z'} \equiv [\quad]_{x'x'}$$

Note that the square brackets with subscripts have special meanings in the equations.

Similar results can be obtained for the differential with respect to y. A set of governing differential equations for an incompressible atmosphere with Boussinesq approximation, after chopping off the prime for transformed coordinates, can be written as:

$$(u)_t + [u^2]_x + [vu]_y + [wu]_z = -[\Phi]_x + fv + f_1 w + [K_v^{(m)}(u)]_z + \nabla_H \cdot (K_H \nabla u) \qquad (2)$$

$$(v)_t + [uv]_x + [v^2]_y + (wv)_z = -[\Phi]_y - fu + \left[K_V^{(m)}(v)_z\right]_z + \nabla_H \cdot (K_H \nabla v) \tag{3}$$

$$[\Phi]_{xx} + [\Phi]_{yy} + (\Phi)_{zz} = \lambda(\theta)_z + f\left\{[v]_x - [u]_y\right\} + f_1\left\{(u)_z - [w]_x\right\}$$

$$- \left\{[u]_x^2 + [v]_y^2 + (w)_z^2 + 2[u]_y[v]_x - 2[w]_x(u)_z + 2[w]_y(v)_z\right\}$$

$$+ \left([K_v]_x(u)_z + [K_v]_y(v)_z + (K_v)_z(w)_z\right) + \left[[K_H]_x[u]_x + [K_H]_y[v]_x + (K_H)_z[w]_x\right]_x$$

$$+ \left[[K_H]_x[u]_y + [K_H]_y[v]_y + (K_H)_z[w]_y\right]_y \tag{4}$$

$$[u]_x + [v]_y + (w)_z = 0 \tag{5}$$

$$(\theta)_t + [u\theta]_x + [v\theta]_y + (w\theta)_z = \left(K_V^{(\theta)}\left((\theta)_z - \varepsilon\right)\right)_z + \left[K_H^{(\theta)}[\theta]_x\right]_x + \left[K_H^{(\theta)}[\theta]_y\right]_y \tag{6}$$

where $(\ )_t$, $(\ )_z$, etc = partial differential with respect to t, and z, etc respectively in transformed coordinates.

u,v,w = velocities in the x-, y-, and z- axes directions,

and $\bar{\Phi}$ = pressure deviation from the mean at a given height

$= \bar{\theta}\pi'$ $\left(\pi \simeq c_p \left(\frac{p}{p_0}\right)^{\kappa}, \pi' = \pi - \bar{\pi}\right)$

2) The topography

The 2-dimensional valley cross-section and mesh in the x-z plane at y=0 is shown in Figure 1. The x-axis oriented in the cross-valley direction, the y-axis, in the down-valley direction, and the z-axis, in the vertical direction pointed upward from the ground surface. The grid interval in the vertical direction from ground up are 50,50,100,300,500,1000 m up to the sixth grid and 1000m thereafter for every grid interval up to 10km level. The grid size in the x- or y-axis direction is even but is different for different computer runs. The grid size in the x-axis direction ranges from 333m to 8km, and in the y-axis direction, from 5km to 15km depending upon the run. Experiments with combinations of different size grids in the x- and y-axes directions are made for purposes of comparison. The time interval chosen depends upon the grid size used in order to fulfil the Courant-Friedrichs-Lewy linear computational stability criterion.

The height of ridges above the valley floor is assumed to be constant in the y-axis direction, but it varies from case to case, ranging from 100m to 1.5km. The height of valley floor at the valley head is 300m above that at the valley mouth at the bottom of the valley. The cross-section along the valley floor is shown in Fig. 2.

3) Boundary layer

Since mountain-valley systems are largely affected by differential heating and terrain features, some fine turbulent characteristics over the uneven lower boundary are indeed important to the investigation. It would be interesting to have some good knowledge of vertical and horizontal

eddy viscosity and diffusivity particularly suited to the valley terrain. Unfortunately, little literature about this in a valley is known. Because of lack of the precise knowledge in this matter, the eddy viscosity and diffusivity over homogeneous plane surface formulation may be adapted or a simple constant with a relatively large numerical value is to be used. The relatively large value is used because of the basically strong turbulent nature over rough mountainous surface. In this report we have undertaken the study with both approaches.

Adapting the basic formulation due to Businger(1973), we can compute eddy viscosity and diffusivity by solving well-known equations. We first determined the Richardson number, R_i, from the mean wind speed at one height (say the first grid point above ground surface) and temperature at two heights (say, first grid level and surface). By using the profile Richardson number, $R_i = \frac{g}{\theta}\frac{\partial \theta}{\partial z} \Big/ \left(\frac{\partial |V|}{\partial z}\right)^2$, may be expressed as

$$Ri = \begin{cases} \dfrac{0.74\hat{z}(1-15\hat{z})^{1/4}}{(1-9\hat{z})^{1/2}} & \text{for } \hat{z} \le 0 \\ \dfrac{0.74\hat{z} + 4.7\hat{z}^2}{(1+4.7\hat{z})^2} & \text{for } \hat{z} > 0 \end{cases} \qquad (7)$$

where $\hat{z}$ is non-dimensional height which is the ratio of the height above the ground, z, and the Monin-Obukov length. Determining $\hat{z}$ from the last equation and therefore Monin-Obukov length from formula $L = z/\hat{z}$ lead to the determination of non-dimensional momentum and temperature, ϕ_m and ϕ_θ respectively, from the following relationships with $\hat{z}$,

$$\phi_m = \begin{cases} (1-15\hat{z})^{-1/4} & \hat{z} \le 0 \\ 1+4.7\hat{z} & \hat{z} > 0 \end{cases} \qquad (8)$$

$$\phi_\theta = \begin{cases} 0.74\,(1-9\hat{z})^{-1/2} & \hat{z} \le 0 \\ 0.74 + 4.7\hat{z} & \hat{z} > 0 \end{cases}$$

where

$$\phi_m = \frac{kz_*}{u_*}\frac{\partial \bar{u}}{\partial \hat{z}}, \text{ and } \phi_\theta = \frac{kz_*}{\theta_*}\frac{\partial \bar{\theta}}{\partial \hat{z}} \qquad (9)$$

The integrated version of the profiles are, respectively,

$$u_* = \frac{k\bar{u}}{\ln(\frac{\hat{z}}{\hat{z}}) - \psi_1}, \qquad \theta_* = \frac{k(\bar{\theta} - \bar{\theta}(z_0))}{0.74\left(\ln\frac{\hat{z}}{\hat{z}} - \psi_2\right)} \qquad (10)$$

where

$$\psi_1 = \begin{cases} 2\ln\left(\frac{1+\lambda}{2}\right) + \ln\left(\frac{1+\lambda^2}{2}\right) - 2\tan^{-1}\lambda + \frac{\pi}{2}, & \hat{z} \le 0 \\ -4.7\hat{z} & \hat{z} > 0 \end{cases}$$

$$\psi_2 = \begin{cases} 2\ln\left(\frac{1+0.74\Delta}{2}\right) & \hat{z} \le 0 \\ -6.35\hat{z} & \hat{z} > 0 \end{cases} \qquad (11)$$

and

$$\lambda = (\phi_m)^{-1}, \qquad \Delta = (\phi_\theta)^{-1}$$

The values of ϕ_m and ϕ_θ will allow first determination of ψ_1 and ψ_2 through the above set of equations and then u_* and θ_* with known z_o and $\bar{\theta}(z_o)$. Once θ_* and u_* are determined, we determine vertical eddy viscosity and diffusivity, $K_v^{(m)}$ and $K_v^{(\theta)}$ respectively in the surface layer by

$$K_v^{(m)} = \frac{k u_* z}{\phi_m} \qquad K_v^{(\theta)} = \frac{k u_* z}{\phi_\theta} \qquad (12)$$

and $\frac{\partial}{\partial \hat{z}} K_v^{(m)}$ and $\frac{\partial}{\partial \hat{z}} K_v^{(\theta)}$ by

$$\frac{\partial K_v^{(m)}}{\partial \hat{z}} = \frac{K_v^{(m)}}{L}\left(\frac{1}{\hat{z}} - \frac{1}{\phi_m}\frac{\partial \phi_m}{\partial \hat{z}}\right)$$

$$\frac{\partial K_v^{(\theta)}}{\partial \hat{z}} = \frac{K_v^{(\theta)}}{L}\left(\frac{1}{\hat{z}} - \frac{1}{\phi_\theta}\frac{\partial \phi_\theta}{\partial \hat{z}}\right) \qquad (13)$$

The determination of these quantities is consistent with additional assumptions. Above the surface layer we use O'Brien 's (1970) interpolation, i.e. let K stand for $K_v^{(m)}$ or $K_v^{(\theta)}$

$$K = K_{vi} + \begin{cases} 0 \\ \left(\frac{\hat{z}_i - \hat{z}}{z_i - \delta}\right)^2 \left\{ K(\delta) - K(z_i) + \right. \\ \left. (\hat{z} - h)\left[\frac{\partial K}{\partial \hat{z}}\right] + 2\,\frac{K_\delta - K_{zi}}{z_i - \delta} \right\} \end{cases} \qquad (14)$$

where δ = depth of the surface layer,

z_i = the height at the top of the planetary boundary layer.

$K_v(z_i)$ will be set 1 $cm^2 sec^{-1}$ and z_i will be forecasted by an equation proposed by Deardorff(1974) and tested by Pielke and Mahrer(1975).

$$\frac{\partial z_i}{\partial t} = -u\frac{\partial z_i}{\partial x} + \bar{w}_i + \frac{1.8\left(w_*^3 + 1.1\,u_*^3 - 3.3\,u_*^3 f(z_i)\right)}{g\,\frac{z_i^2}{\theta_s}\frac{\partial \theta^+}{\partial z} + 9\,w_*^2 + 7.2\,u_*^2} \qquad (15)$$

where $w_* = \begin{cases} \left(-\frac{g}{\theta_s} u_* \theta_* z_i\right)^{1/3} & \theta_* \leq 0 \\ 0 & \theta_* > 0 \end{cases}$

$\frac{\partial \theta^+}{\partial z}$ = the stability immediately above z_i

w_* = the vertical velocity at z_i.

The depth of the surface layer, δ, will be taken as 0.04 z_i.

4) The boundary and initial conditions

At the top boundary where z = H = 10km, the horizontal velocity is specified as u = U and v = 0. Since the top boundary is taken as a flat solid surface, it is natural to assume

$$w = \tilde{\phi} = \frac{\partial \theta}{\partial z} = 0$$

At the ground it is assumed that no slip condition is used for wind (i.e. u=v=w=0). The air temperature at surface can be calculated from the energy balance equation at the ground. In order to apply the present model, an analytical expression of the ground surface temperature and heat flux at each small time step in terms of solar and long wave radiation, geometrical factors of the terrain, and initial surface temperature has been derived. Details of the investigation is shown in Appendix A. In this report, however, only specified temperature variations on the ground are used. The computed temperature will be incorporated into the present model in the next phase. The boundary conditions for $\tilde{\phi}$ can be obtained from the third equation of motion. At lateral boundaries all are assumed to be periodic.

The initial condition is chosen such that all quantities are zero in space except for the specified vertical distribution of mean U with height. In order to avoid the creation of relatively strong disturbances at the initial stage, we let the mountain be flat in the beginning. More details will be discussed in subsection (5).

5) Other numerical considerations

The forward time difference and center space difference in general are used. Except for $\tilde{\phi}$, all dependent variables are evaluated at each grid

point.Eq. 4 is solved by the block relaxation method. Because of reflection of spurious energy of the internal gravity wave from the upper boundary originally set up by mountain valley terrain, the reflected wave energy leads to undesirable computation results. The spurious wave energy can be partly eliminated by introducing some Rayleigh friction hear the upper boundary. The Rayleigh friction terms may be written as -k(u-U), and -kv if V = 0. In addition, since the horizontal eddy exchange terms are not included in the model, a simpler smoothing approach is used instead. A three-point smoothing formula for each variable is given as follows:

$$\bar{F} = (1-s)F_{i,j,k} + s\left(F_{i+1,j,k} + F_{i-1,j,k}\right)/2$$

where s is a constant to be chosen.

As mentioned in the preceeding sub-section, the mountain was assumed to be flat initially and will be gradually built up over 26 time steps until the final desired ridge heights are reached. The undesired initial disturbance can be eliminated.

III. Computation results

Several computer runs were made for a combination of various boundary conditions for both wind and temperature, different geometrical factors of the mountain-valley terrain, and different turbulence parametrization in the surface layer. Table 1 shows the various basic inputs for different runs. In each computer run, the isopleths of the three wind components u, v, w, and T for cross-sections in the x-z plane at J = 7 and/or J = 4 are illustrated. The x-, y-, and z-axes directions represent the cross-valley horizontal, but pointing toward upvalley, and vertically upward

directions, respectively. To be explicit, a positive u is the horizontal wind blowing from the left to the right in Fig. 1a; a positive v is the horizontal wind blowing upvalley into the paper; a positive w is the vertical wind blowing bottom upward. The cross-section at J = 7 will illustrate the circulation and thermal situation for the middle of the valley and the cross-section at J = 4 will illustrate the information at the lower part of the valley. At J = 4, the valley floor and side ridges start to level out. Several cases, e.g. Figs. 10,11,12, show that the height of the valley side ridges above the valley floor start to drop to zero at J = 4. In other words, there is a completely flat plain between J=1 and 4, while a valley slope exists from J=4 to 10. Between J=10 and 11 it is a flat plateau. The horizontal grid size and height of ridge above the valley floor vary from case to case although the same diagram is used. The vertical grid size is fixed. Therefore the mountain scale is somewhat out of proportion with the mesh scale used in the illustration. The isopleths for u,v,w are isotechs of the corresponding wind components in m sec^{-1}. The isopleths for T are temperature deviations from horizontal mean in ^{o}C. Since the gradients of these quantities can be very large, the interval of isopleths used in the following figure are not always uniform and all isopleths will be labeled.

Results of Run # 1 are shown in Fig. 3. The striking feature is the tilt of positive and negative axes of u, w, and T toward the upstream direction (negative x-axis) of the basic flow. The maximum +u is correlated very well with the -w and -T over the lee near the ridge. In 3a an area of negative isotech was situated near the center of the valley but it covers nearly half the windward slope. This signifies the development of the

return flow and a separatedcell near the bottom of the valley, when the resultant wind in the x-z plane is computed by using the w-component. The development is possible because a negative and a positive w area are situated over the windward and small part of lee slope in the bottom center of the valley. Owing to the tilts of the u and w fields, waves in the x-z plane at J=4 and 7 with tilts axes resulted, similar to many mountain wave patterns. However the wavelength is larger but the corresponding wave amplitude is smaller because the present boundary conditions are somewhat different from the typical investigation of mountain wave problems. For the small or meso-scale circulation, the periodic condition seems to be more reasonable than the boundary conditions used in the mountain wave studies with a single mountain.

Cross-sections of the flows in the valley axis direction at J=4 and J=7 are shown in 1.b and 1.f. It is found that the upvalley flows are maximum near the center of the valley at about 500m above the valley floor. In comparing the magnitudes of v at J=4 and at J=7, the magnitude of v component is greater halfway along the valley (J=7) than near the valley mouth (J=4). Comparison of resultant u and w in the x-z plane show there is not much difference in strength.

The temperature deviation from the mean, T, for cross-sections at both J=4 and J=7 are of little difference. Again the inclination is toward the upstream direction. Large negative T covers most of the windward slope, whereas a very small section is found near the ridge at the lee. For the center of the valley from the ground up to 2km are positive values. The 2-dimensional results obtained here are reasonable and similar to results obtained by Tang (1976).

Run # 2 is computed for a 24km wide valley and a valley slope of 7×10^{-3} terrain for about 2 hours and is shown in Fig. 4. Except for the relative narrowness of the valley and the steeper slopes both in the valley sides and axis directions, the assumptions are basically the same. The patterns of u and w are similar. The wind speeds u at lower levels are relatively small. The v component, however, near the center of the valley, is about 0.30m sec^{-1} higher. The level of maximum v is again about 500m above floor. At the 4 to 5 km level there is a return flow in the down-valley direction and it appears very reasonable. The appearance of the T field has changed somewhat and is dominated by positive deviations. The negative area shrinks. The air returns warmer in the valley center than over valley sides. The general warming is believed to be attributed to the stronger downward motion above the steeper slope of the ground.

An even narrower and steeper valley is used as a terrain model for the study. The width is 4 km and the valley slope is 33×10^{-3}. Since the time interval used for the integration cannot be larger than 5 sec, only about 29 minutes (350 steps) of computation have been made for this run. The appearance of the patterns have changed somewhat. The axes become less inclined than the first two cases. The u component near the center of the valley becomes even smaller than that near the ridge level. The return flow region remains in the center of the valley and over the windward slope. The positive and negative w fields become distributed more or less vertically over the windward and leeward slopes respectively. The center of maximum magnitude is about 2km above both slopes between the ridge and the center of the slopes. The maximum magnitude is about 3.5 m sec^{-1}. Therefore the troughs of the wave in the x-z plane will be more or less vertical The maximum amplitude of the wave is about 2km above valley side slopes.

The T field has large negative values near the center but is warmer than over the slopes. The coldest spot in the air is near the top of the windward slope. The flow in the horizontal direction of the valley axis direction is largest for the last cases. The maximum valley wind is about 1.5 m sec^{-1} between 200m and 500m above the ground, the maximum down-valley wind is about 1.4 m sec^{-1} at about 5 to 6 km above ground.

The first 2 cases are computed for a sloping valley. The top and bottom of the valley are assumed to be horizontal by assuming that the variations of all quantities in the y-axis direction are zero. For the following cases the boundary conditions in the y-axis is again assumed to be cyclic. For Runs 4, 5, 6 and 7 the height of the ridges above the valley floor is constant, but it may be a different constant for different cases. Other runs are for cases where the height of the valley side ridges start to drop off from position at J=7 to zero at J=4, a typical valley-plain topography.

Runs #4 and #5 are for valley with a 64 km wide valley. Run #4 is made with a warmer valley slope which cools with an assumed rate as time goes on. Results are illustrated for cross-section at the middle of the valley slope where J=7 at time 20100 sec ($\sim$ 5 hrs). Run #5 is made with a heating case. The axes of these patterns are slightly inclined downstream of the basic flow. However, since the vertical velocity field w is very weak and is essentially vertical, the wave trough will remain vertical, and energy propagating downward is negligible. The characteristics of the return flow for these cases are again in agreement with earlier findings. The intensity under the cooling condition is stronger than that under the heating condition. The flow along the valley is toward the down and up valley directions for Runs #4 and #5 respectively. This is reasonable. The down-valley component (-3.5 m sec^{-1}) in the cooling case is stronger

than the up-valley flow (+2.4 m sec^{-1}). This is in general agreement with observational results obtained in Vermont valleys.

Similar to the assumption used in Runs 4 and 5, Runs 6 and 7 are computed with a valley only half as wide as the valleys in Runs 4 and 5. In comparing these two sets, again patters are very similar to corresponding cases and a similar conclusion can also be drawn. Between Runs 4 and 5 the cooling surface condition leads again to stronger intensity than with the heating condition.

Runs #8 and #9 are computed for u, v, w, and T at position J=7 under the same assumption except for the corresponding surface cooling and heating conditions on a realistic valley-plain terrain. The variation with time in each case are illustrated by the results obtained at t=10100 sec and at t=20100 sec. The one with the cooling surface condition produces stronger intensity than the one with the heating surface condition in general. As time increases to about 5.5 hrs, nothings changes noticeably. The only quantity that is intensified is the upvalley or downvalley flow.

Run #10 is the experiment with surface layer formulation based on the equations used in Section II.3. Since the time step has to be very small when the surface layer formulation is included, computation has been made for 750 sec. Results are shown in Fig. 12. The patterns of the isopleths are very similar to those shown in Fig. 4 except that the basic wind profile in the vertical direction decreases with height in the upper layer, which can be attributed to the input profile and small mountain slope used in Fig. 4. It appears that using the surface layer formulation has made little difference upon the gross features of the circulation. However, further experiments including the surface layer should be pursued.

The present numerical model has produced several interesting and encouraging results of a three-dimensional model for mountain-valley wind systems. By no means is this an ultimate model for prediction. While pursuing the improvement, some results obtained here may be used for comparison with observations available at hand. Based on studies by Davidson (1960), for a valley with ridge height of 800m the maximum winds are found at about 400m level which is halfway to the ridge level. The comparison of the level of maximum down-valley wind with the results obtained here is shown in Fig. 13. With the assumed topography used here we have obtained the maximum down-valley wind, generally occuring at the 500m level which is in close agreement with observation. Even for many computations the down-valley wind speed is small, the level of maximum remains in the neighborhood of the middle level of the valley. In the slope wind theory for an infinitely long slope the level of maximum wind is only about 50m above the ground. It cannot be used to explain the valley wind phenomenon. A simple three-dimensional linear theory cannot explain this phenomenon either. It is believed that the non-linear theory has a contribution to this conclusion.

IV. Discussion

The numerical model developed in this study has included the non-hydrostatic assumption and turbulence parameterizations that are believed to be important in the study of mountain-valley wind systems of steeper terrain. The computations yield reasonable results in the three-dimensional flow over a typical mountain-valley terrain. The mountain-valley wind system resulted from the non-linear interaction between the thermally induced flow in the valley and the upper air flow of the larger scale motion.

This model produces the following conclusions:

1) The positions of the return flow or separated cell in the valley obtained in this study is in agreement with the earlier study.

2) The imposed nighttime thermal surface condition produces down-valley wind, the imposed daytime thermal surface condition produces up-valley wind.

3) The maximum down-valley wind level is about 500m, for a ridge 1km above the valley floor.

4) The up-valley wind is relatively weak as compared to the down-valley wind speed while the other conditions remain the same.

5) The component of cross-valley wind is maximum at the lee near the ridge, or above the ridge.

6) The wave flow pattern in the upper part of the troposphere is similar to some earlier findings.

In the future studies, continuous effort will be placed on the improvement of the accuracy of the model. This may be corrected by modifying the present computation scheme and increasing the numbers of the horizontal grids. In order to be more realistic, cyclic boundary conditions will be modified so that they can be applied to actual conditions. First we will conduct a study based on an analytical model of two mountain ridges and sloping valleys, then later compare the results from the numerical and theoretical models. Actual observational data from the Tularosa Basin will be used to validate the results. Finally an attempt will be made to build a prediction model for the White Sands Missile Range.

Acknowledgement

This research was made possible by the U.S. Army Research Office, Research Triangle Park, N.C., under Contract No. DAAG27-76-C-0007. The authors wish to express deep gratitude to Drs. W. Vickers and M. Lopez at the MITRE Corp for their encouragement and assistance, to Dr. E. Rivas of MIT for helpful discussions, to Dr.C.M.Hui of Johns Hopkins Applied Physics Laboratory and to Ms.C.M.Tang for valuable assistance in numerical programming.

References

Businger, J.A., 1973: Turbulent transfer in the atmosphere surface layer. Workshop in Micrometeorology, Amer. Meteor. Soc., Chap. 2.

Clark, T.L., 1977: A small-scale dynamic model using a terrain following coordinates transformation. J. Computational Phys., 23, 186-215.

Davidson, B. and S. Jaffe, 1960: Observation and theory of local wind systems. Final Report, Contract No. DA-36-039-Sc-78127. 3A-99-07-001-03, College of Engineering, New York University.

Deardorff, J., 1974: Three dimensional numerical study of the height and mean structure of a heated planetary boundary layer. Boundary-Layer Meteor., 7, 81-106.

Mahrer, Y., and R.A. Pielke, 1975: A numerical study of the air flow over mountains using the two-dimensional version of the University of Virginia mesoscale model. J. Atmos. Sci., 32, 2144-2155.

_____, 1977: A numerical study of the air flow over irregular terrain. Beit. Z. Phys. d. Atmos., 50, 98-113.

O'Brien, J.J., 1970: A note on the vertical structure of the eddy exchange coefficient in the planetary boundary layer. J. Atmos. Sci., 27, 1213-1215.

Tang, W. and L. Peng, 1974: Mountain-valley circulation and dispersion of vehicular exhaust gases from a valley highway. Preprint volume, Symposium on Atmospheric Diffusion and Air Pollution, Santa Barbara, Calif., 9-13 Sept., 1974. Amer. Meteor. Soc.

Tang, W., 1976: Theoretical study of cross-valley wind circulation. Arch. Met. Geoph. Biokl., Ser. A, 25, 1-18.

Table 1

Basic inputs for different computer runs

The number of run and time (sec)	Geometrical factors of terrain			Surface thermal condition		
	Maximum ridge height above valley floor and floor height above plain (m)	Valley width (km)	Valley slope (x10-3)	Cooling	Neutral	Heating
1 (5100)	1000+300	64	6.6		*	
2 (7550)	1000-300	24	13		*	
3 (1750)	1000+600	4	33	*		
4 (20100)	1000+600	64	10	*		
5 (20100)	1000+600	64	10			*
6 (22500)	1000+300	32	10	*		
7 (22500)	1000+300	32	10			*
8 (10100-20100)	500+150	64	2.5	*		
9 (10100-20100)	500+150	64	2.5			*
10 (750)	1000+600	8	20		*	

Table 1 (continued)

Run Number	Initial ground temperature ascendant			Initial cross-valley wind speed profile				Values of coefficients of eddy viscosity and diffusivity	Lateral boundary conditions	
	Pos	Neut	Neg	constant above 100m	linear	non-linear	max wind spd	K ($m^2 sec^{-1}$)	no gradient	cyclic
1	*			*			10	10	*	
2	*			*			10	10	*	
3		*			*		10	20		*
4	*				*		10	10		*
5			*		*		10	10		*
6		*			*		10	20		*
7		*			*		10	20		*
8			*		*		10	10		*
9	*				*		10	10		*
10		*				*	5	variable		*

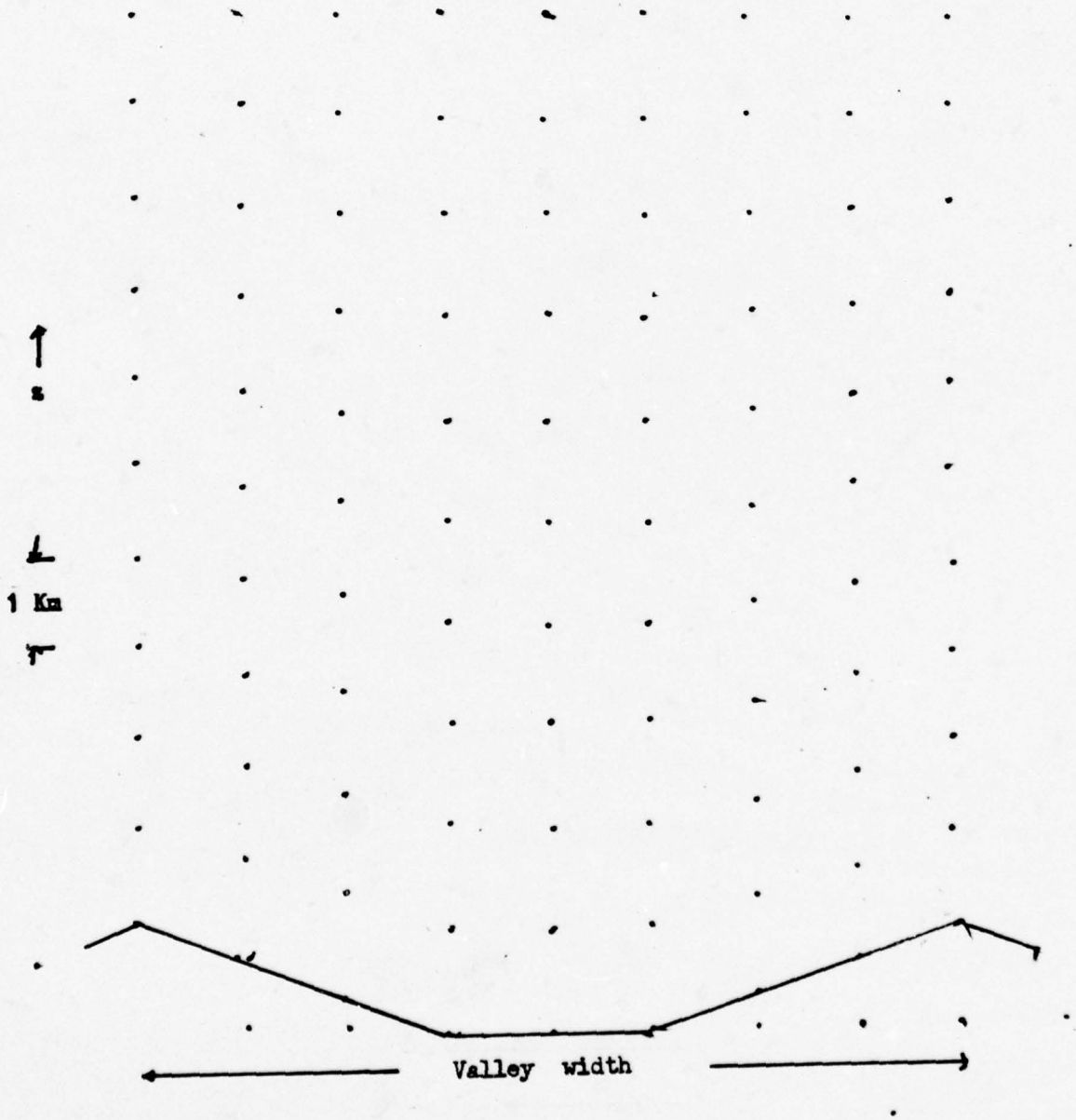

Fig. 1. The two-dimensional valley cross-section and mesh in the x-z plane at y=0.

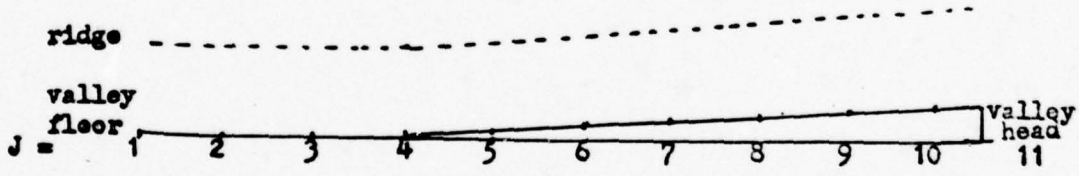

Fig. 2. The height of ridge and height of the valley floor in the y-z plane at the middle of the valley.

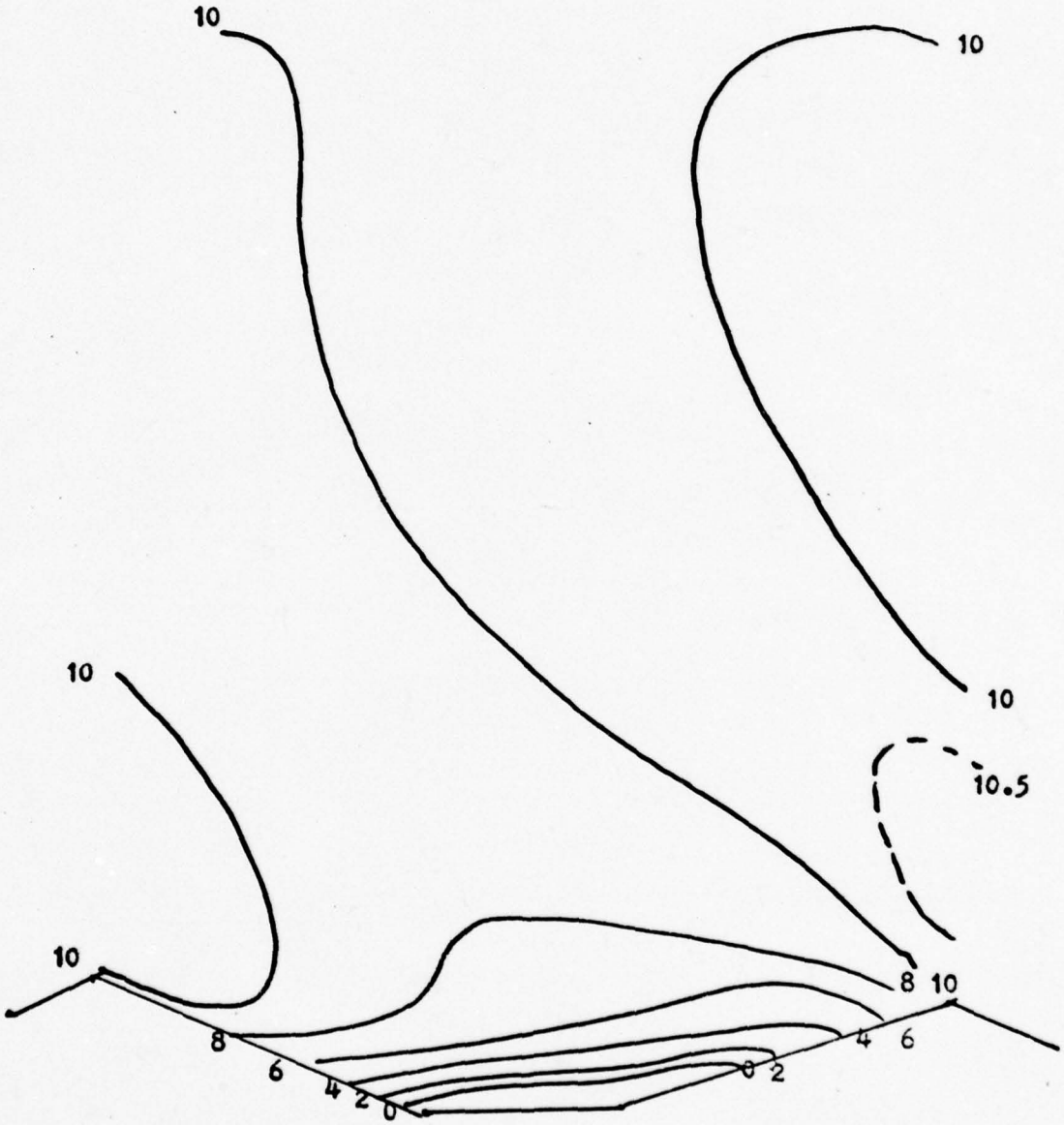

Fig. 3. Isopleths of wind components and temperature deviations for Run #1 at J=4 (a to d) a. u b. v c. w d. T and at J=7 (e to h) e. u f. v g. w d. T

3a. u

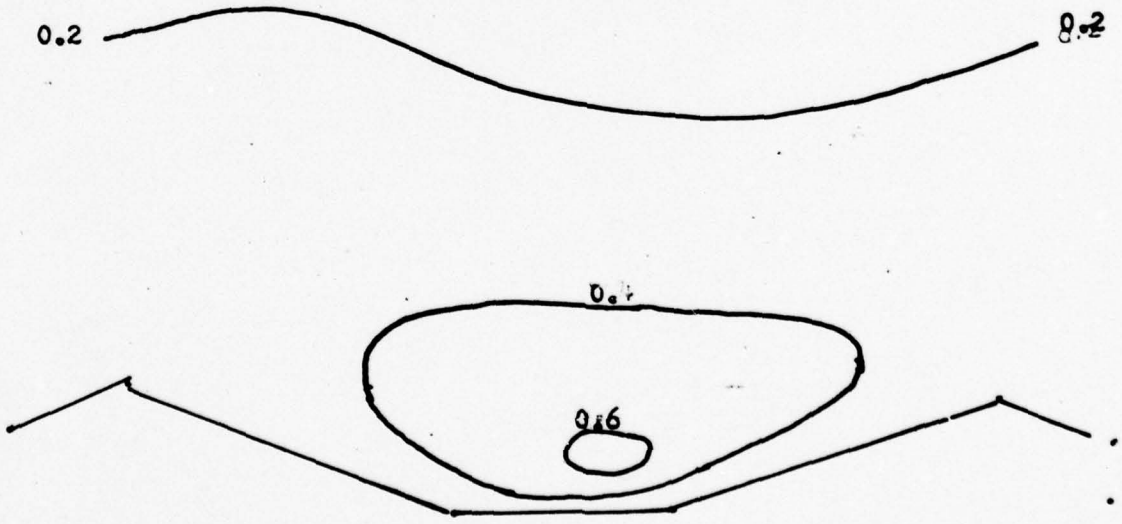

3b.

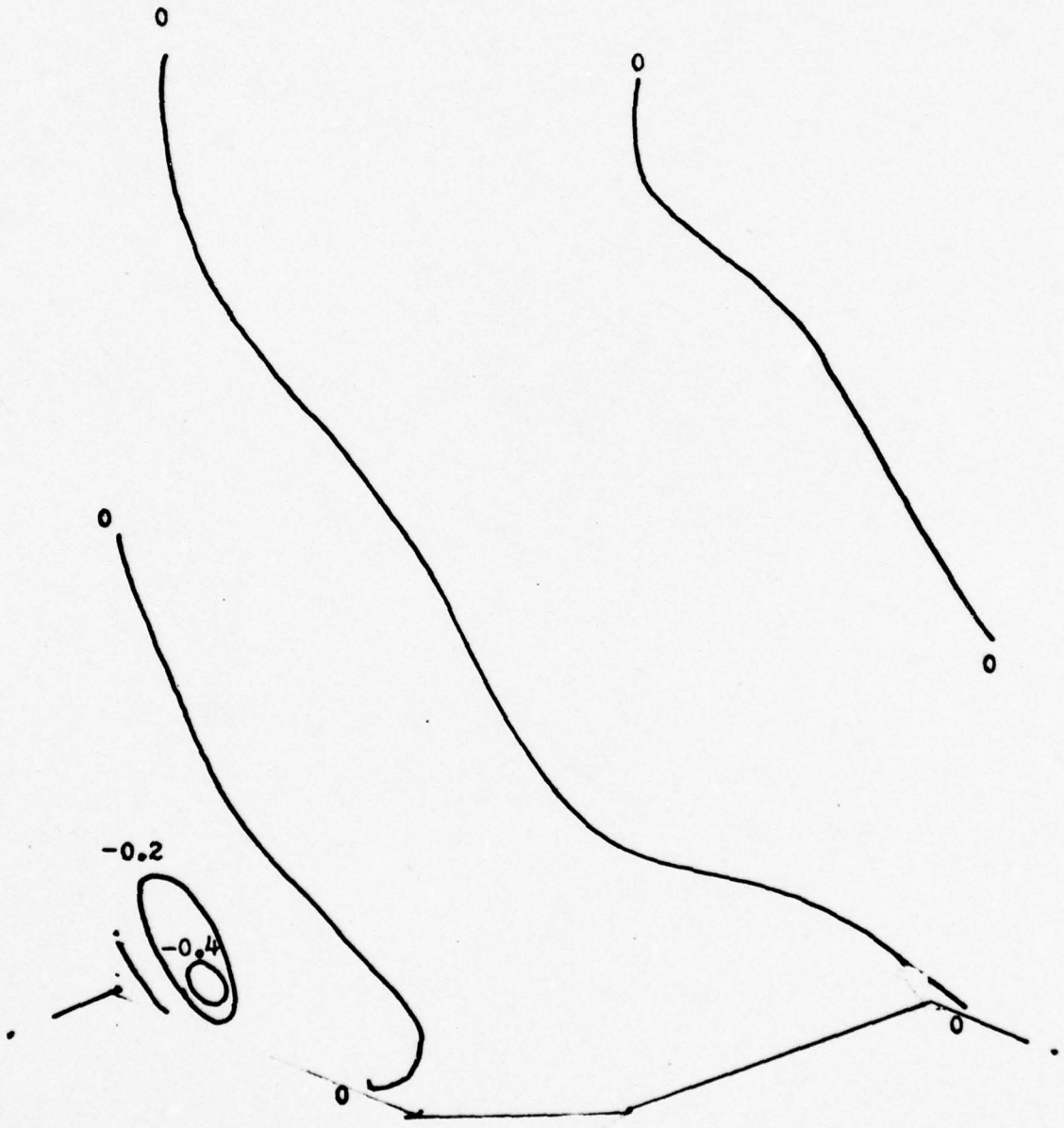

30. W

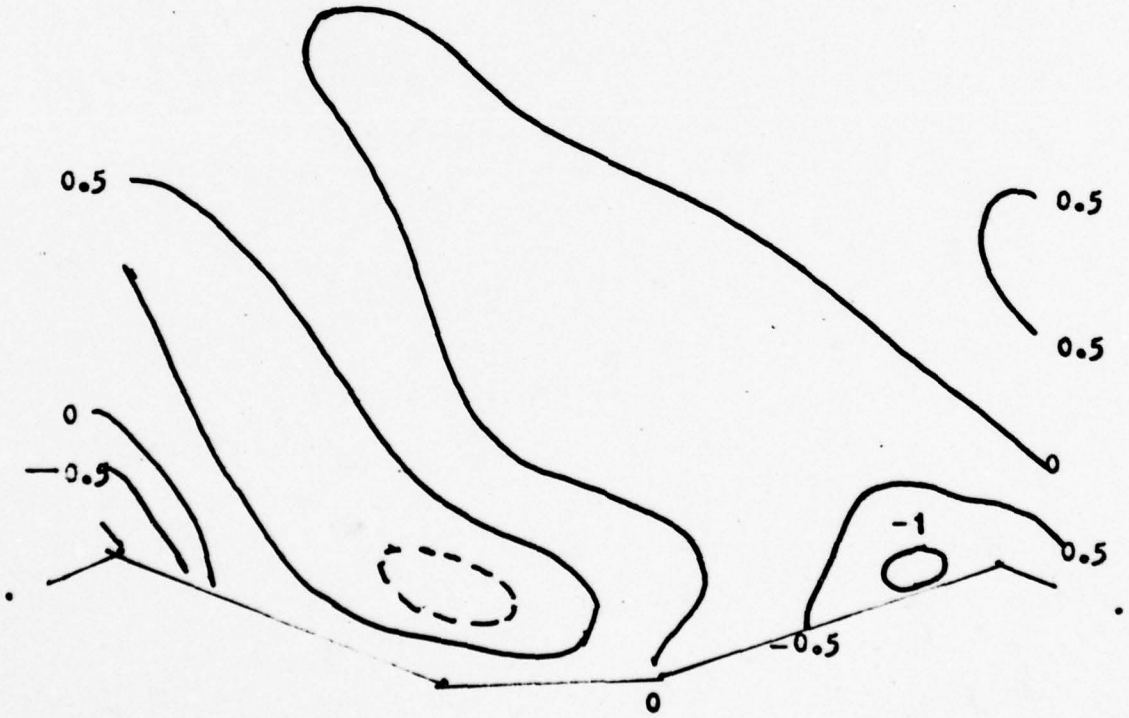

Fig. 7

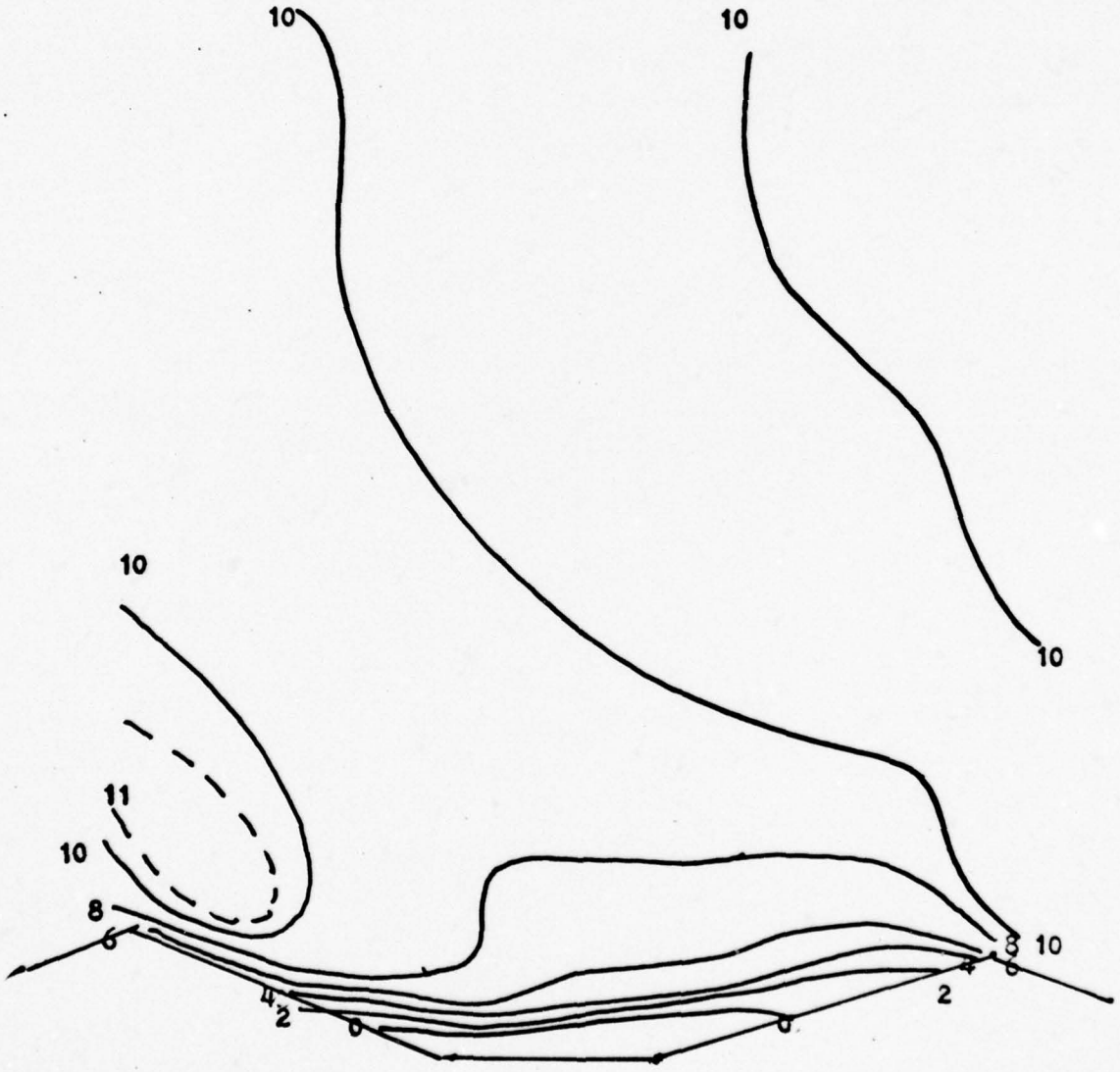

30. u

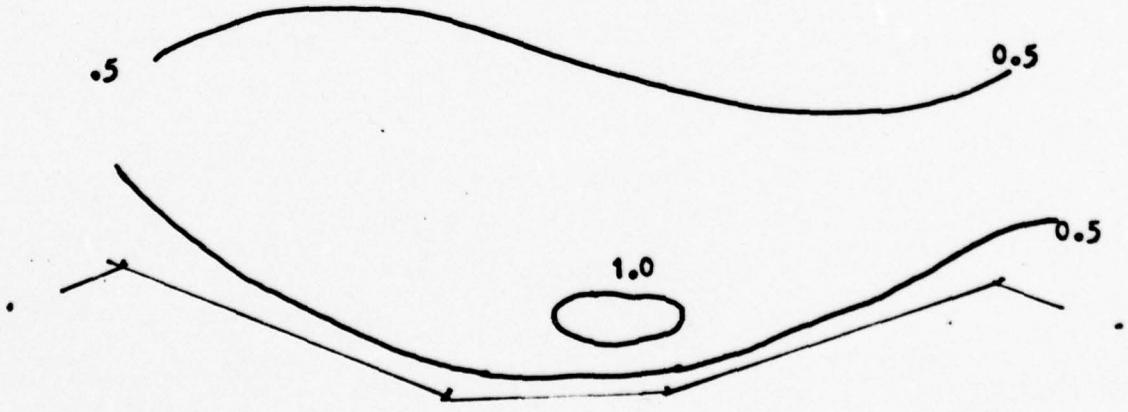

3f. v

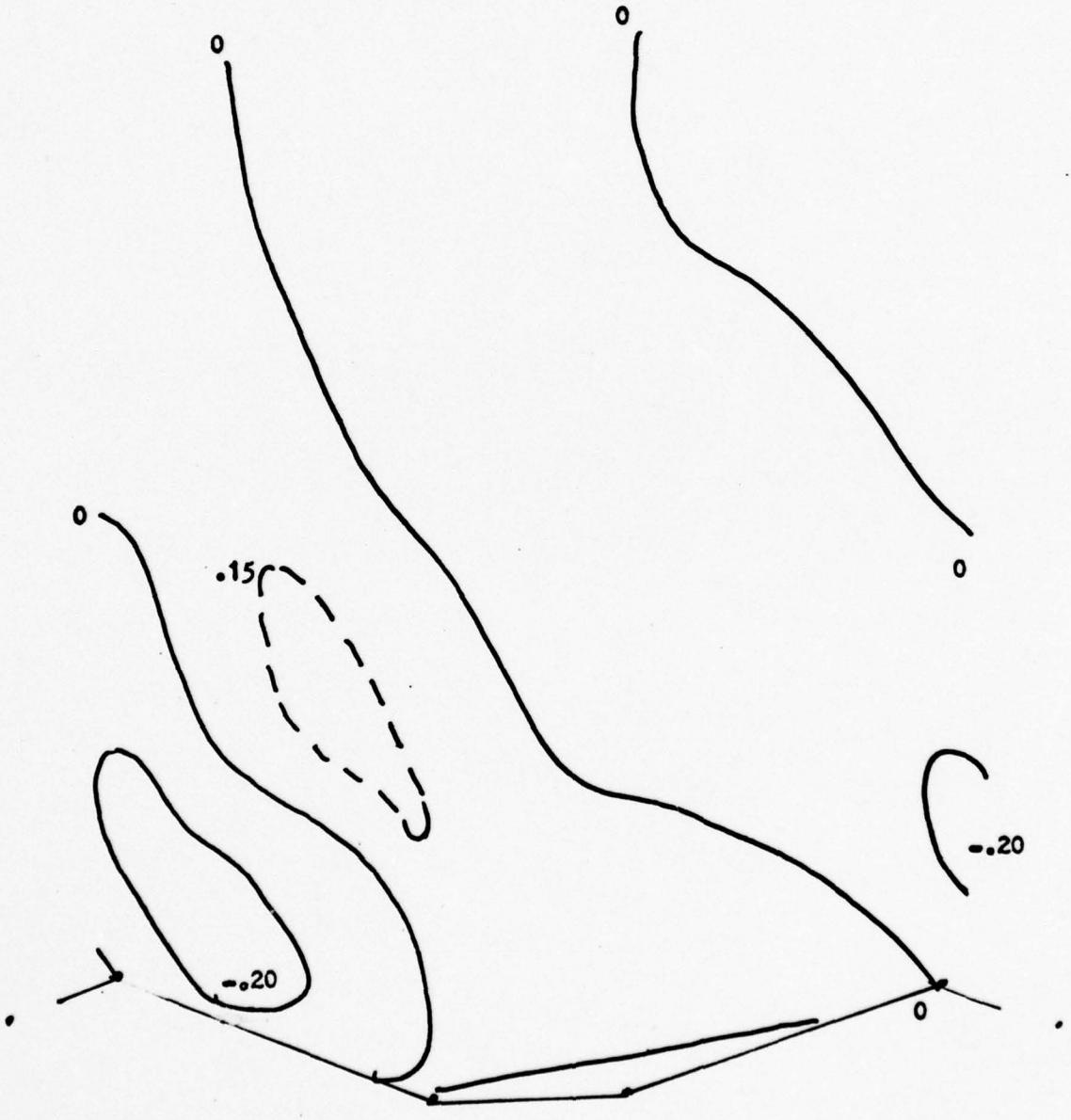

3g. w

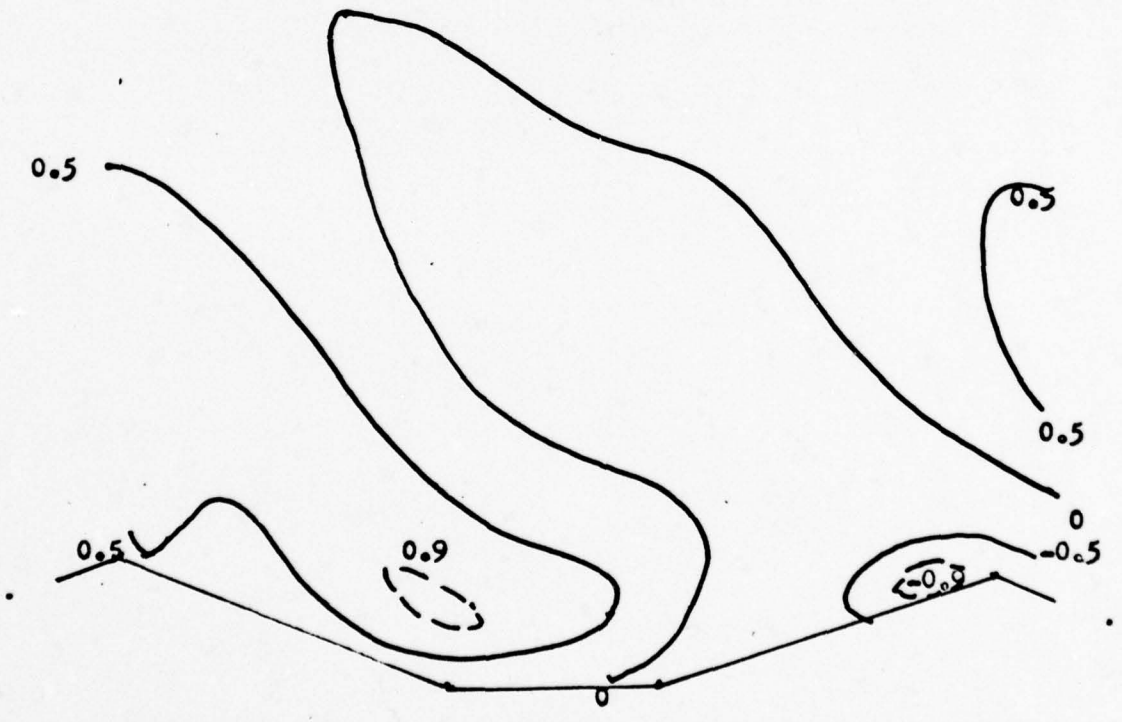

3h. T

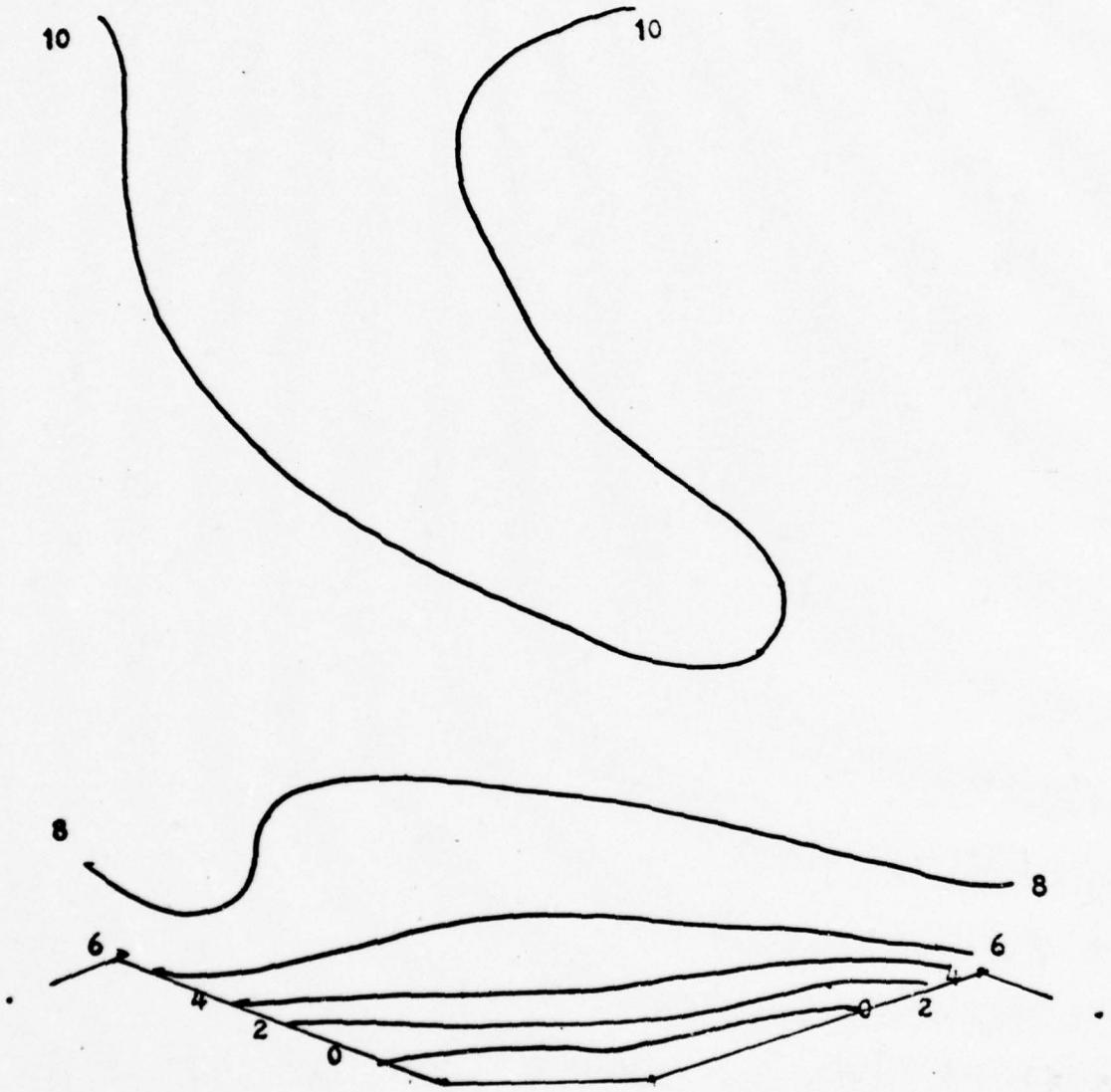

Fig. 4. Isopleths of wind components and temperature deviations for Run #2 at J=4 (a to d) a. u b. v c. w d. T and at J=7 (e to h) e. u f. v g. w h. T

4a.u

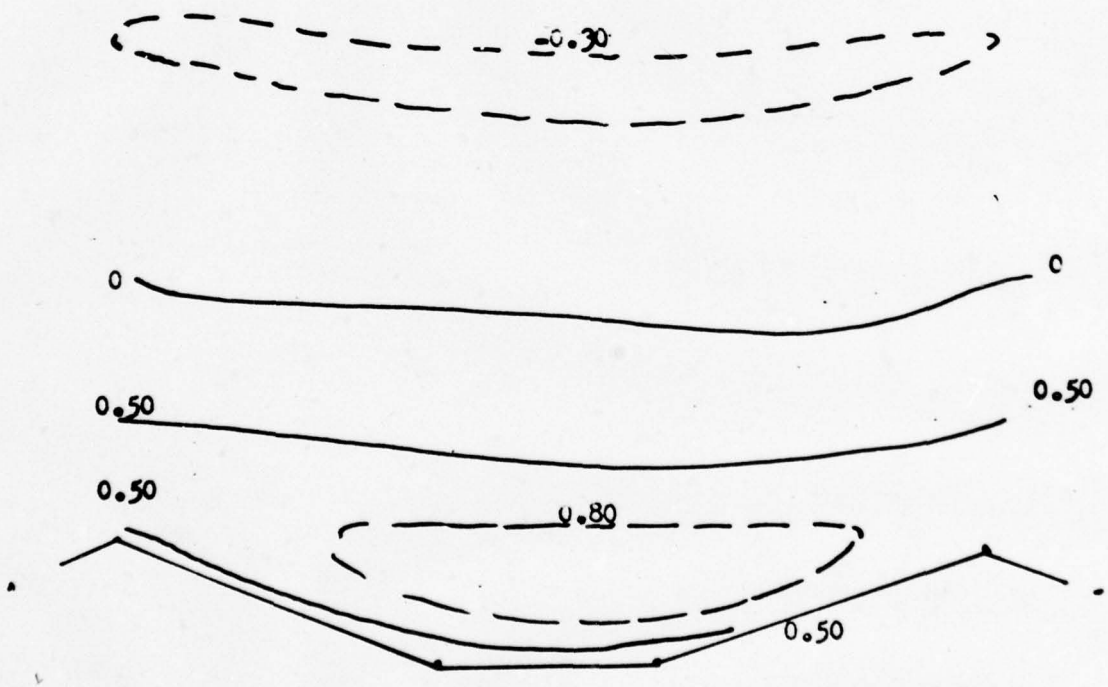

4b. ▼

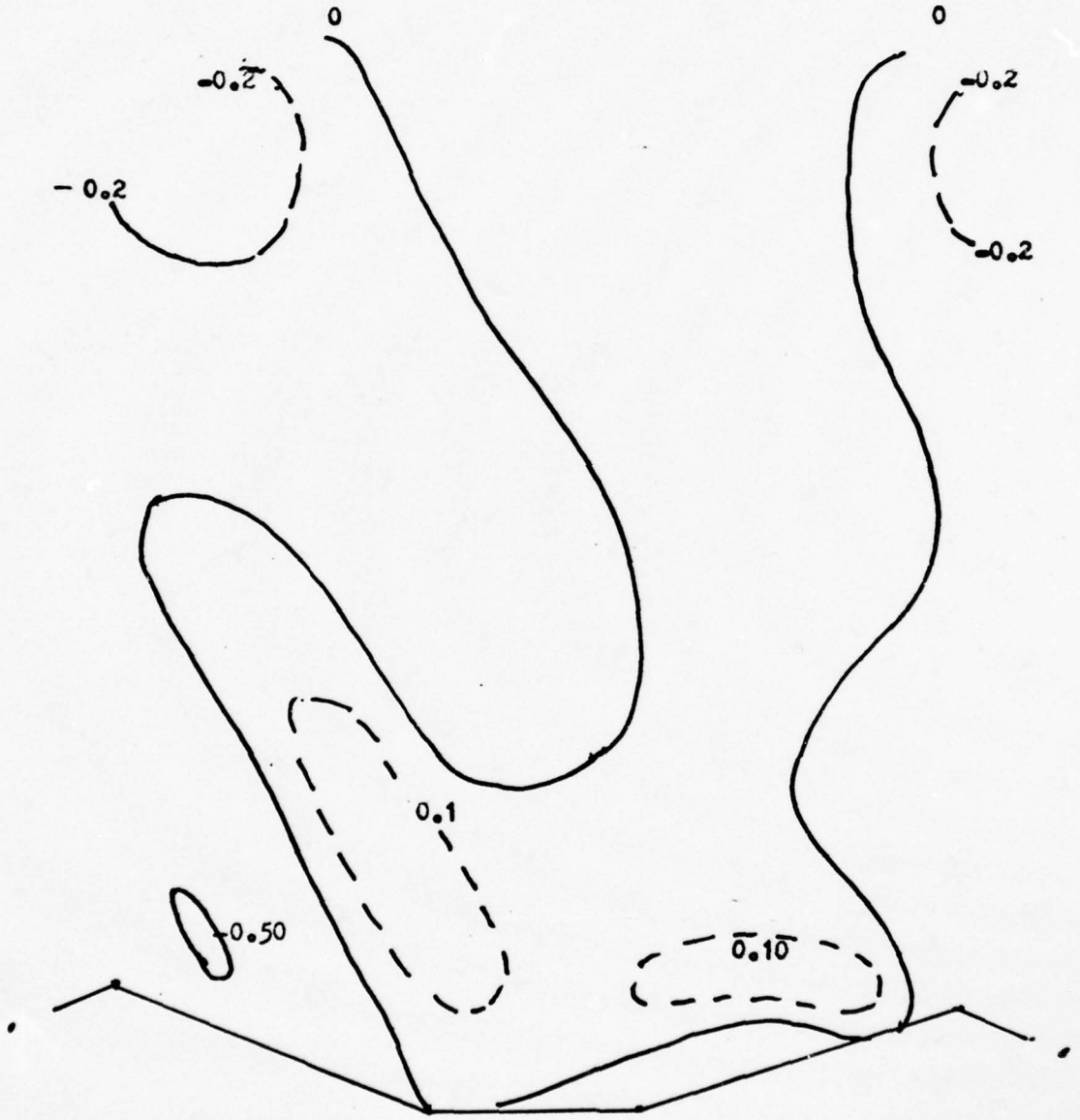

4c. w

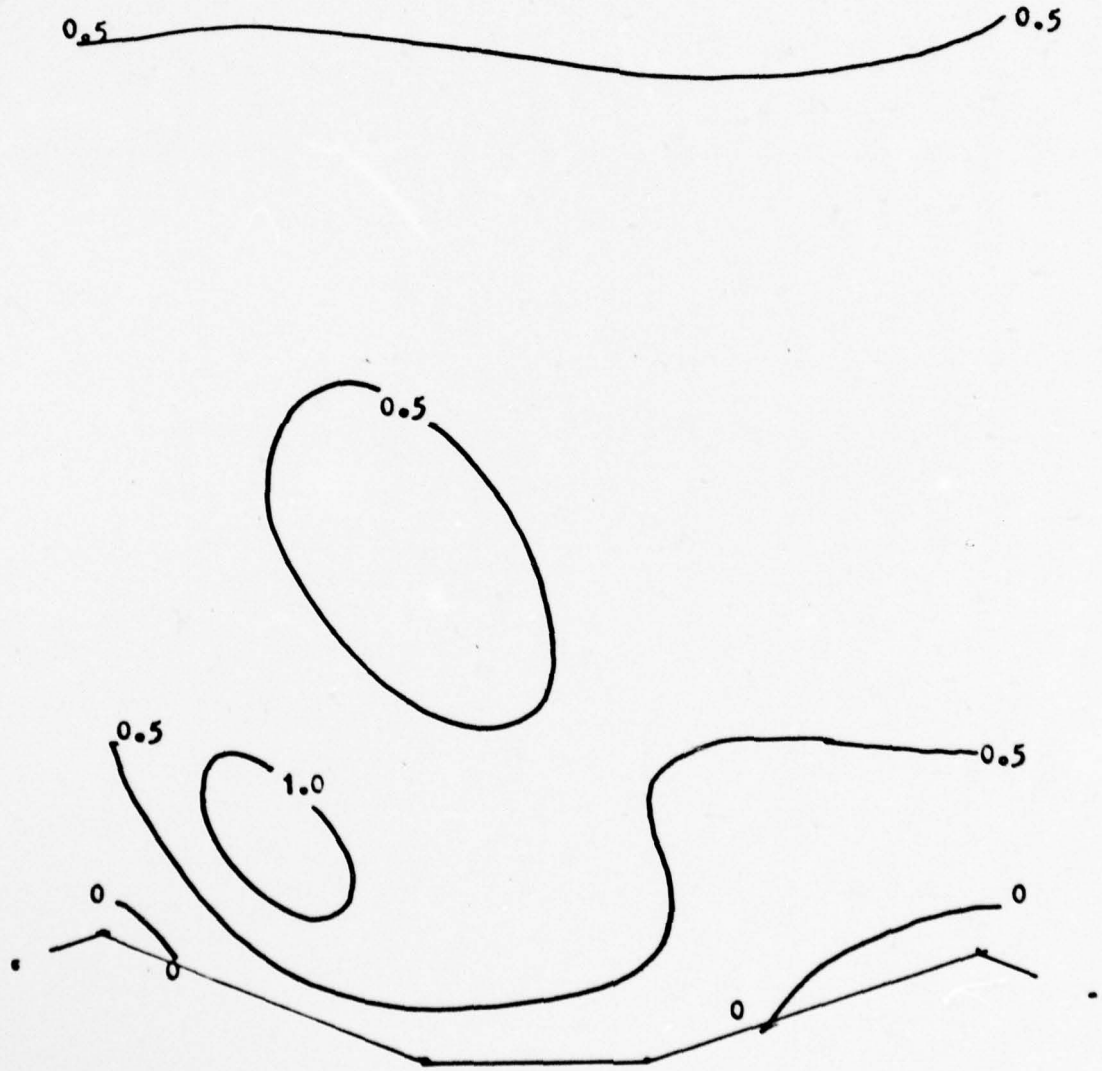

4d.T

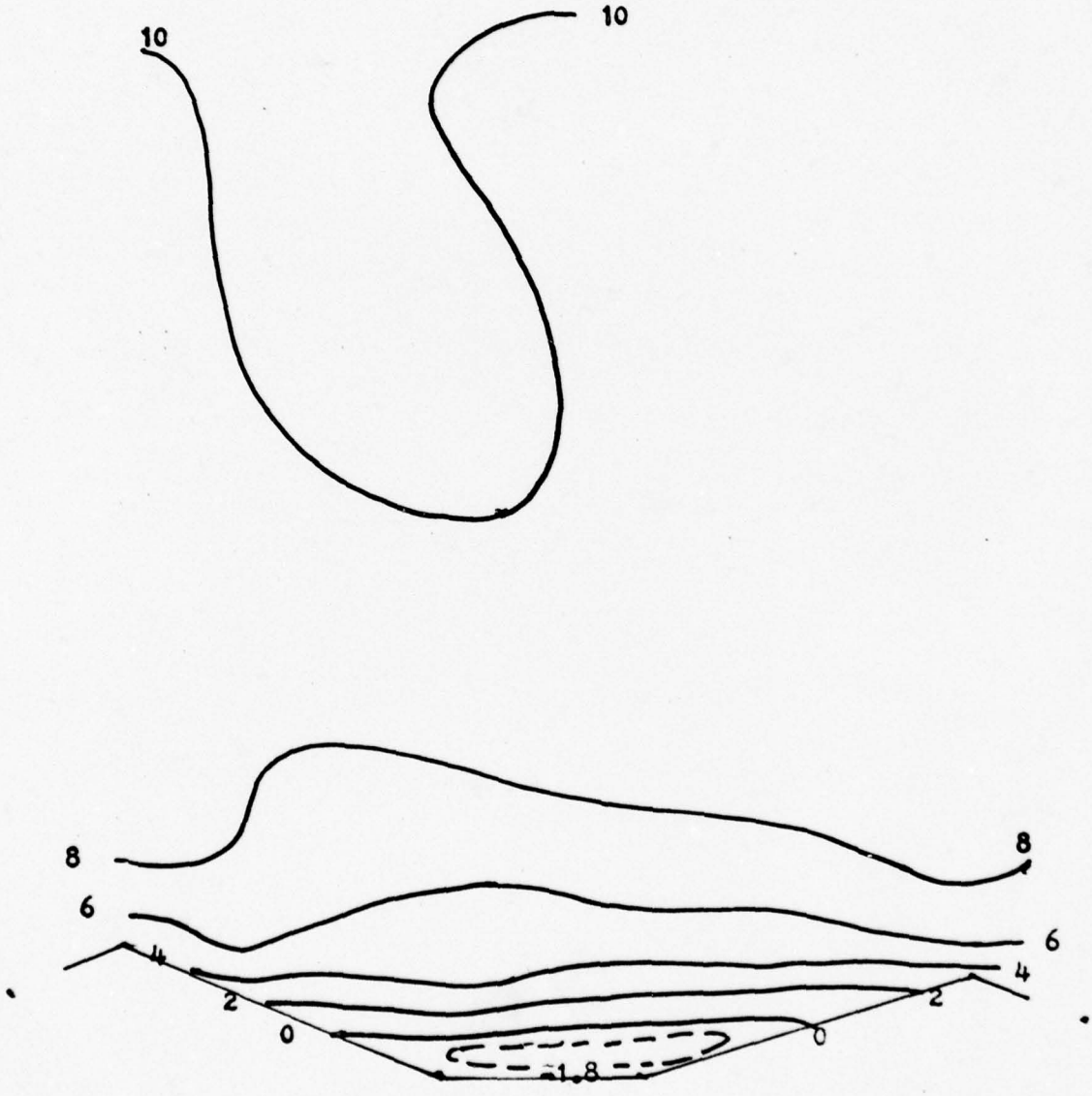

4e. u

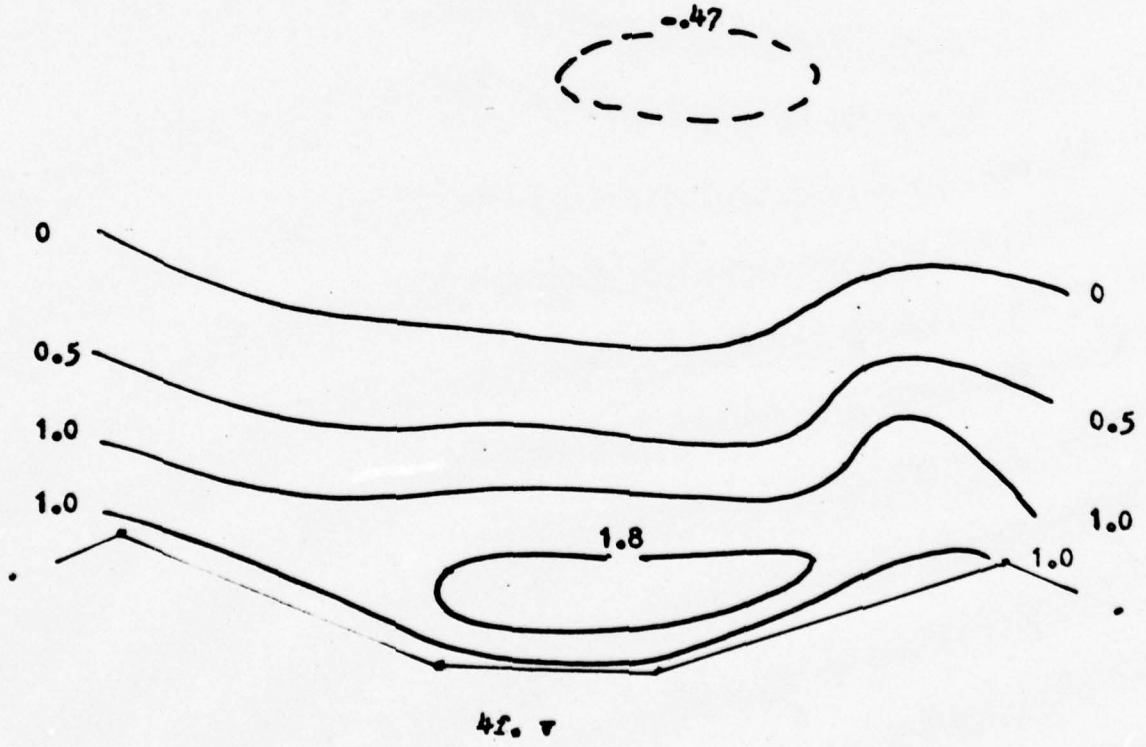

4f. ▼

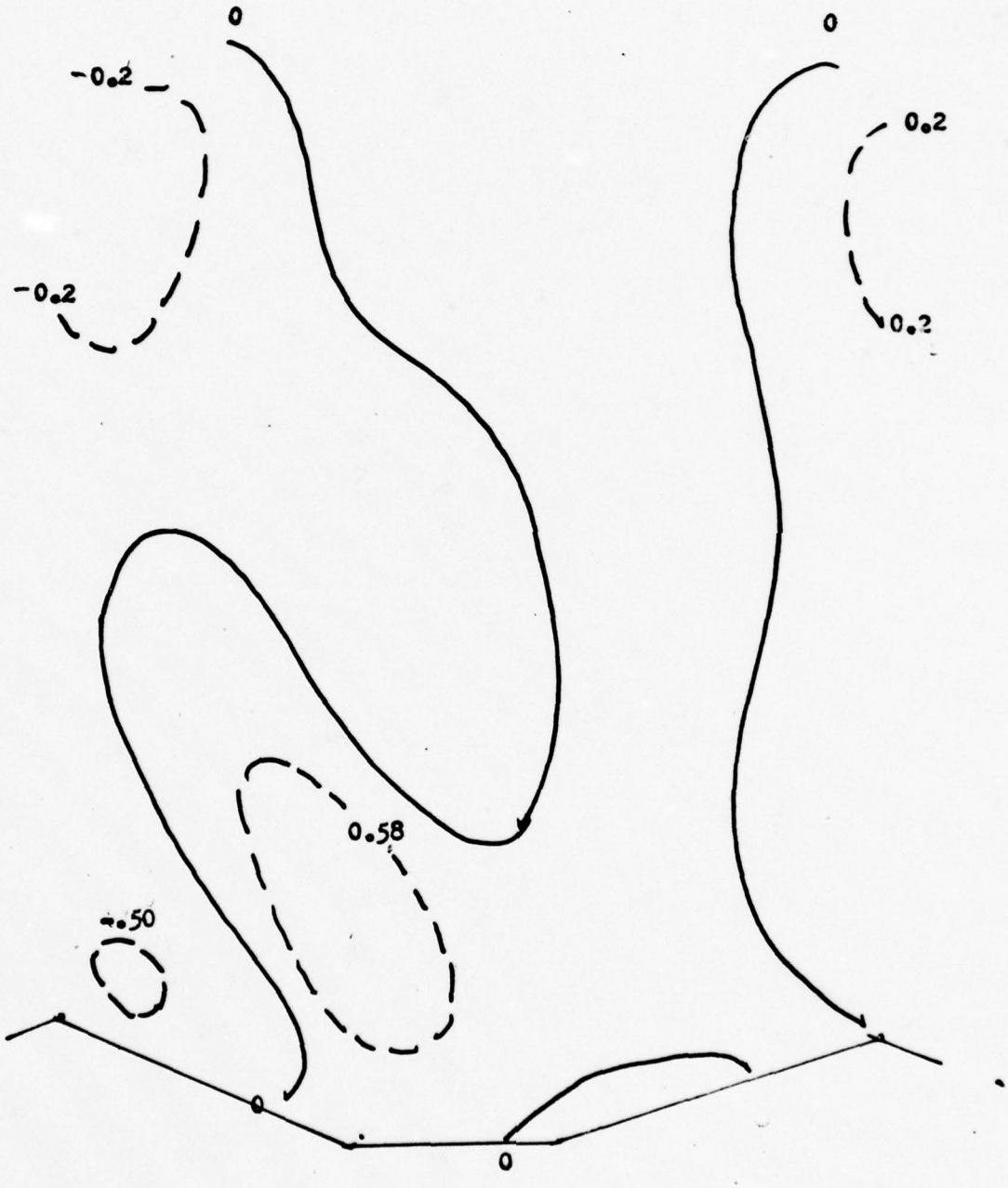

4g. w

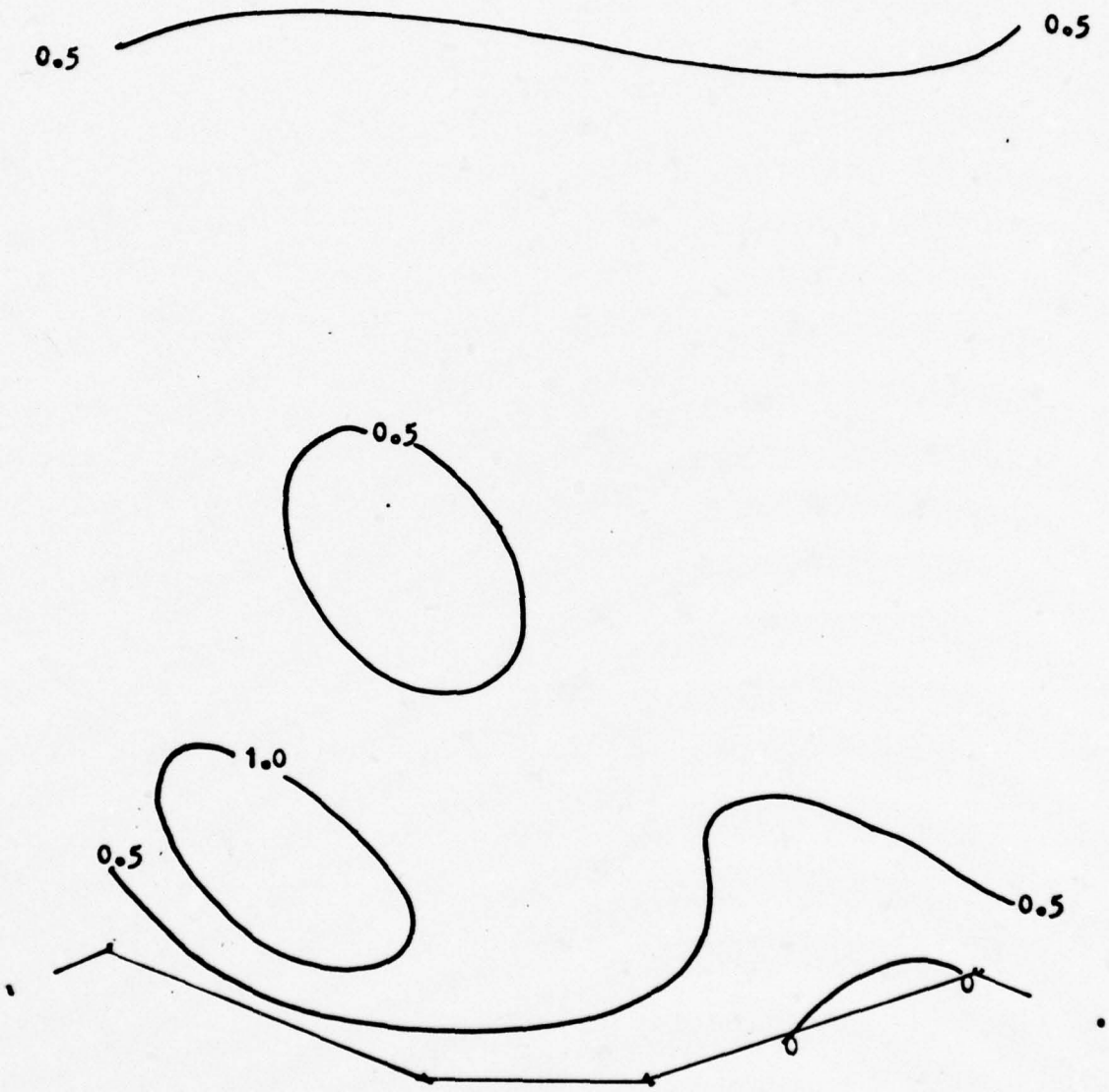

4h. T

T 4

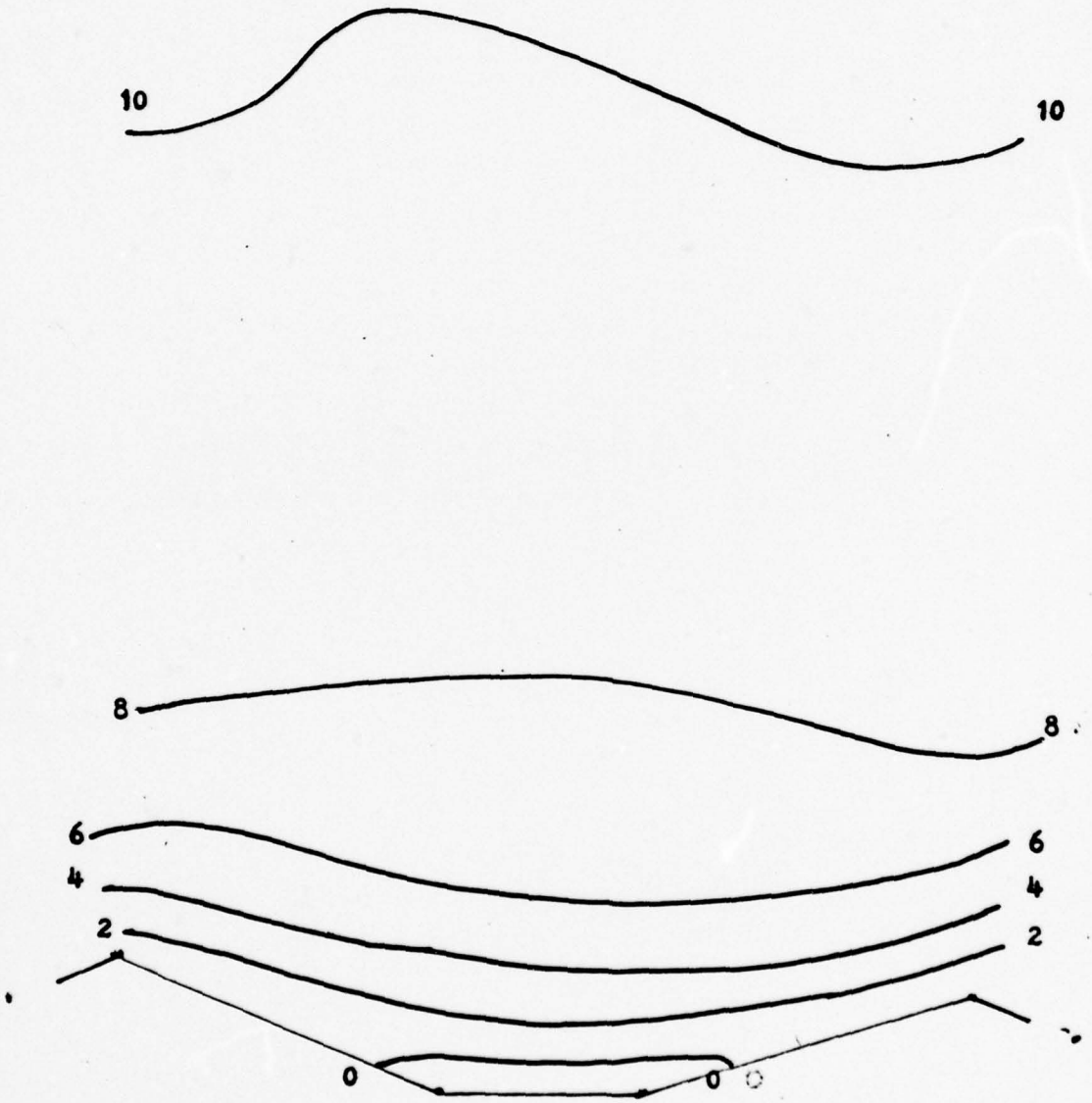

Fig. 5. Isopleths of wind components and temperature deviations for Run #3 at J=4 (a to d) a. u b. v c. w d. T and at J=7 (e to h) e. u f. v g. w h. T

5a. u

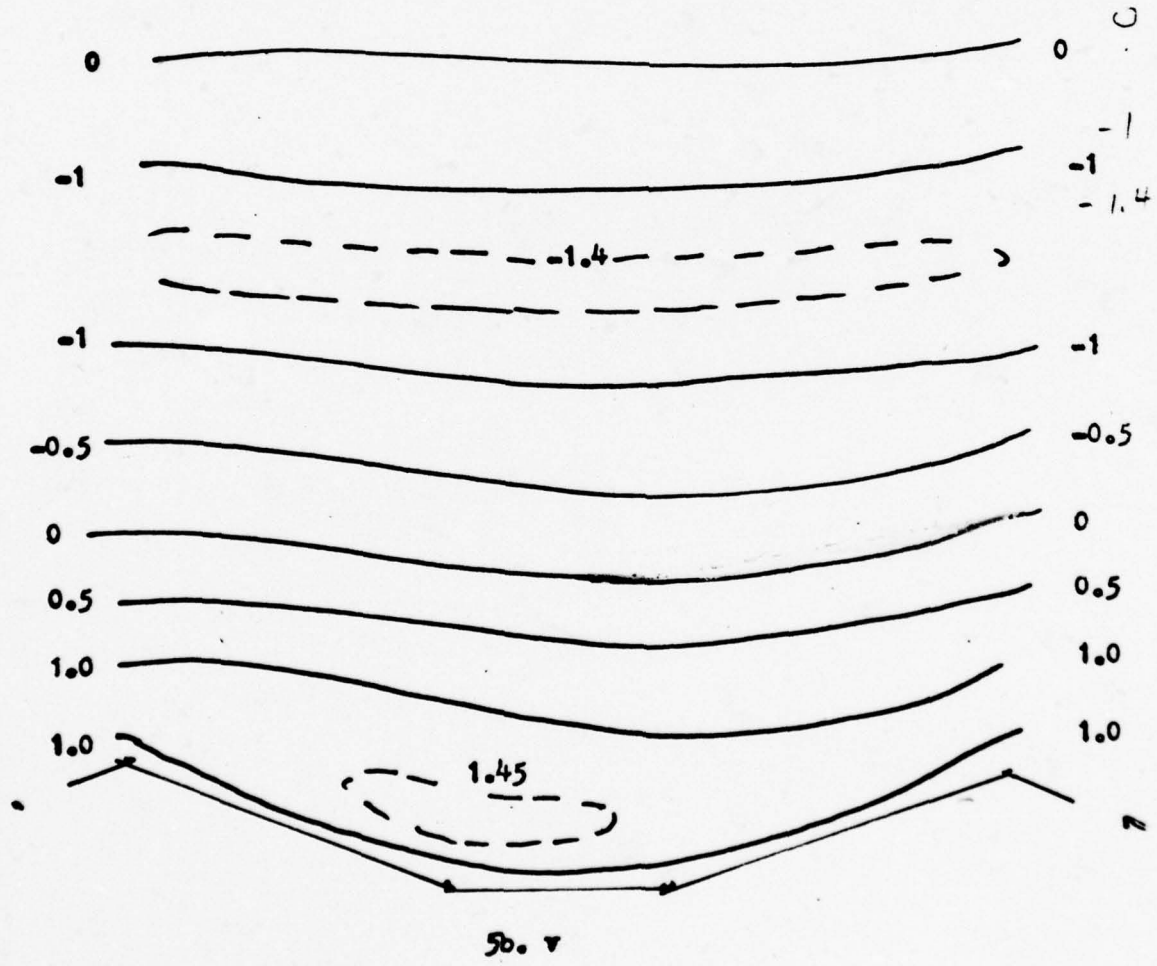
0
0
-1
-1
-1.4
-1
-1
-0.5
-0.5
0
0
0.5
0.5
1.0
1.0
1.0
1.0
1.45
50. V

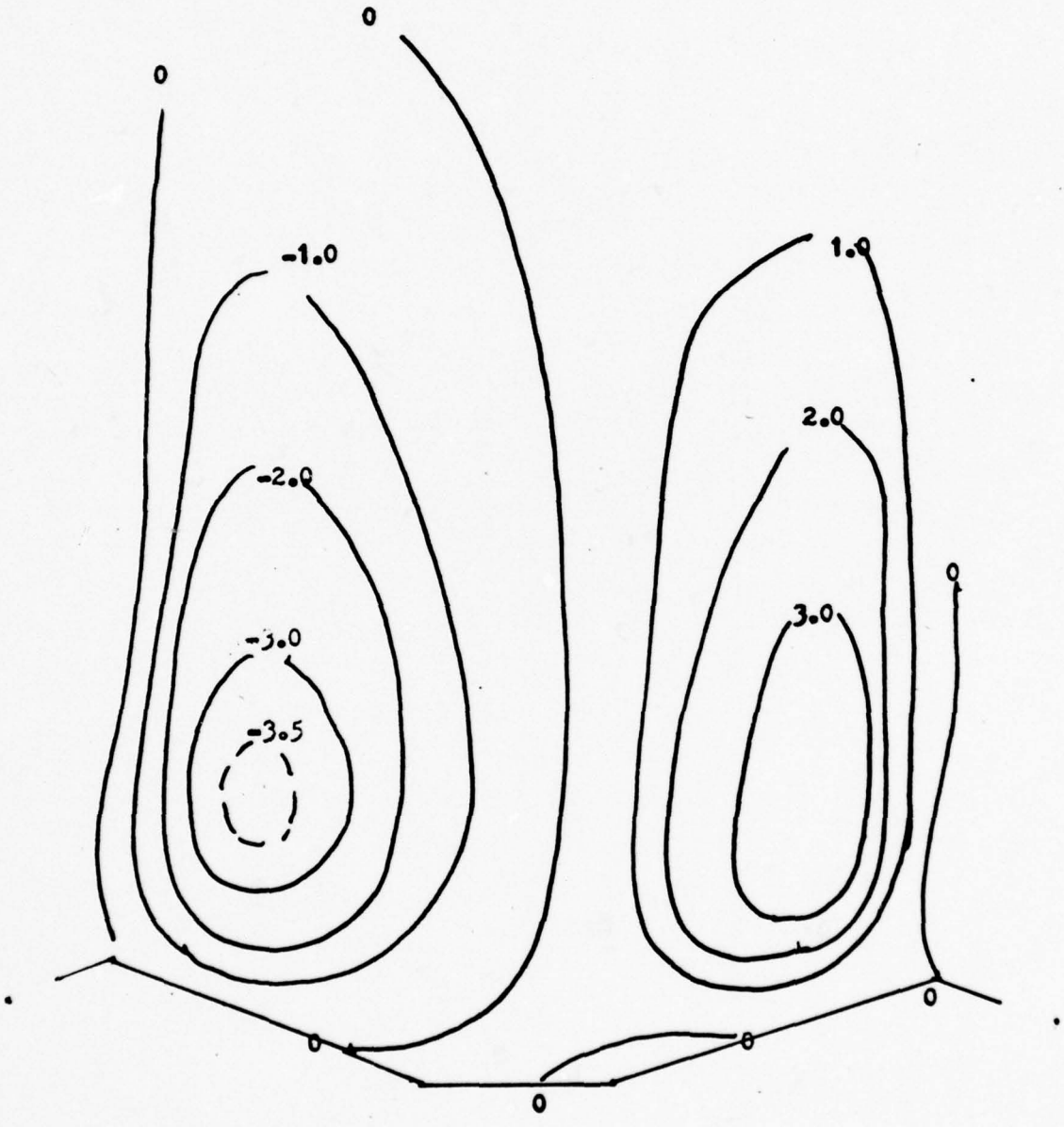
0
0
-1.0
-2.0
-3.0
-3.5
1.0
2.0
3.0
0
0
0
0
0
0
50. W

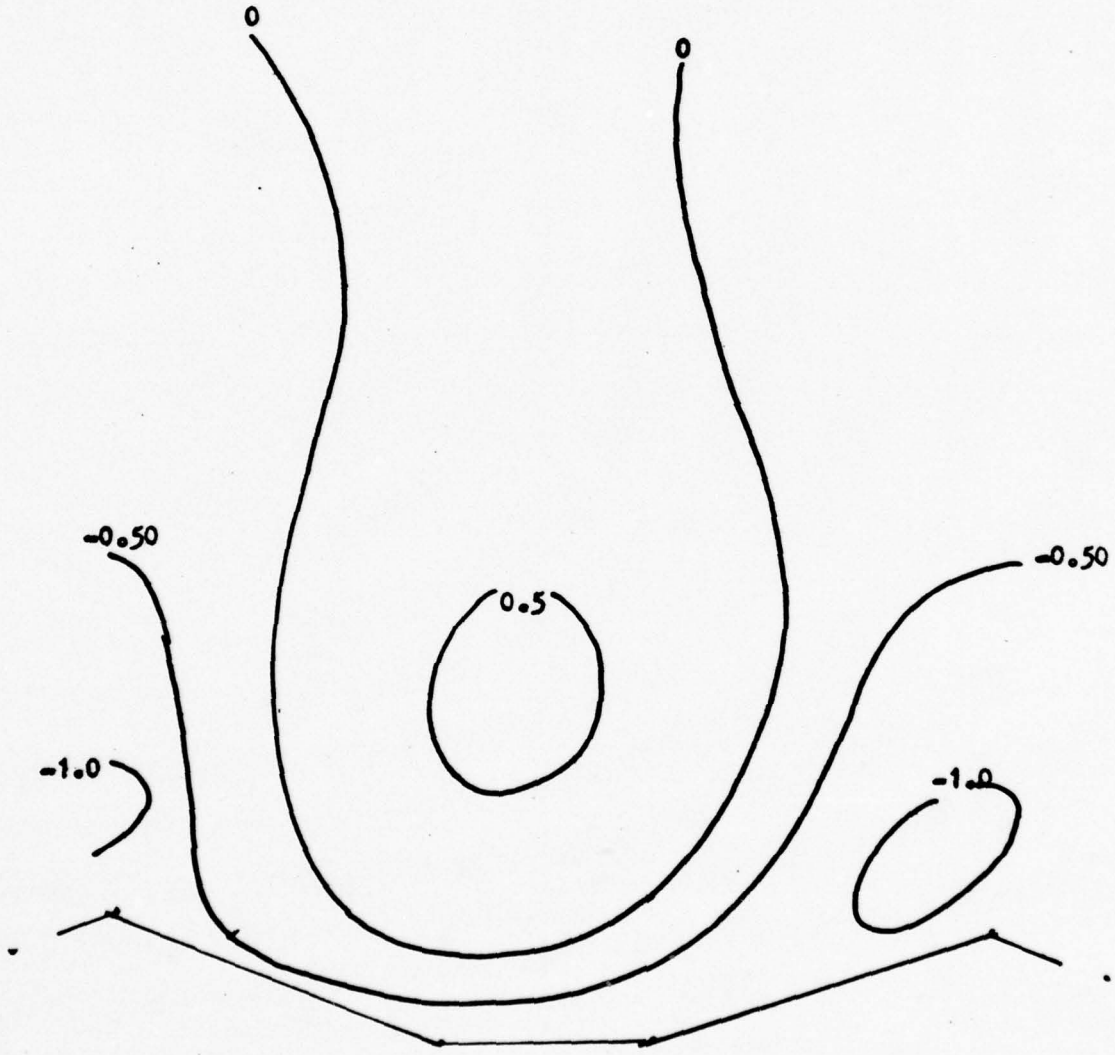

Sd. T

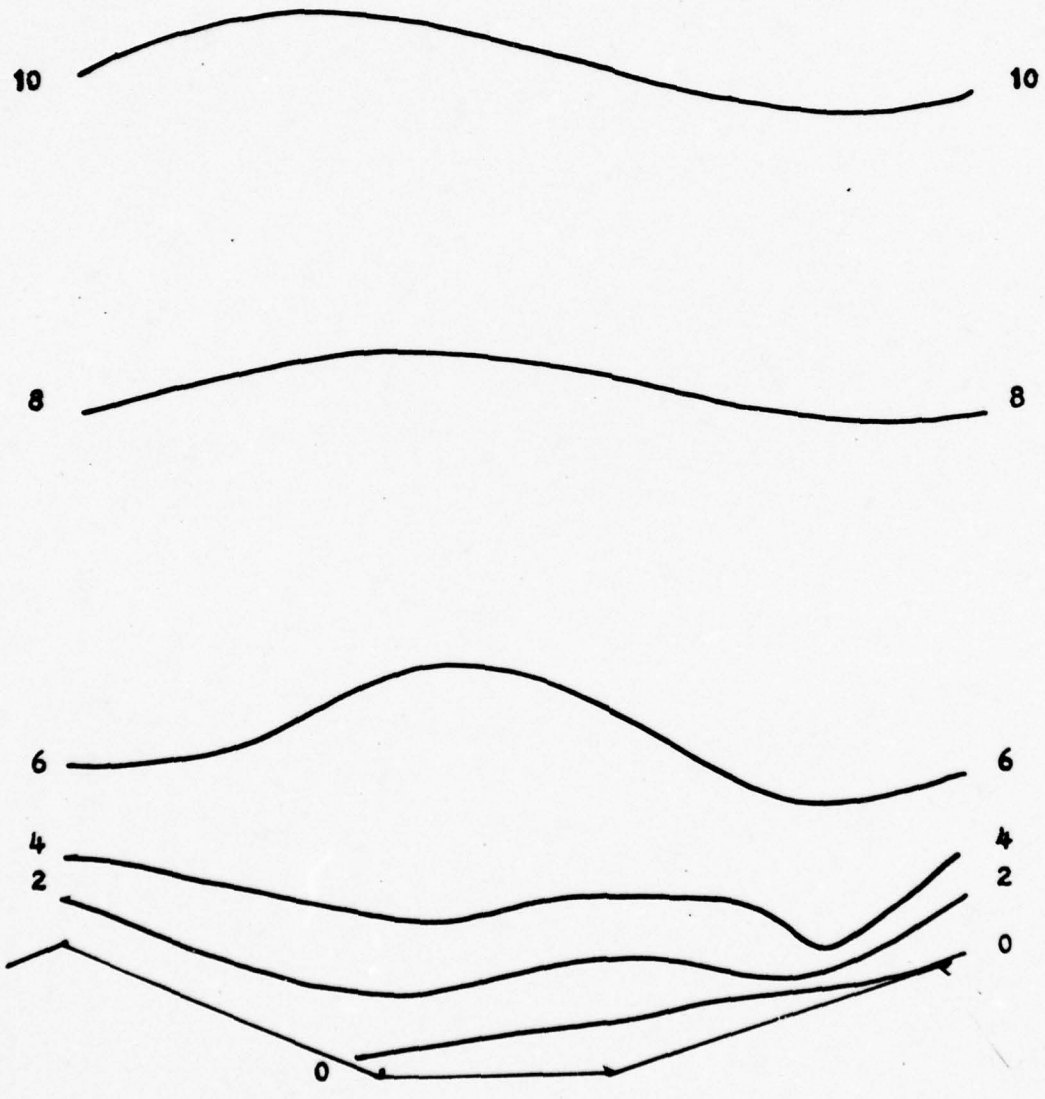

50. u

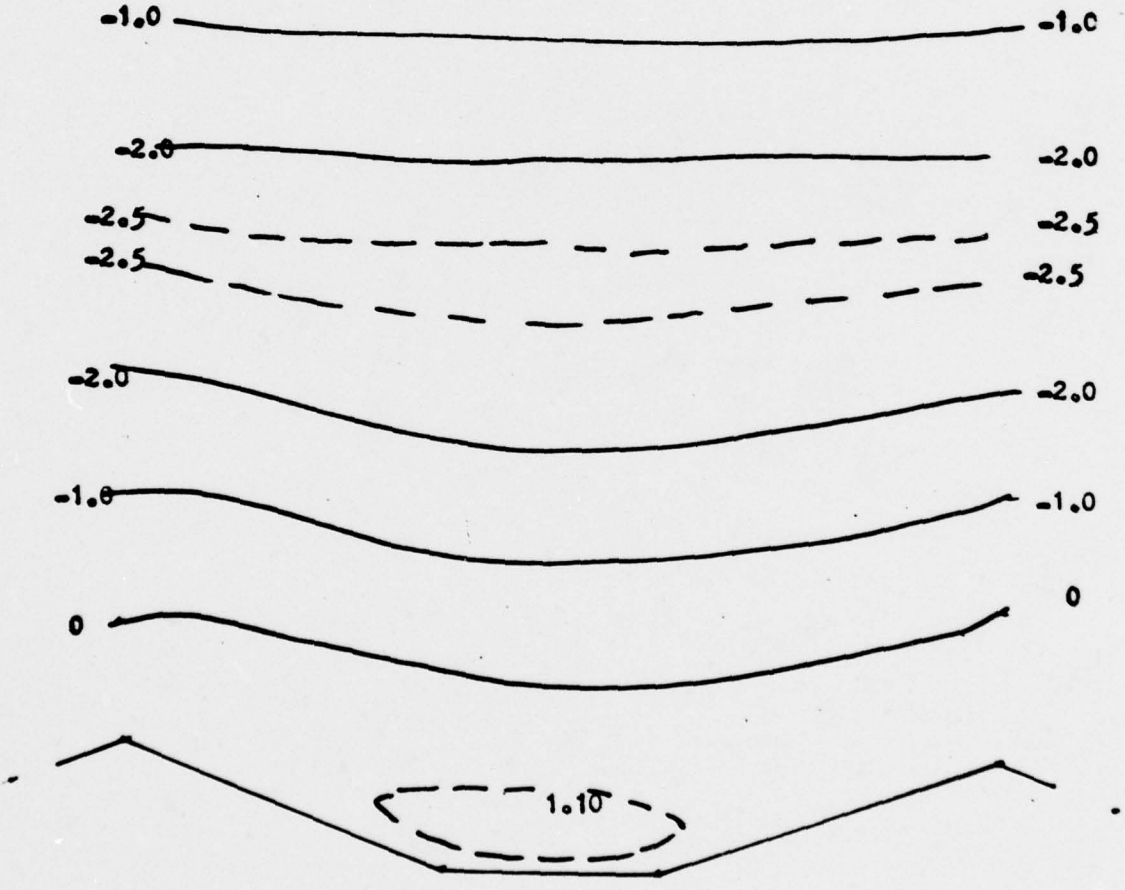

Sf. ▼

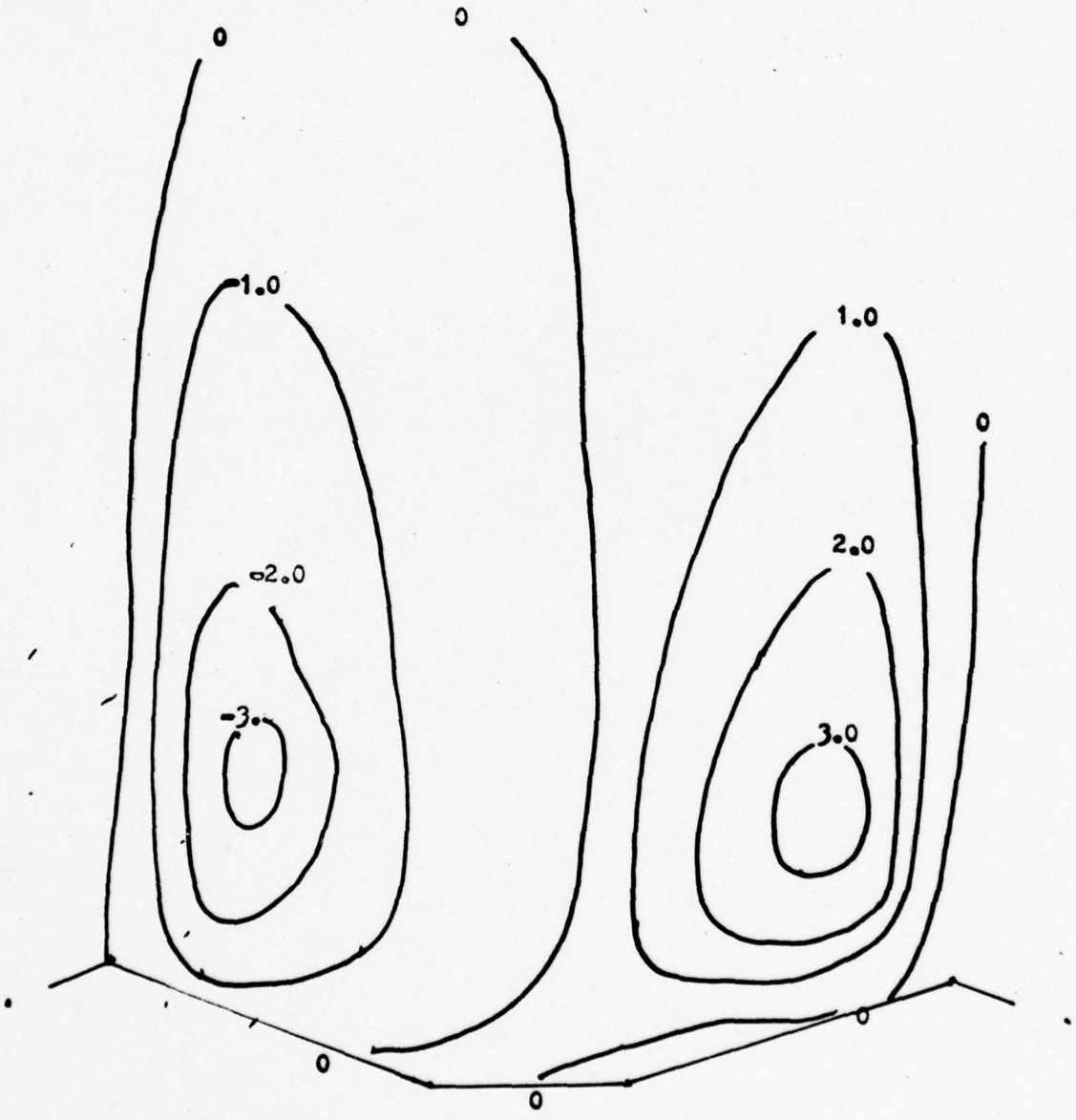

5g. w

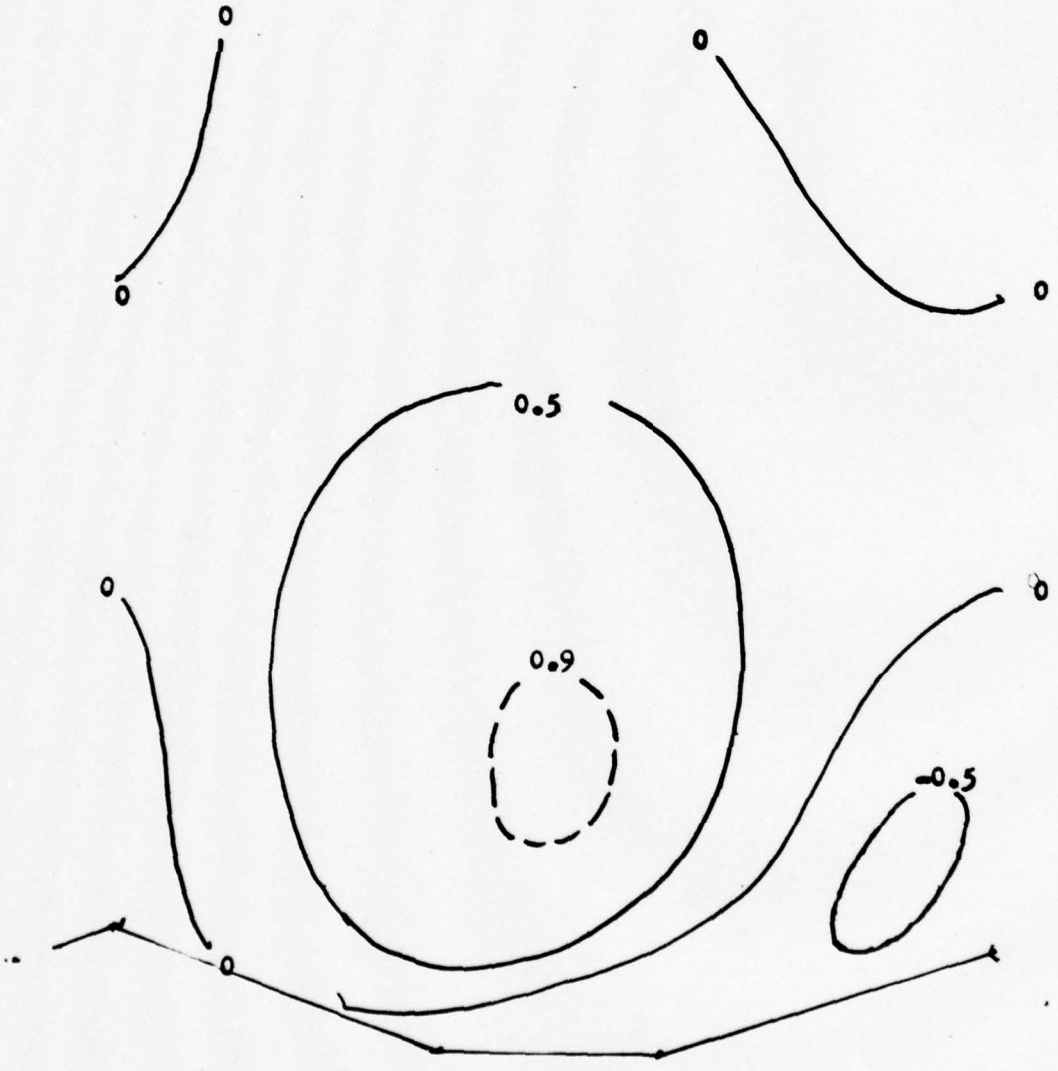

5h. T

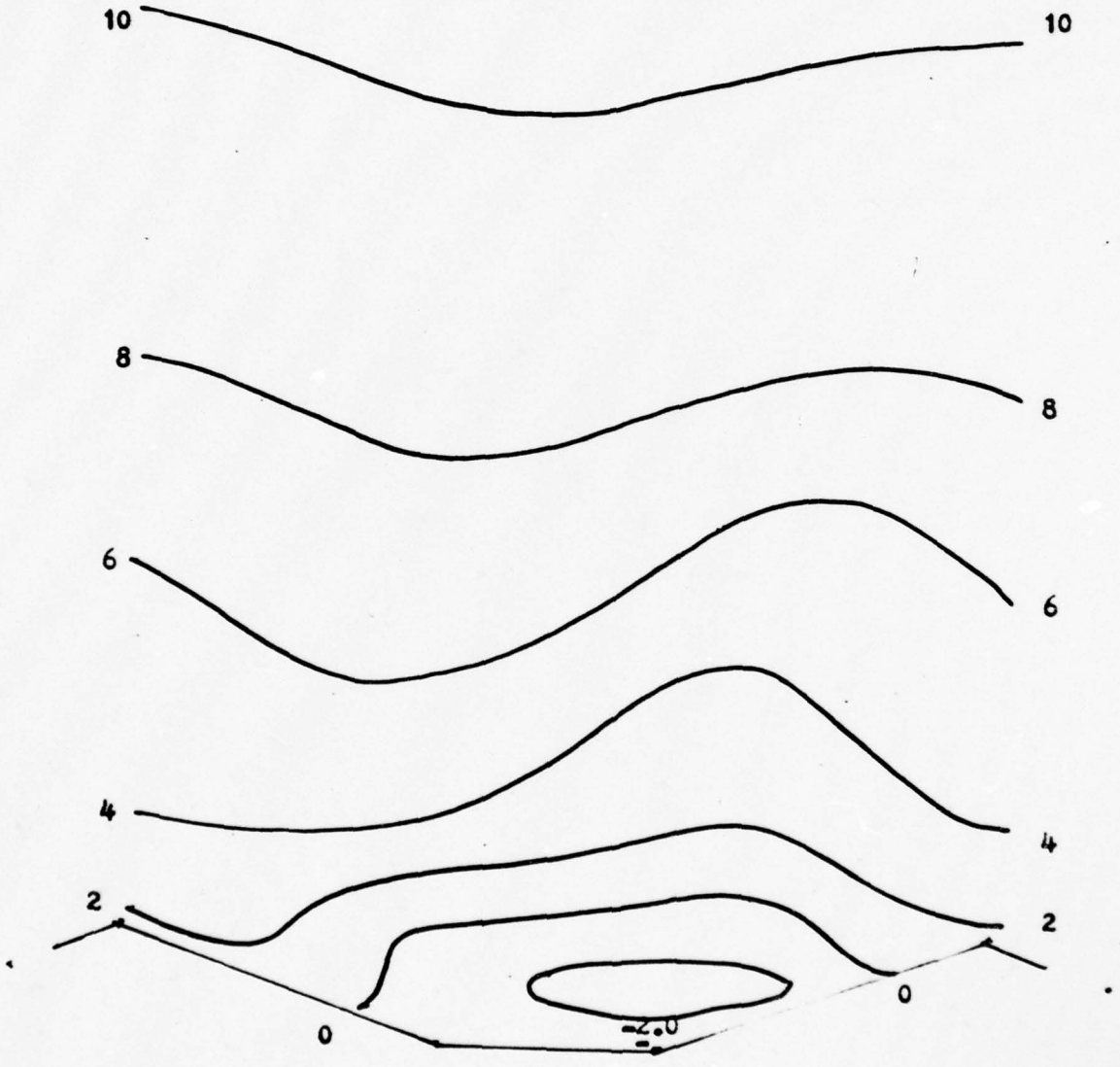

Fig. 6. Isopleths of wind components and temperature deviations for Run #4 at J=7 (a to d) a. u b. v c. w d. T

6a. u

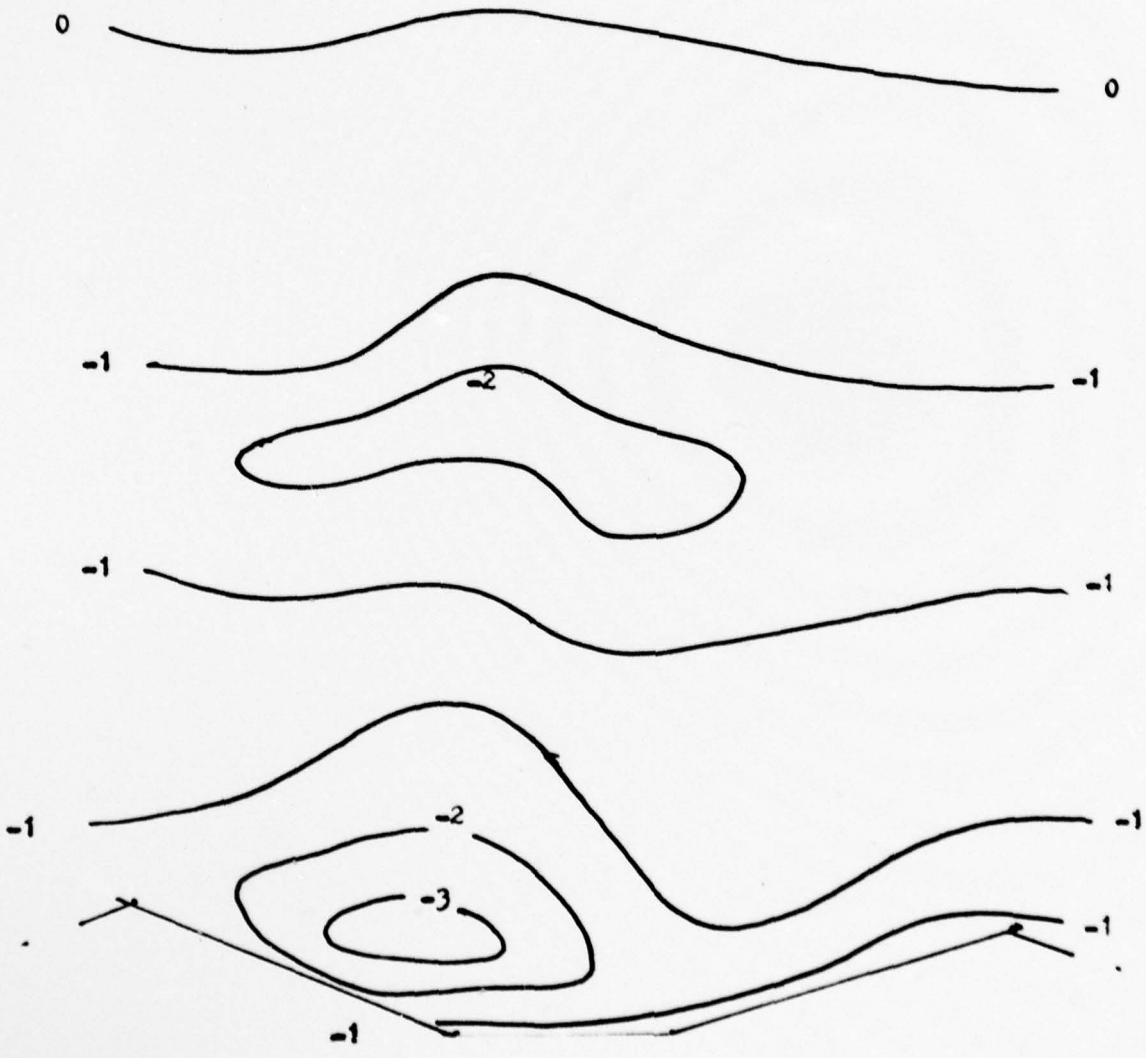

6b. v

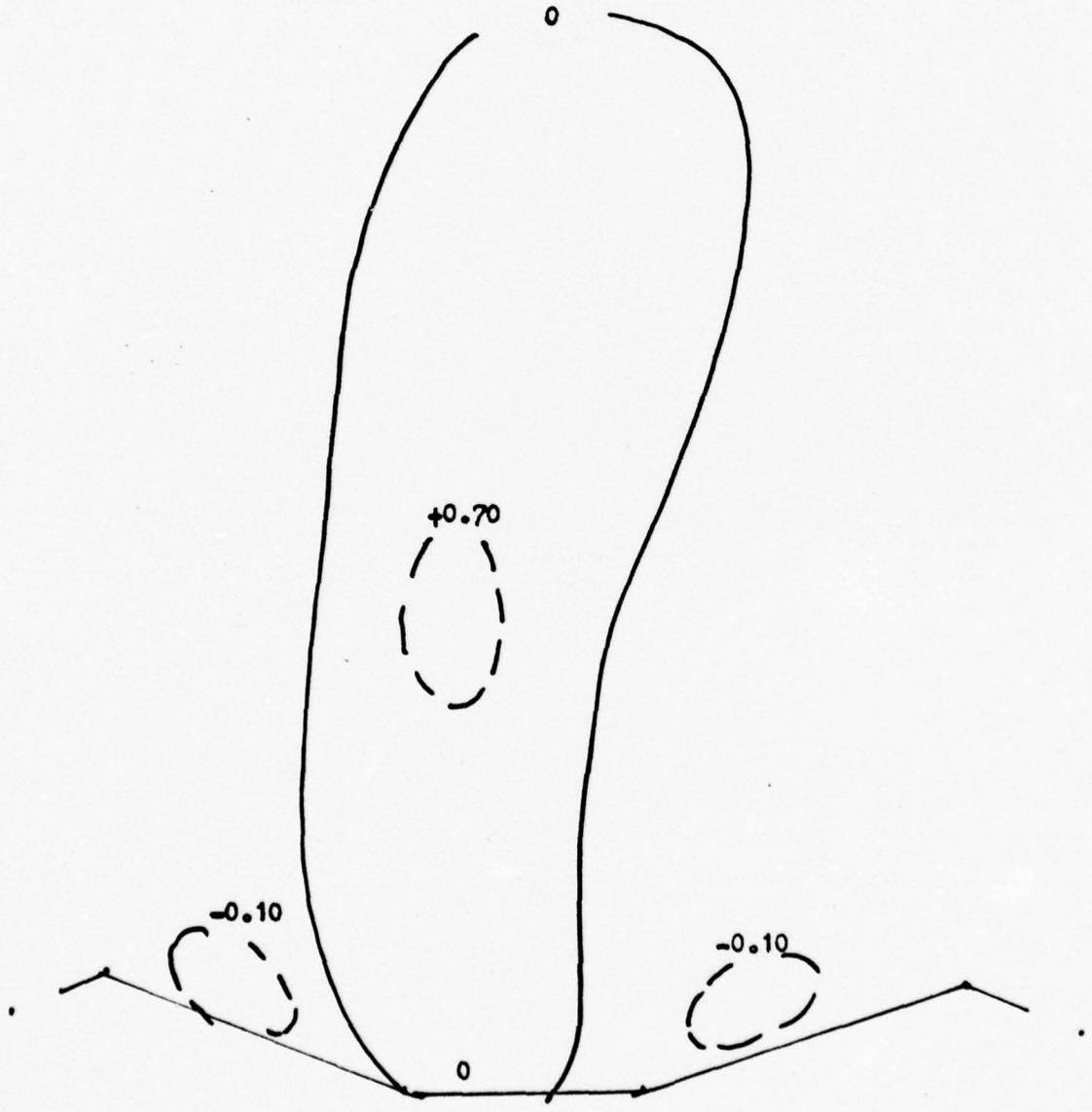

6g. w

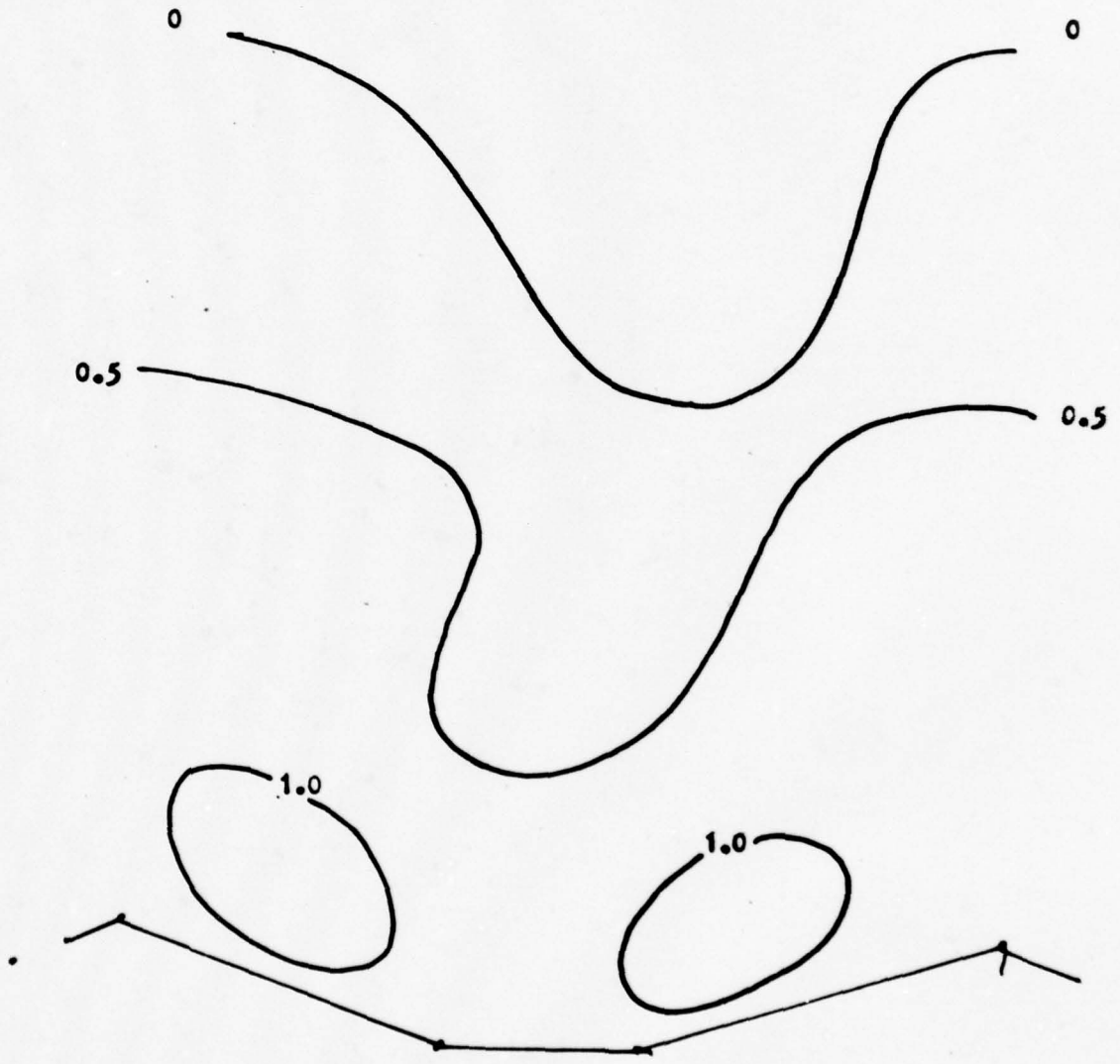

6h. T

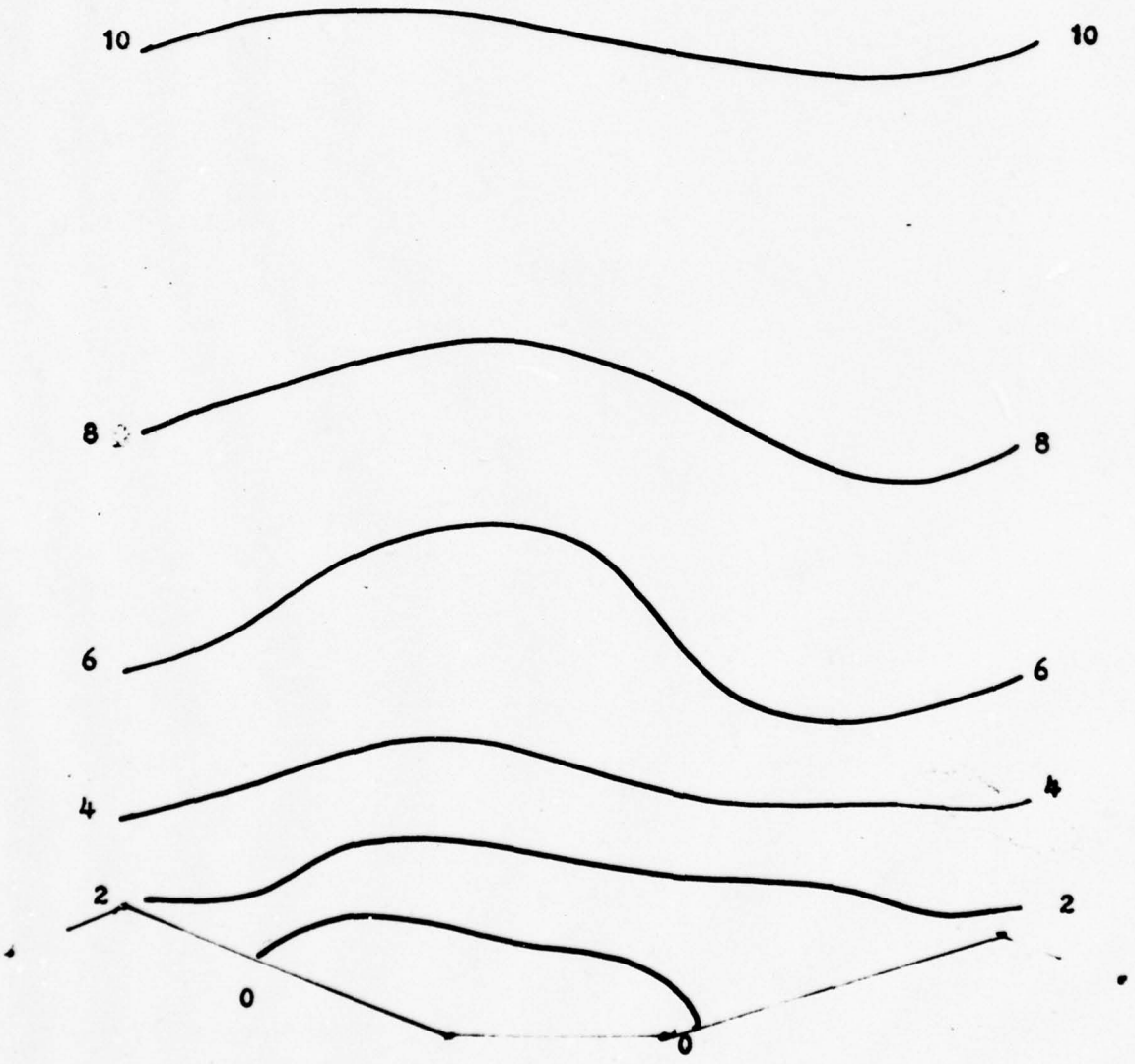

Fig. 7. Isopleths of wind components and temperature deviations for Run #5 at J=7 (a to d) a. u b. v c. w d. T

7a. u

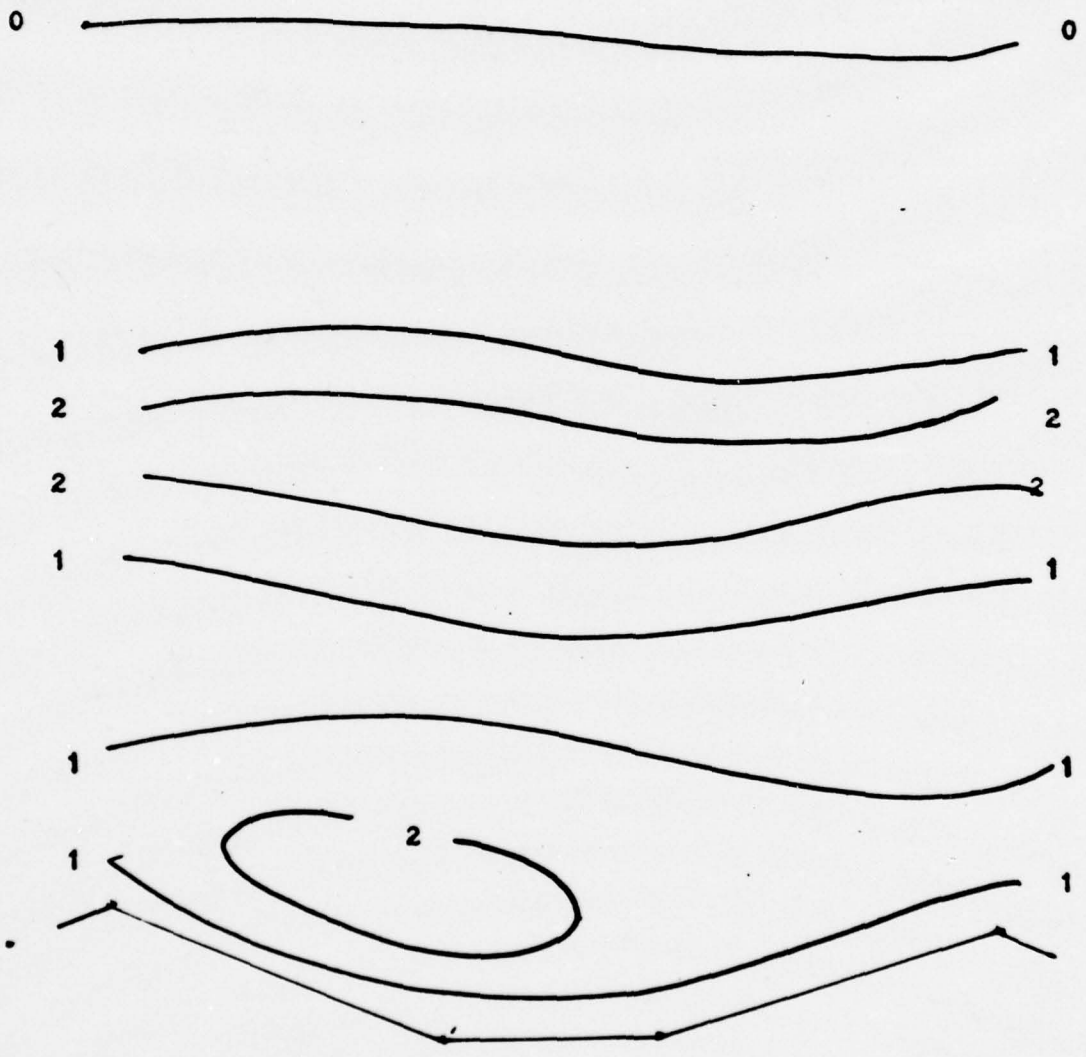

Fig. V

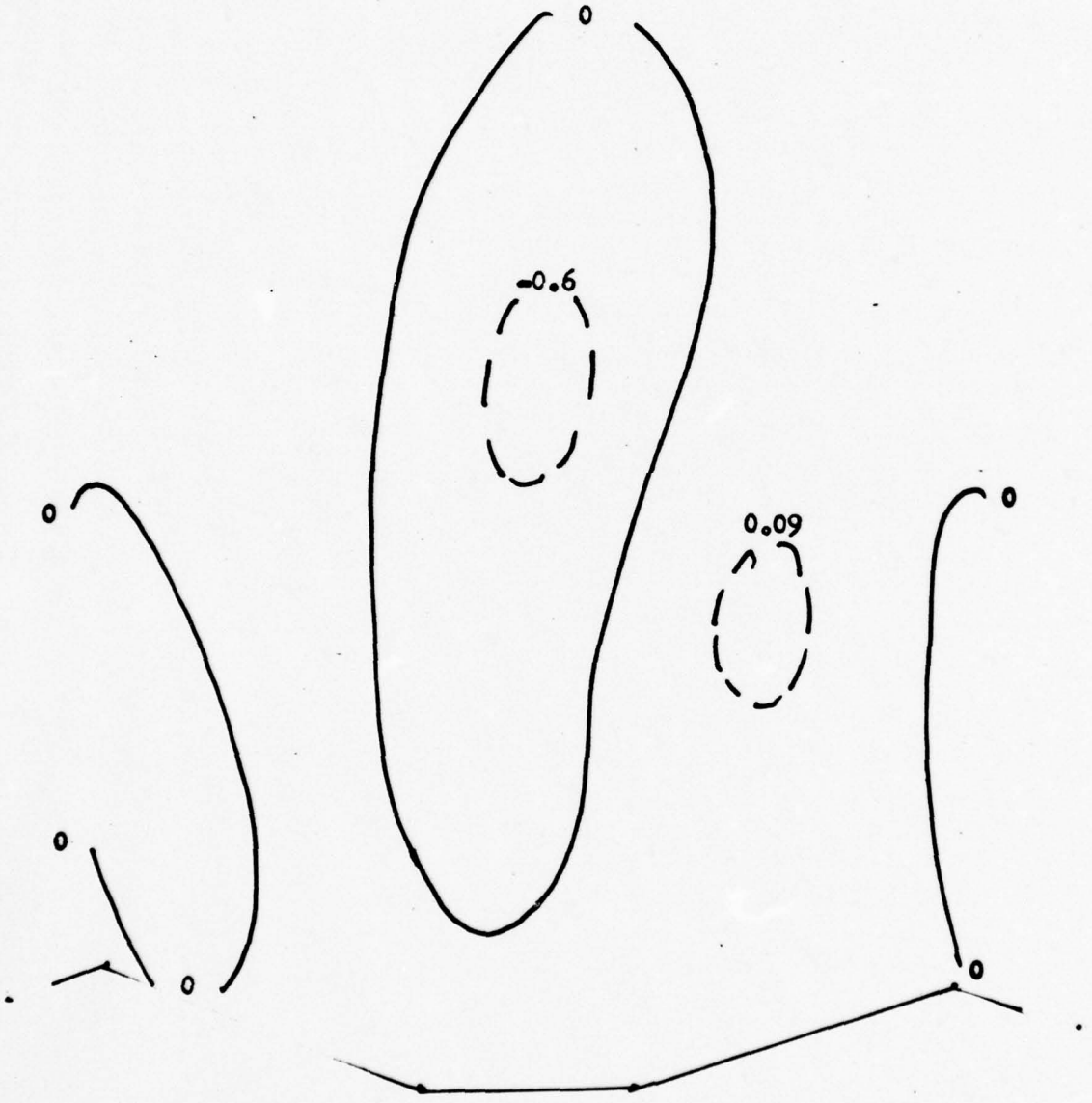
0
-0.6
0
0.09
0
0
0
0
70. W

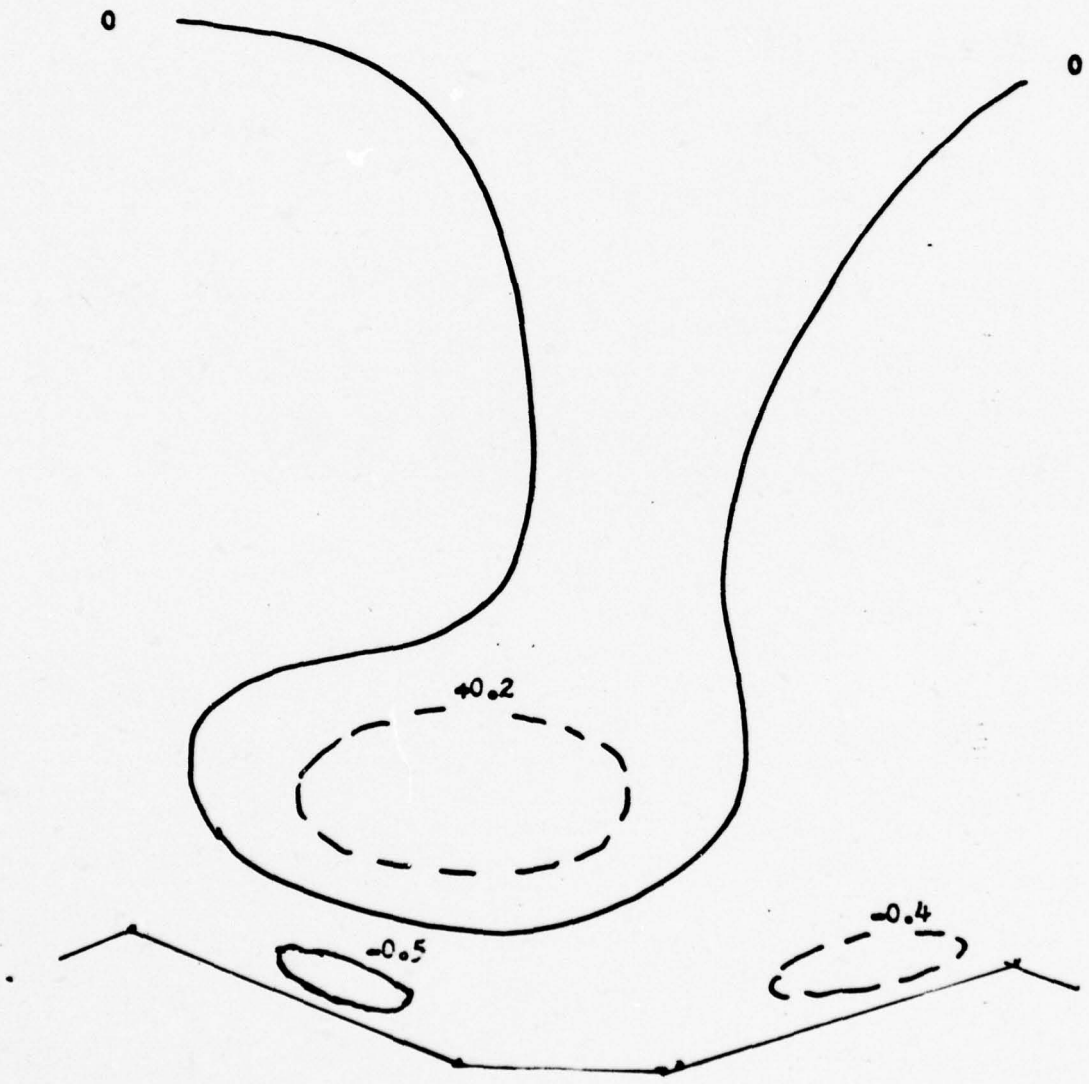

7d. T

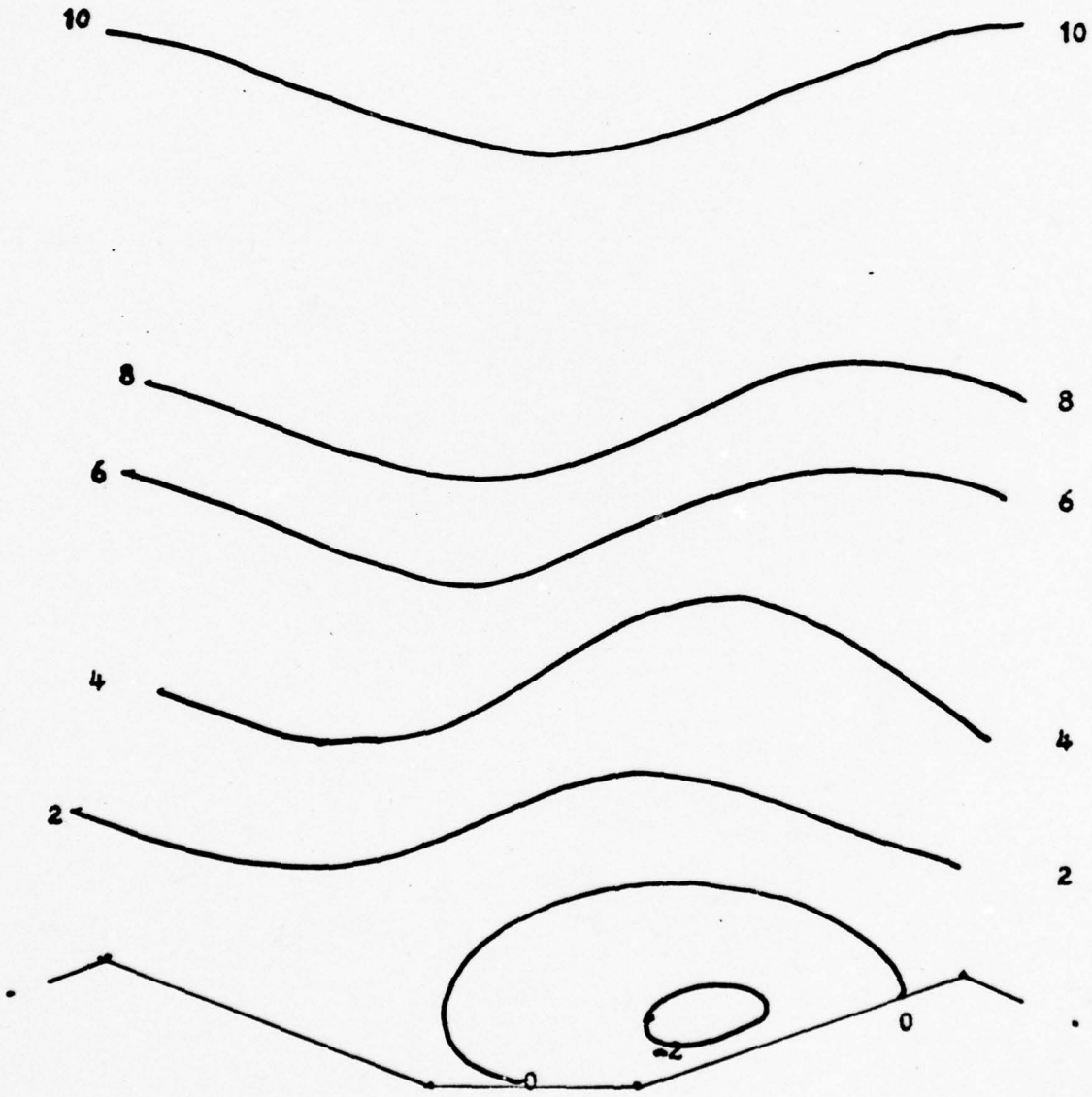

Fig. 8. Isopleths of wind components and temperature deviations for Run #6 at J=7 (a to d) a. u b. v c. w d. T

8a. u

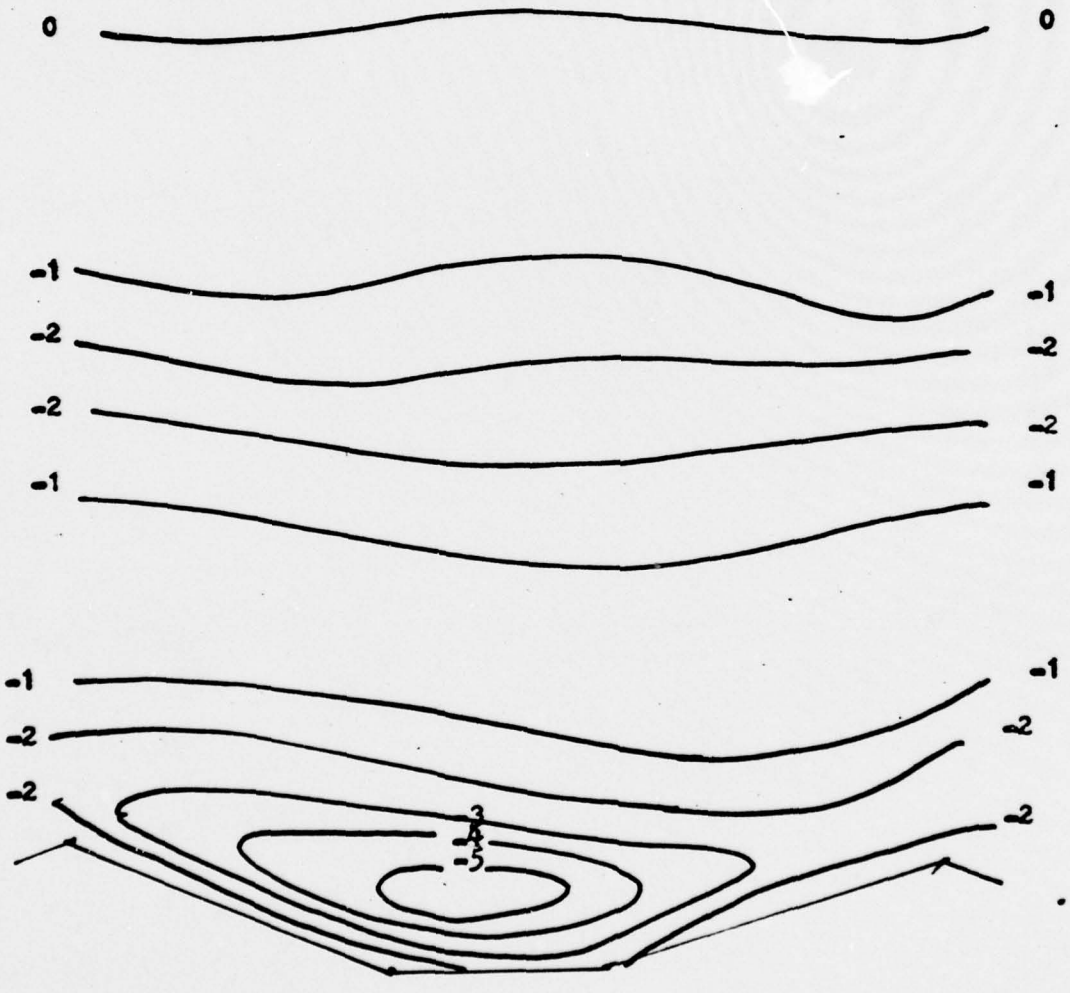

8b. v

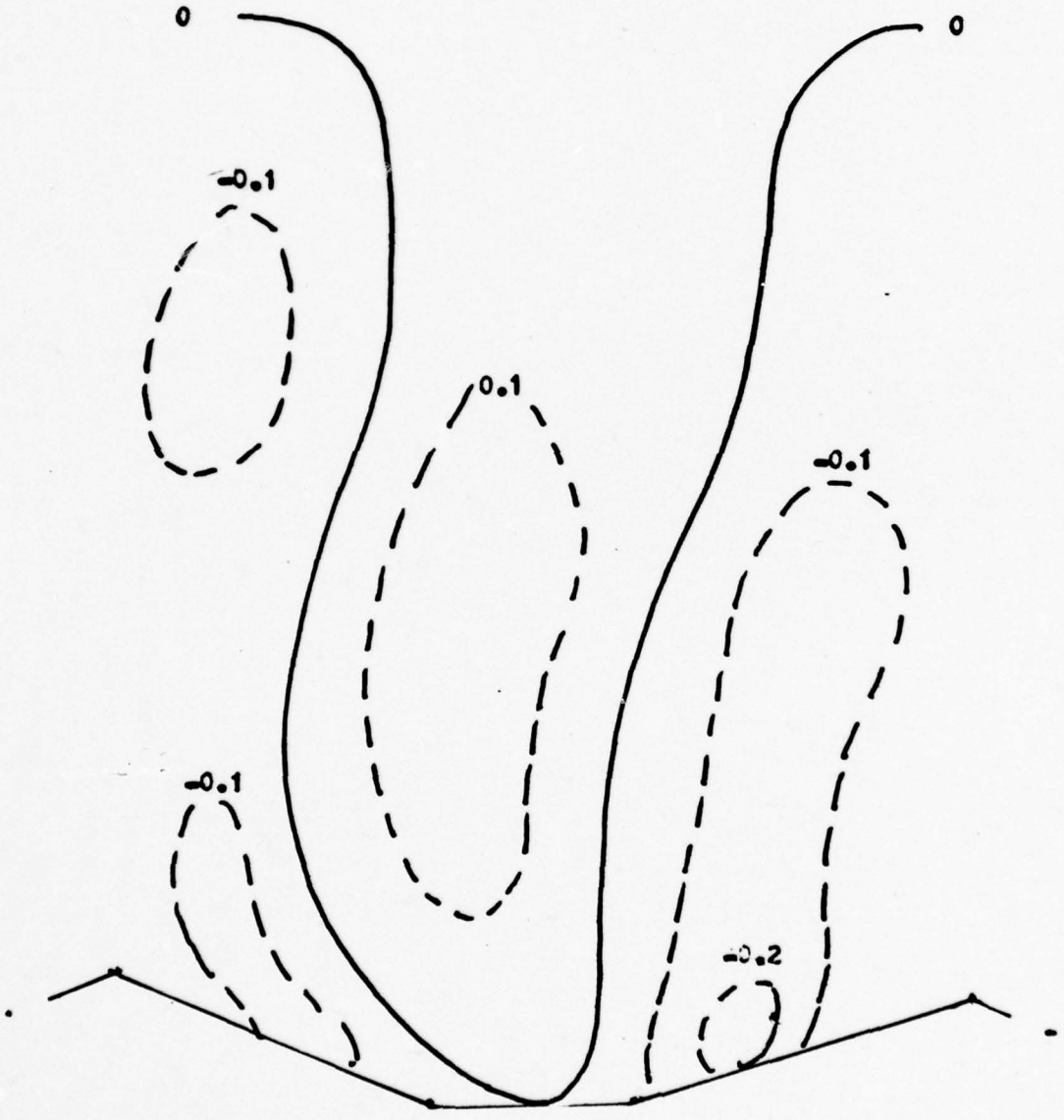

8c. w

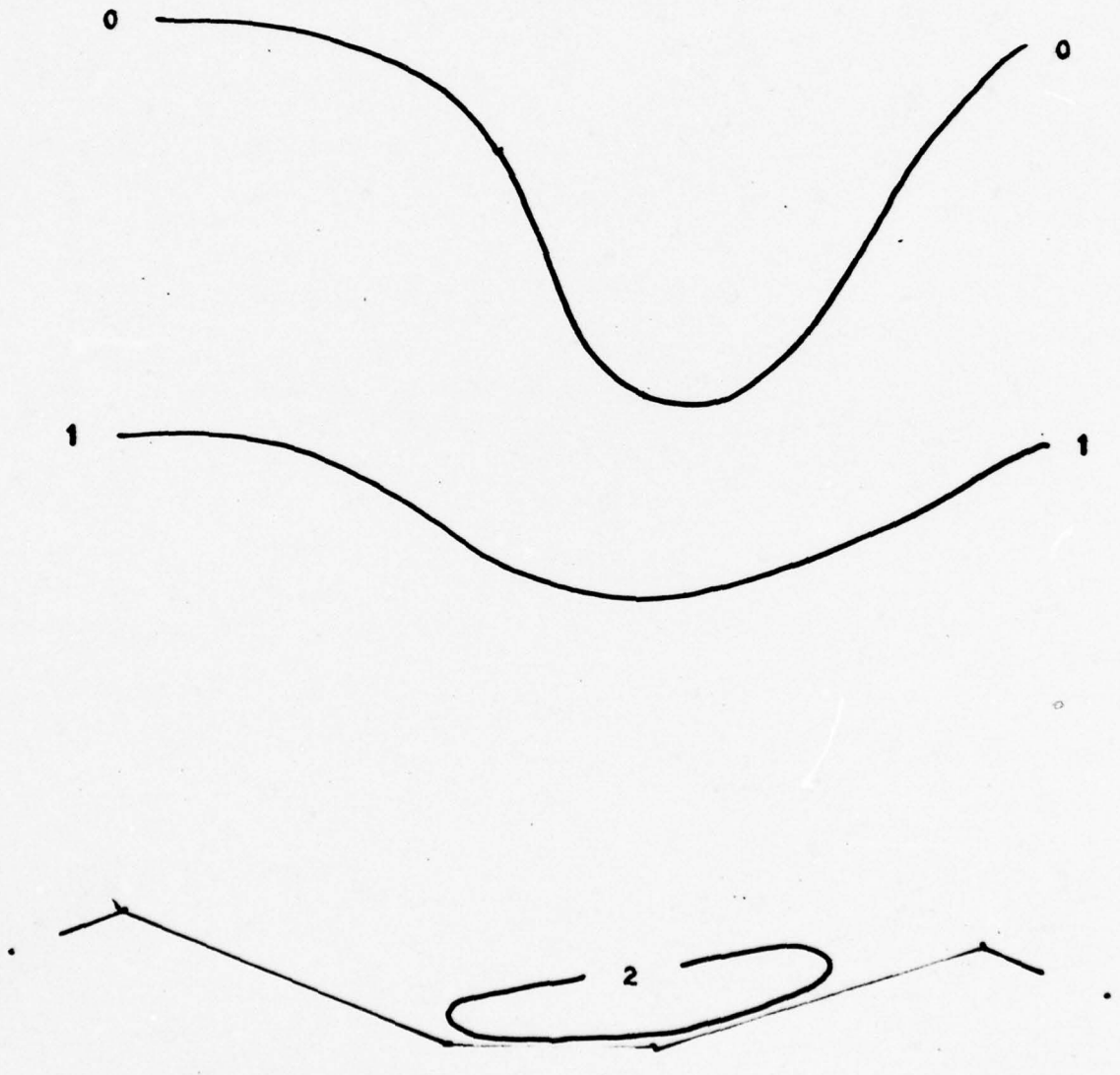

8d. T

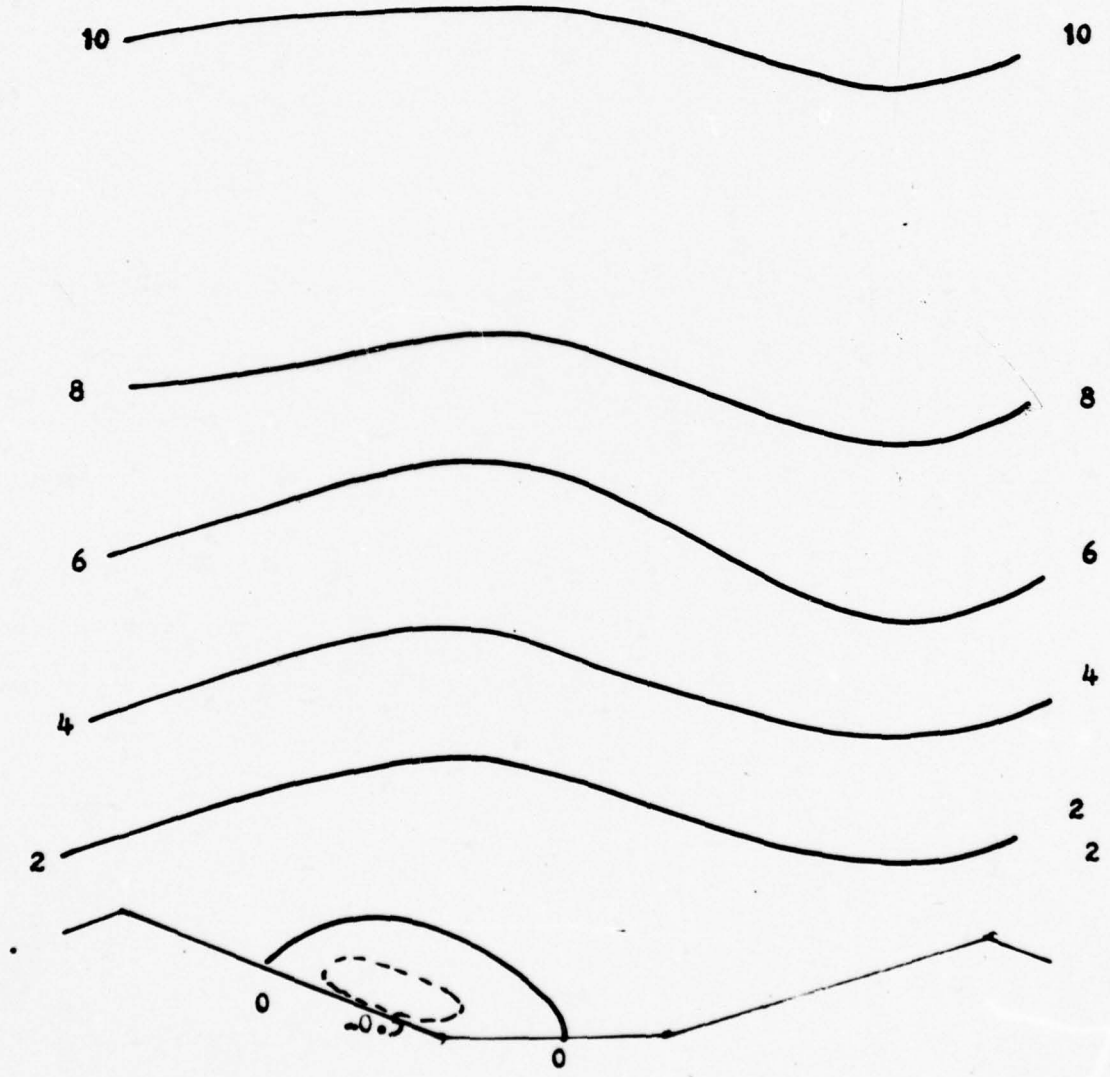

Fig. 9. Isopleths of wind components and temperature deviations for Run #7 at J=7 (a to d) a. u b. v c. w d. T

9a. u

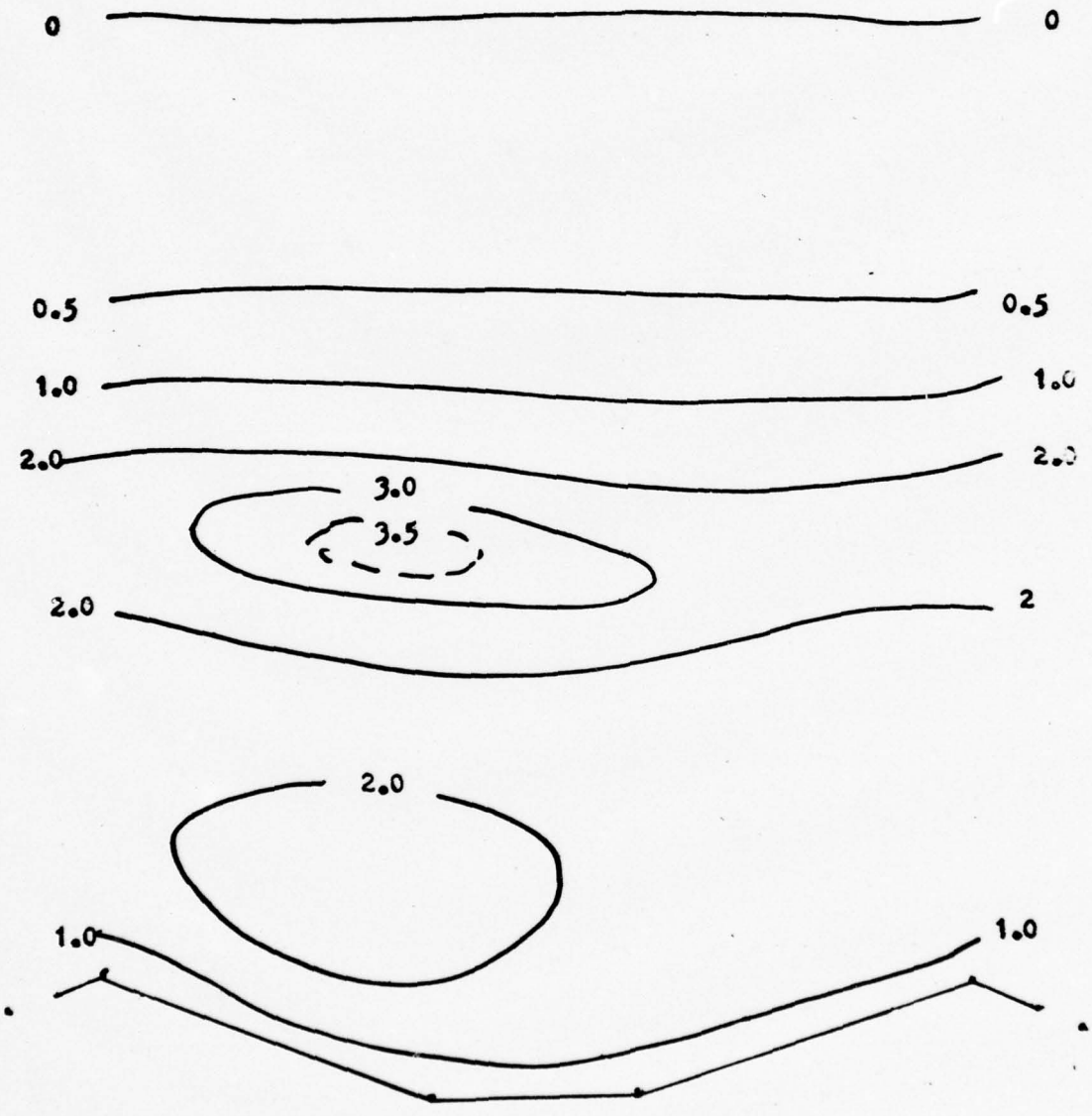

9b. u

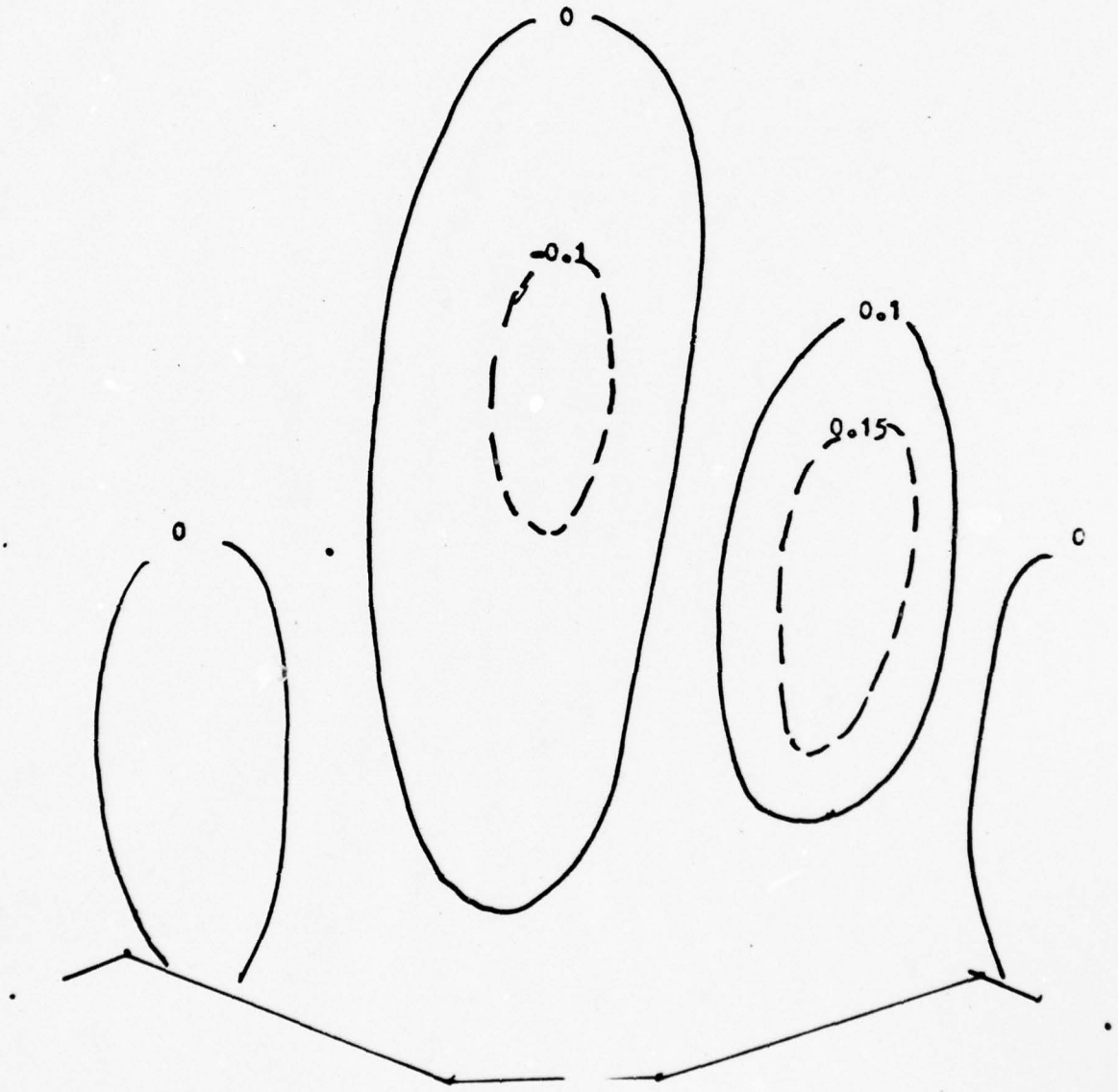

90. w

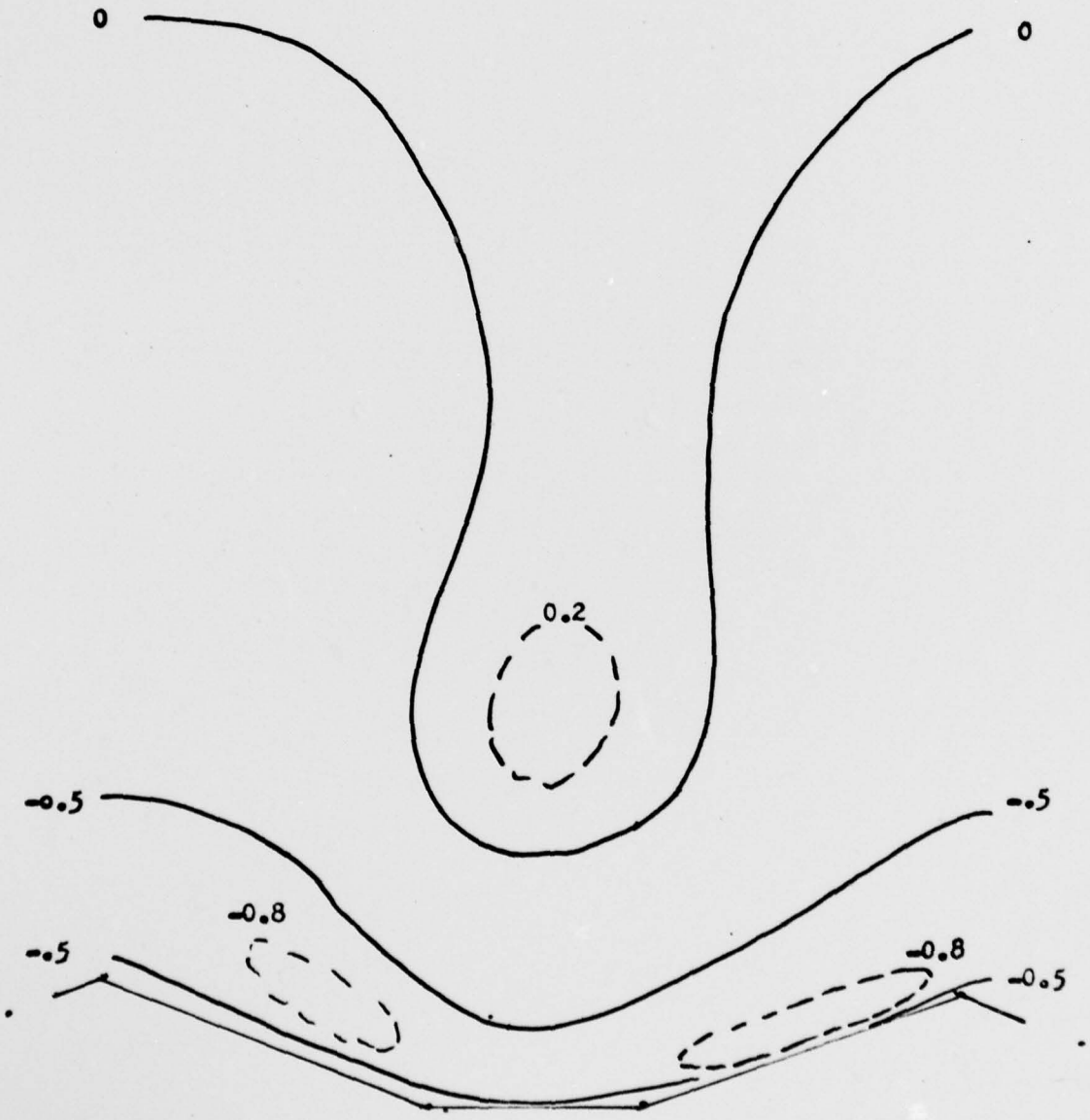

9d. T

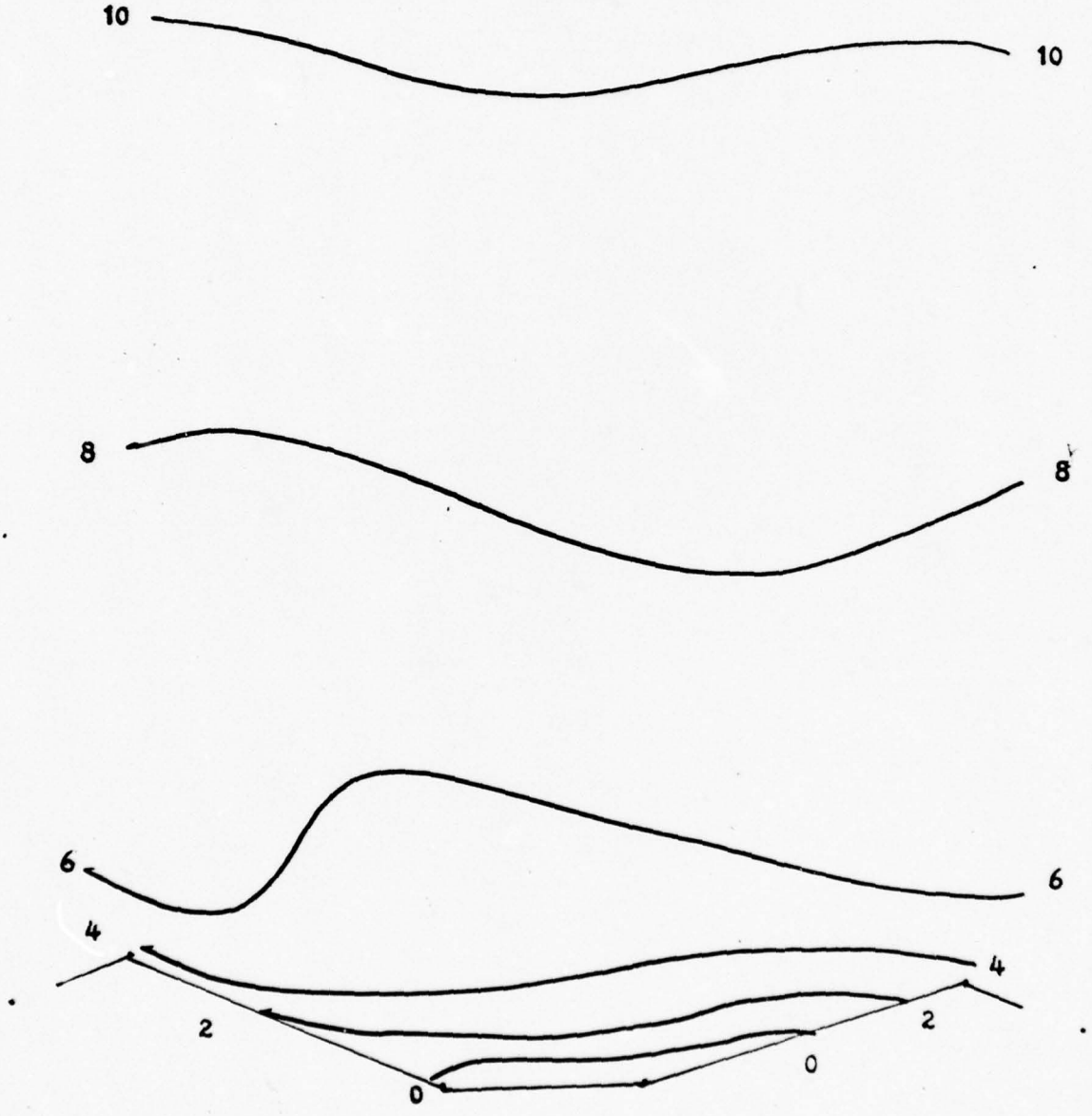

Fig.10. Isopleths of wind components and temperature deviations for Run #8 at J=7 for t=10100sec (a to d) a.u b.v c.w d.T and for t= 20100 sec (e to h)e. u f. v g. w h. T

10a. u

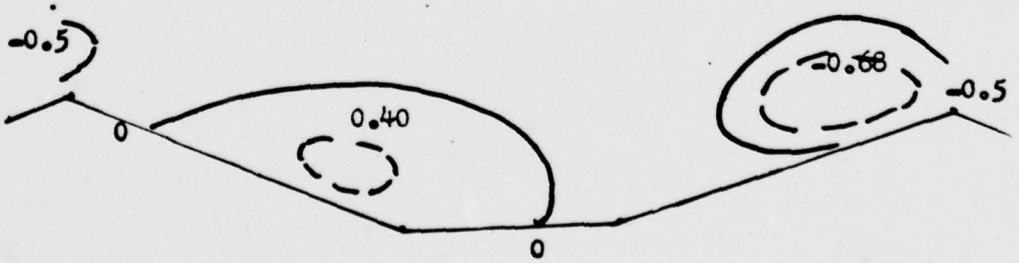

10b. ▼

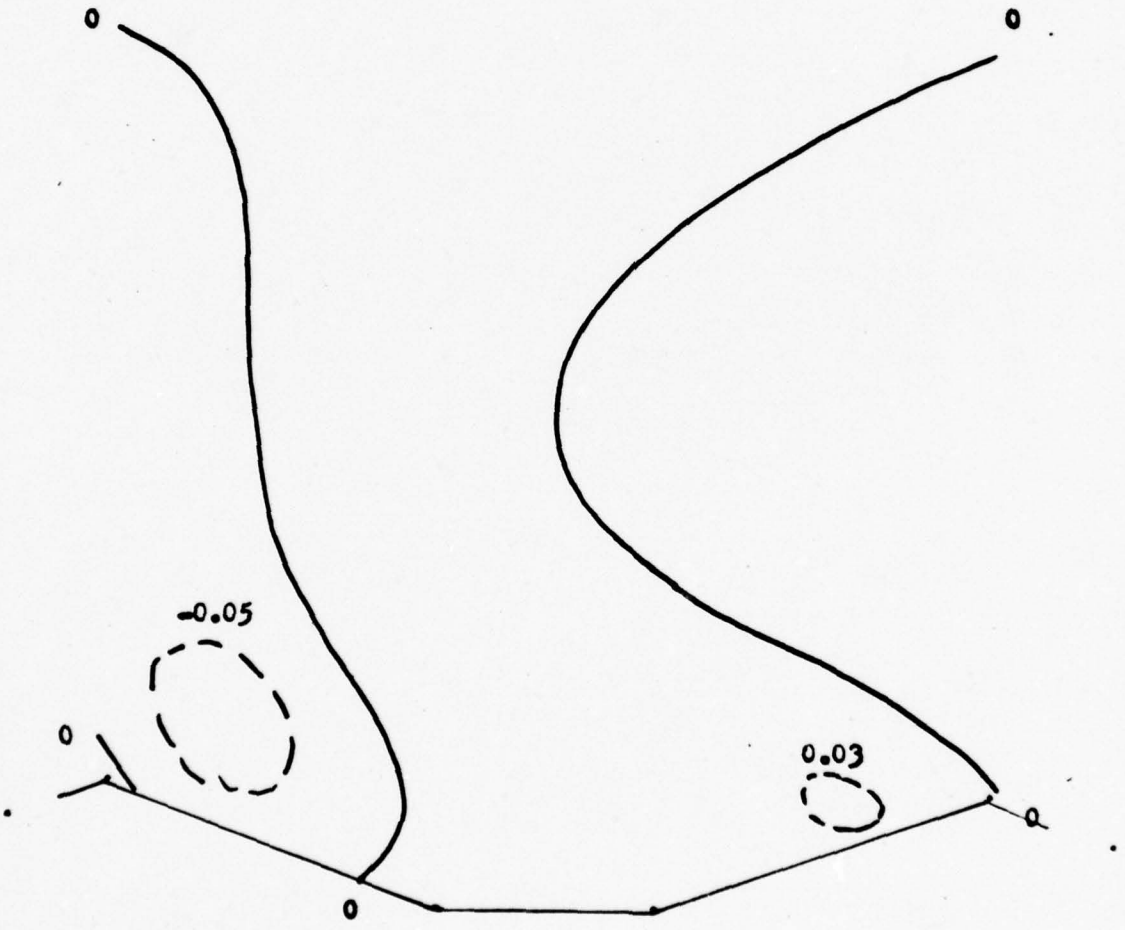
0
0
-0.05
0
0.03
0
0
10 a. w

10d. T

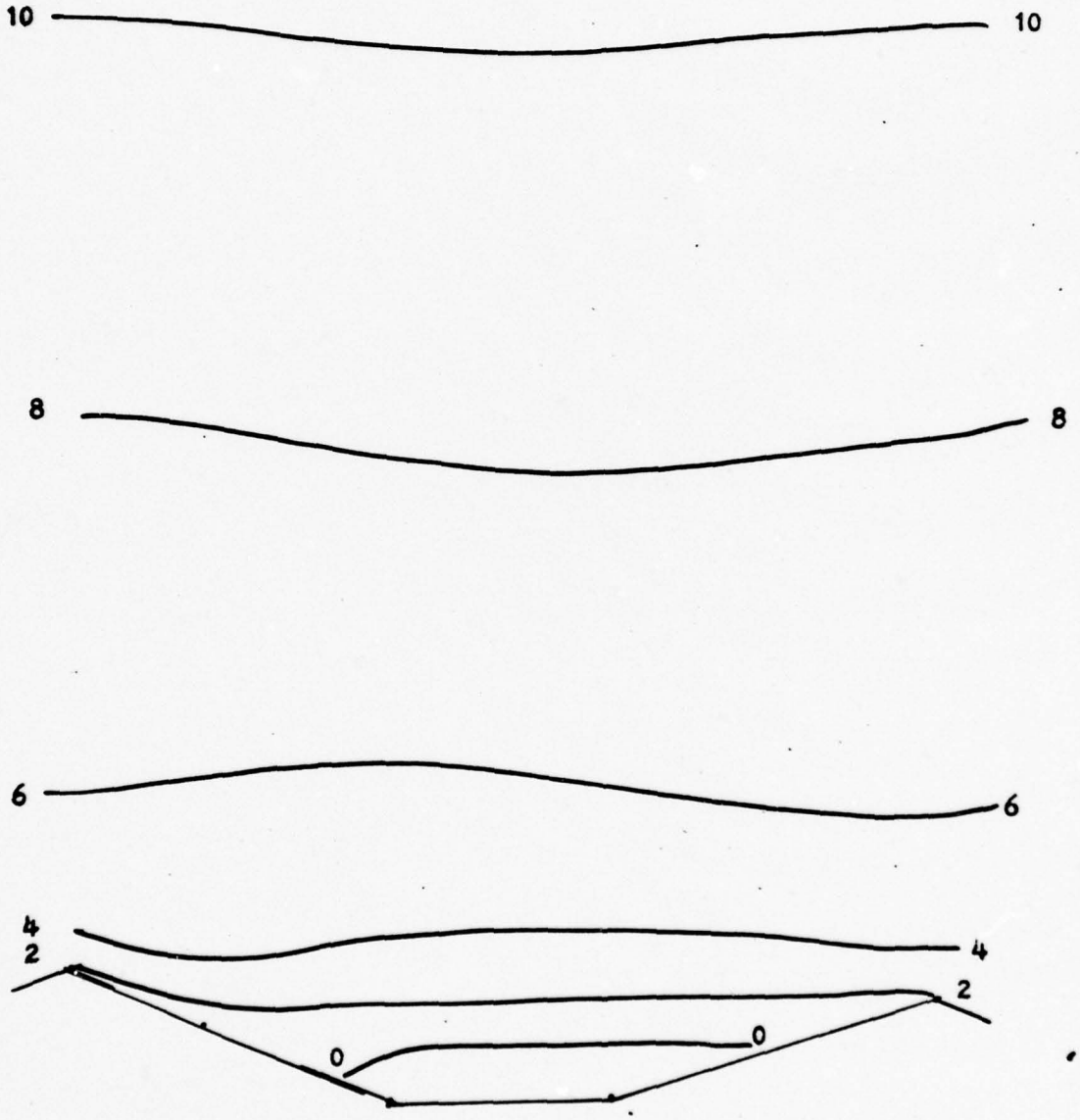

100. u

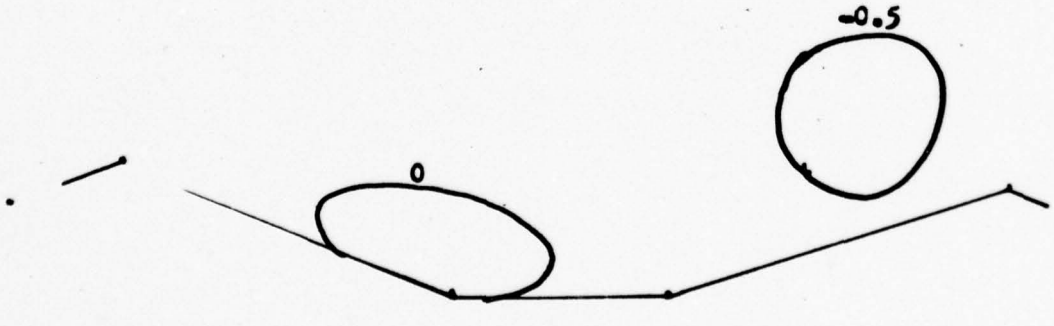

10f. 7

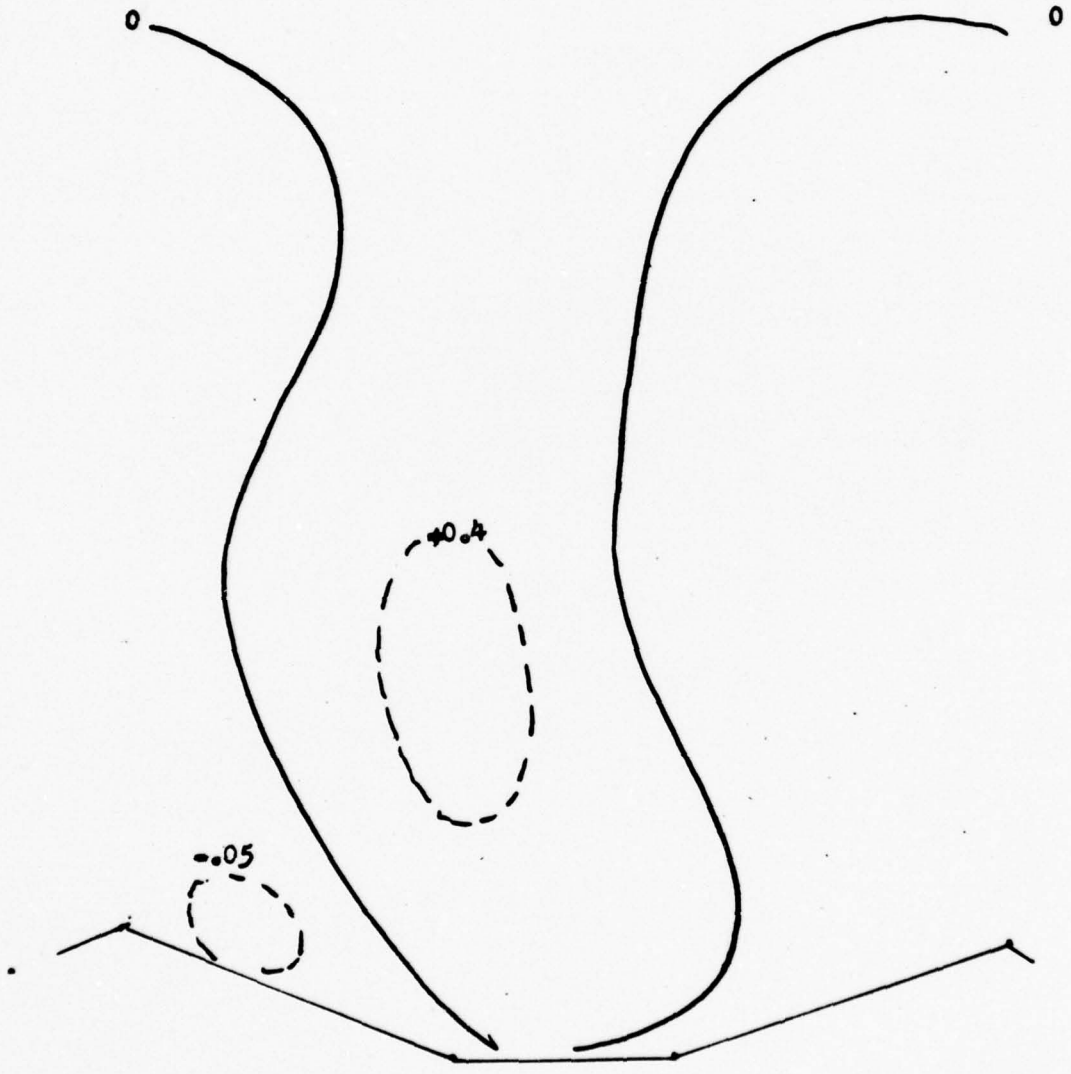

10g. w

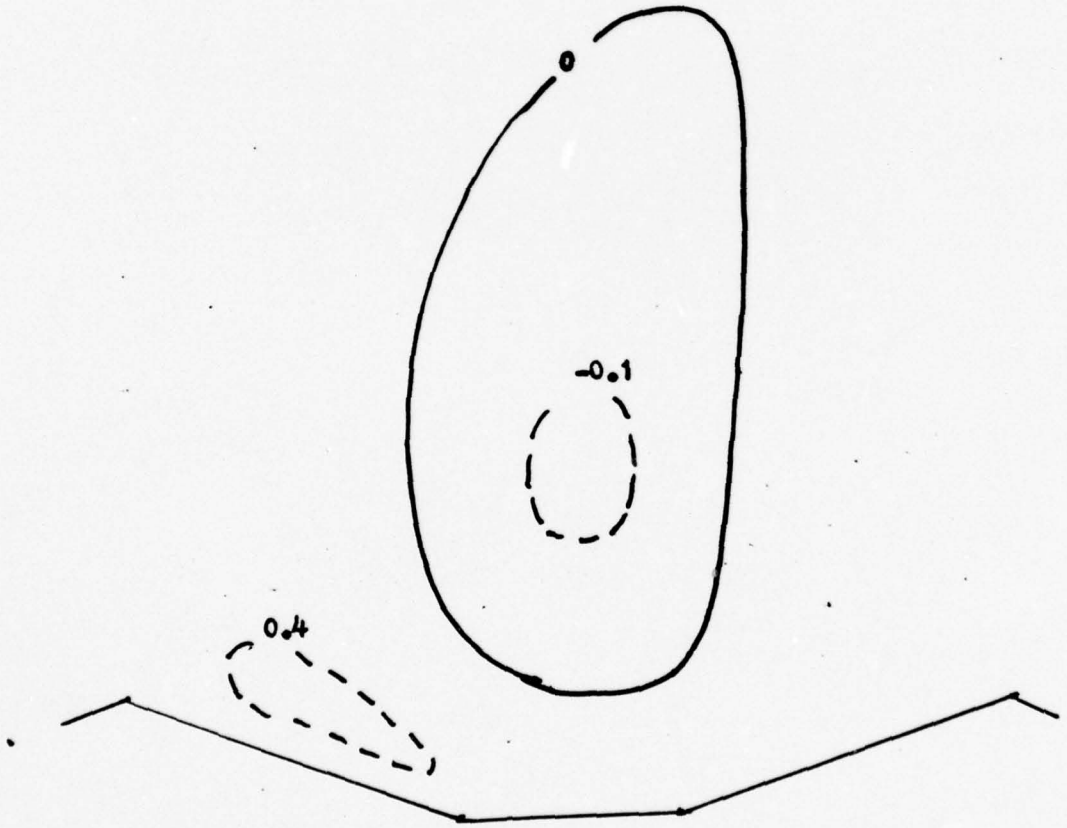

10h. T

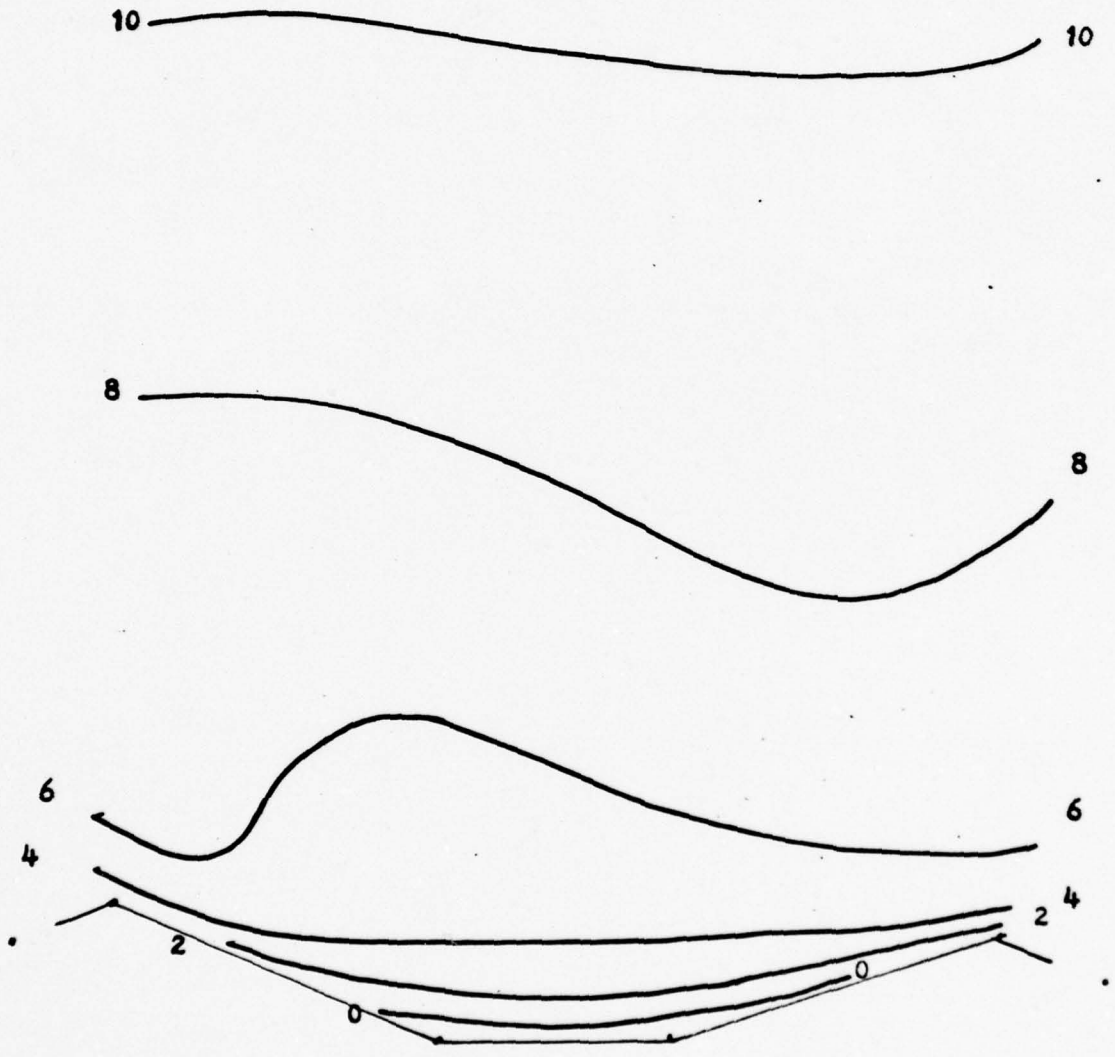

Fig.11. Isopleths of wind components and temperature deviations for Run #9 at J=7 for t=10100sec (a to d) a.u b.v c.w d.T and for t= 20100 sec (e to h)e. u f. v g. w h. T

11a. u

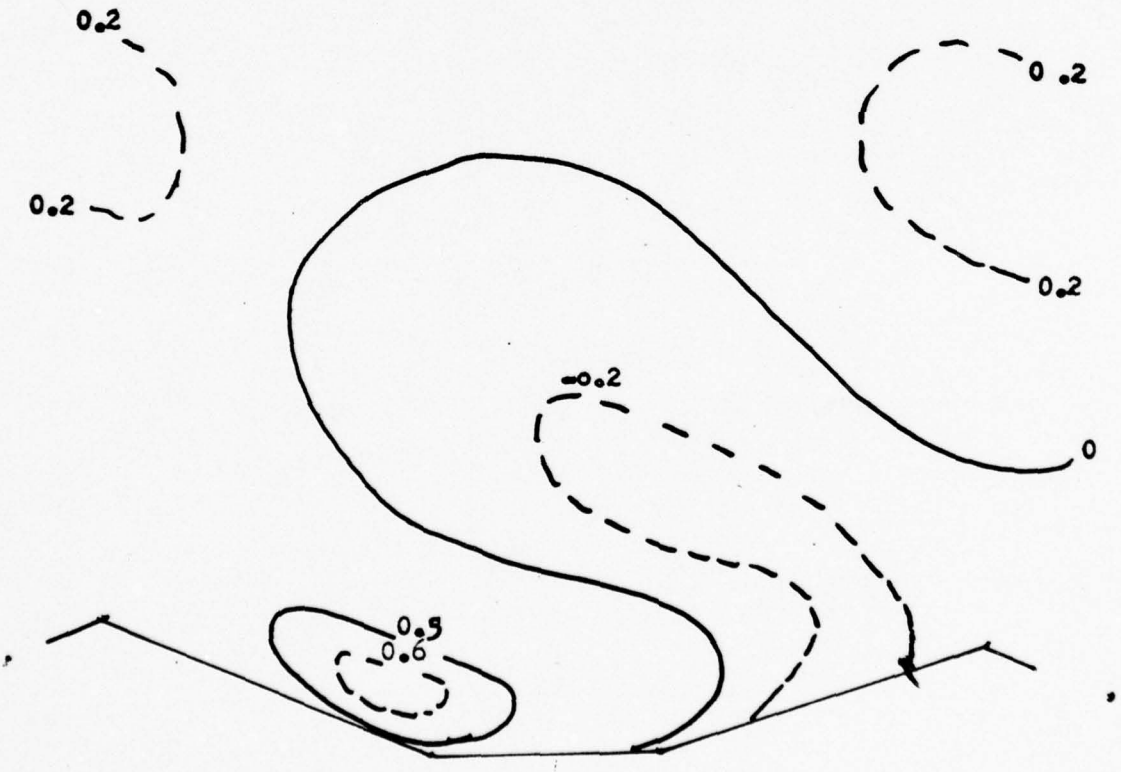

11b. ▼

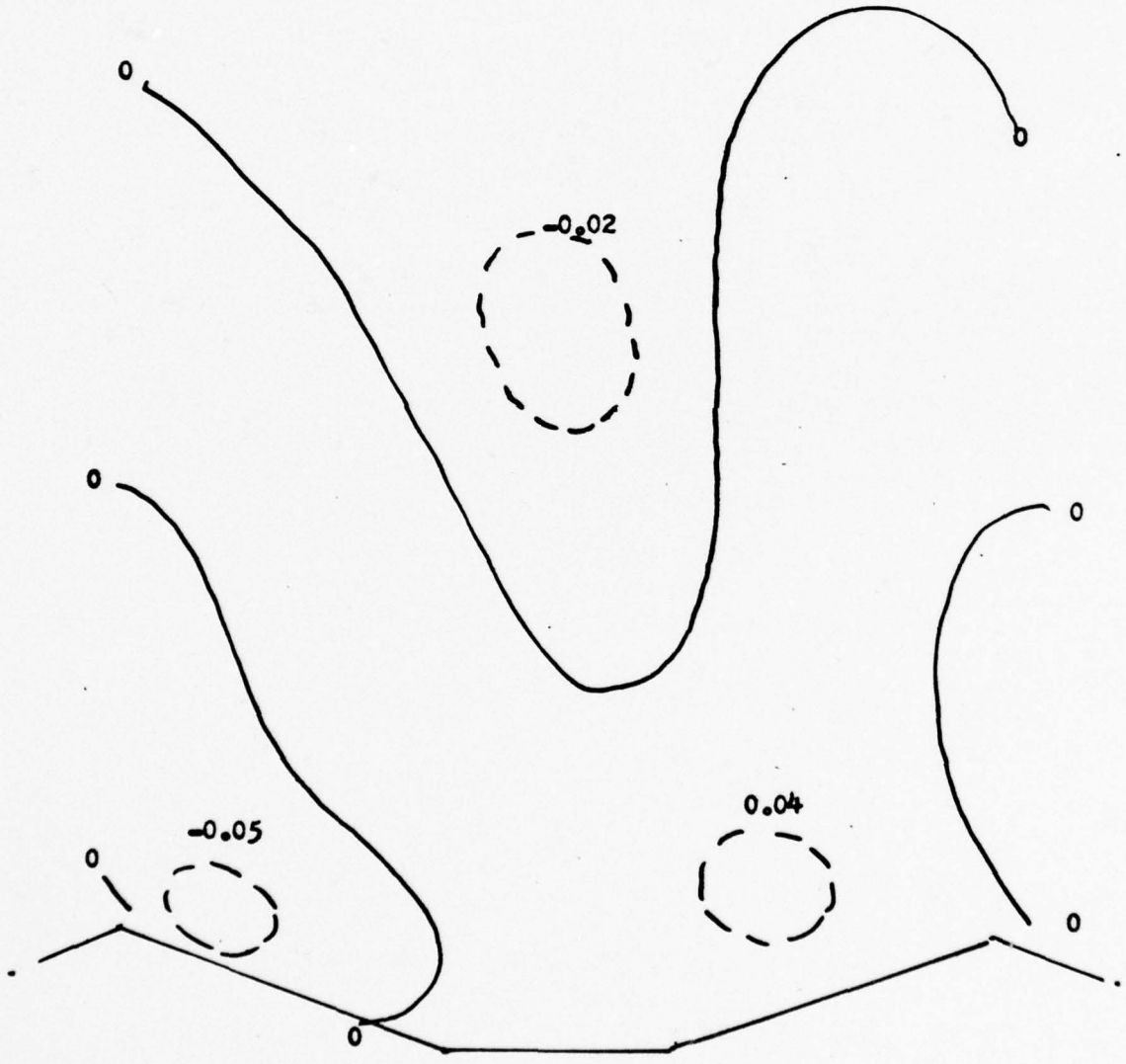

11c. w

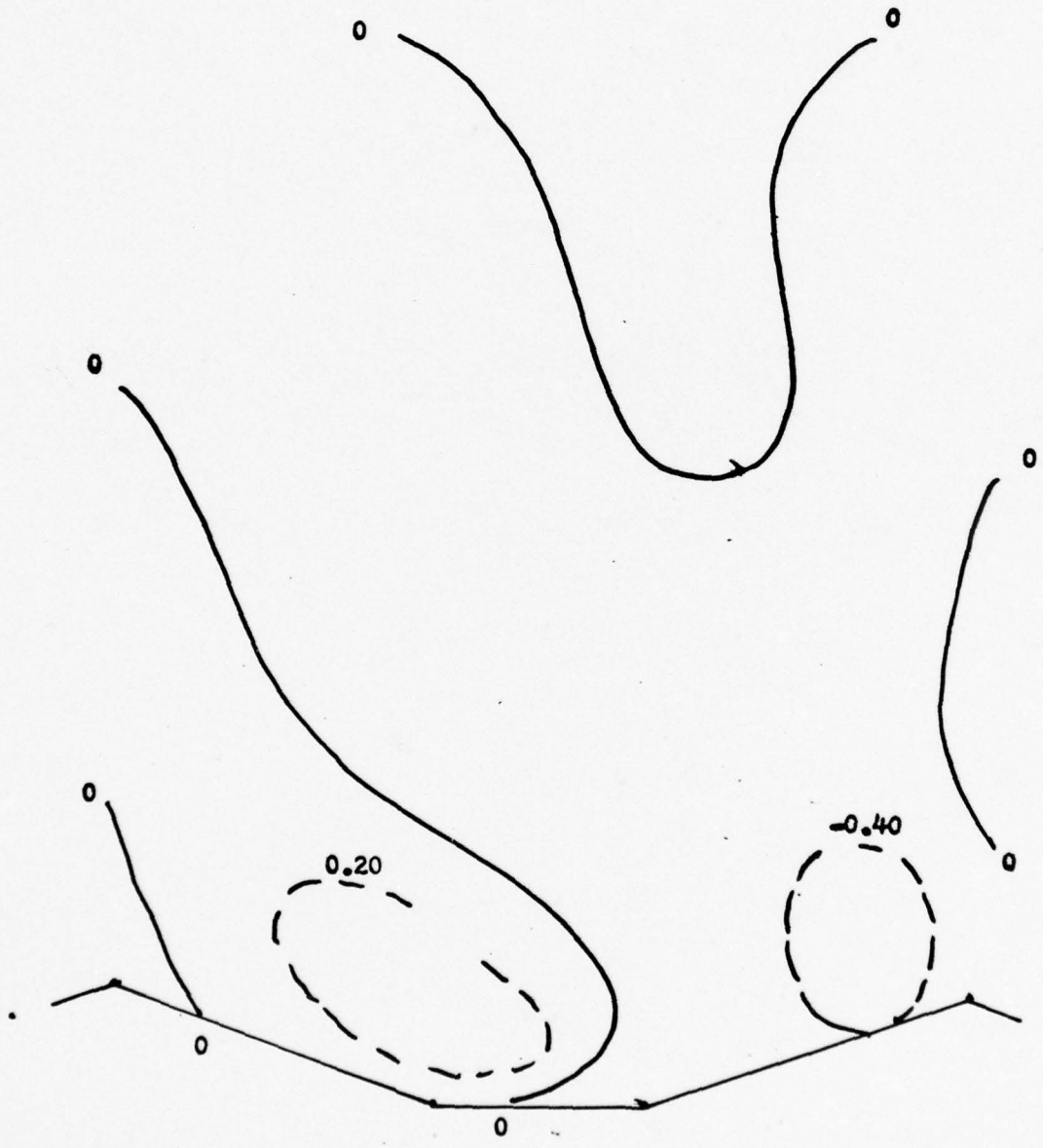

11d.T

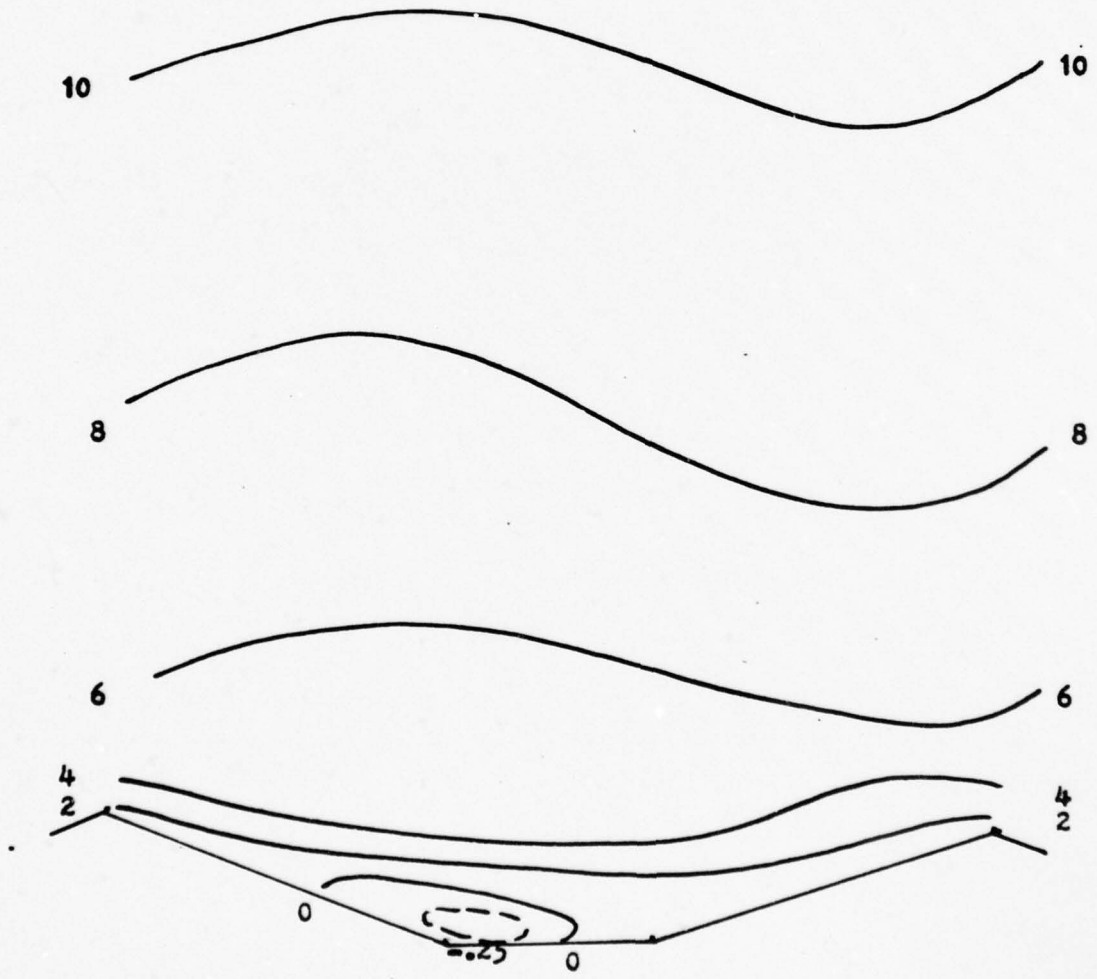

11e. u

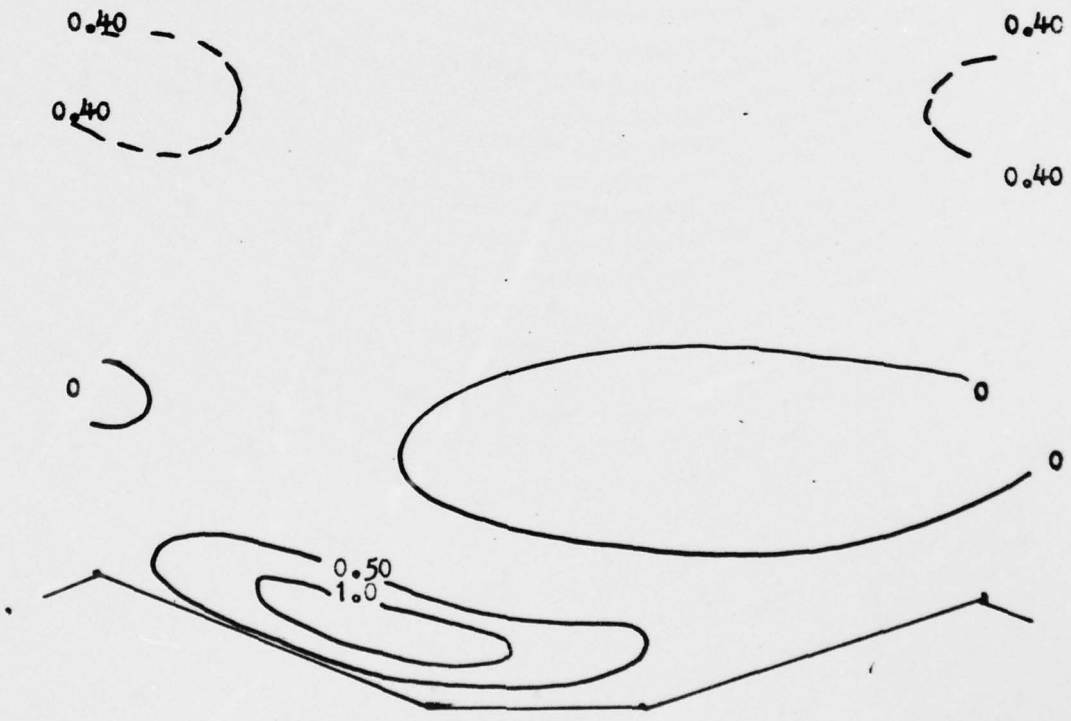

11f. v

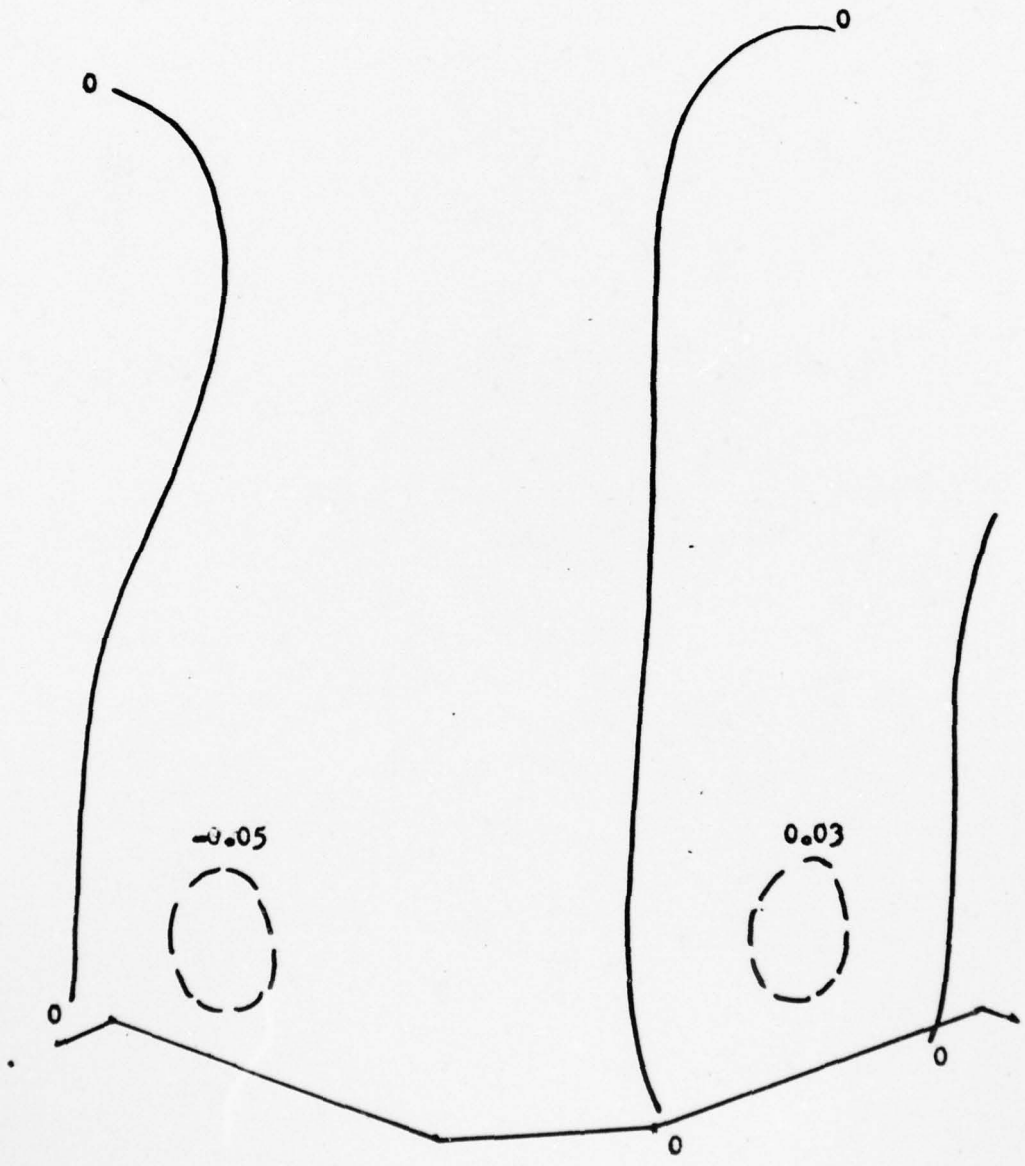

11g. w

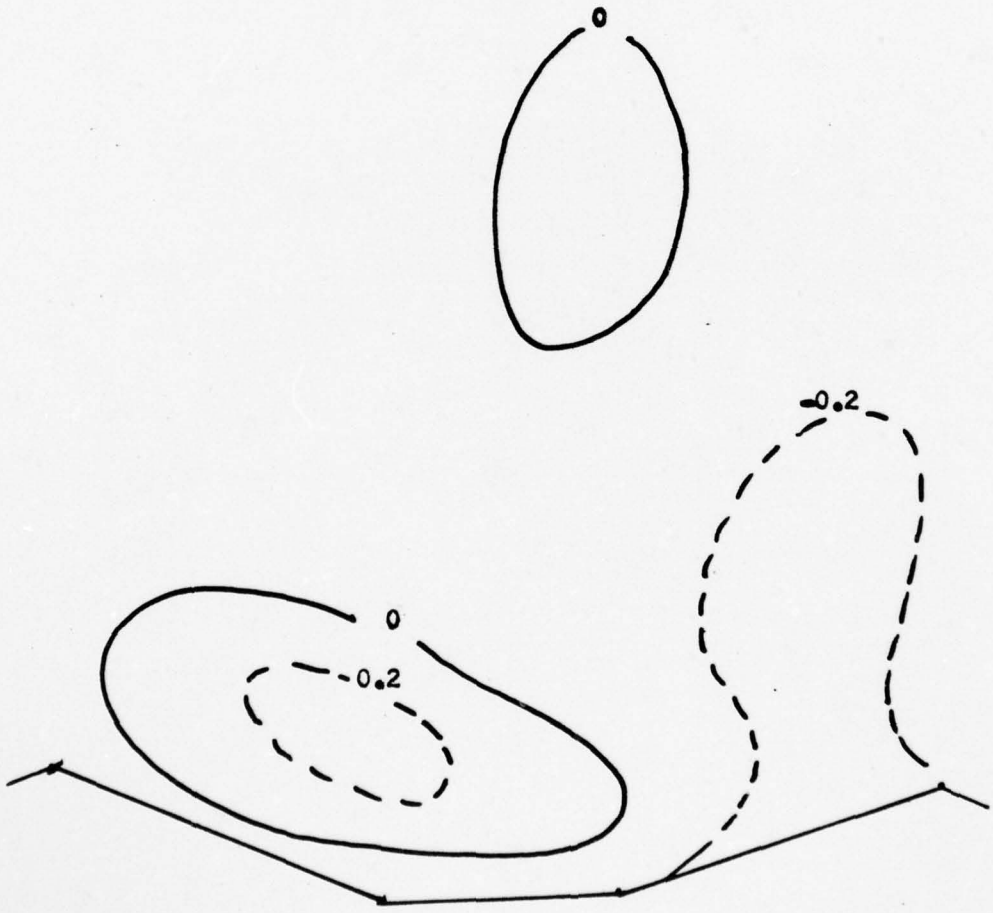

11h. T

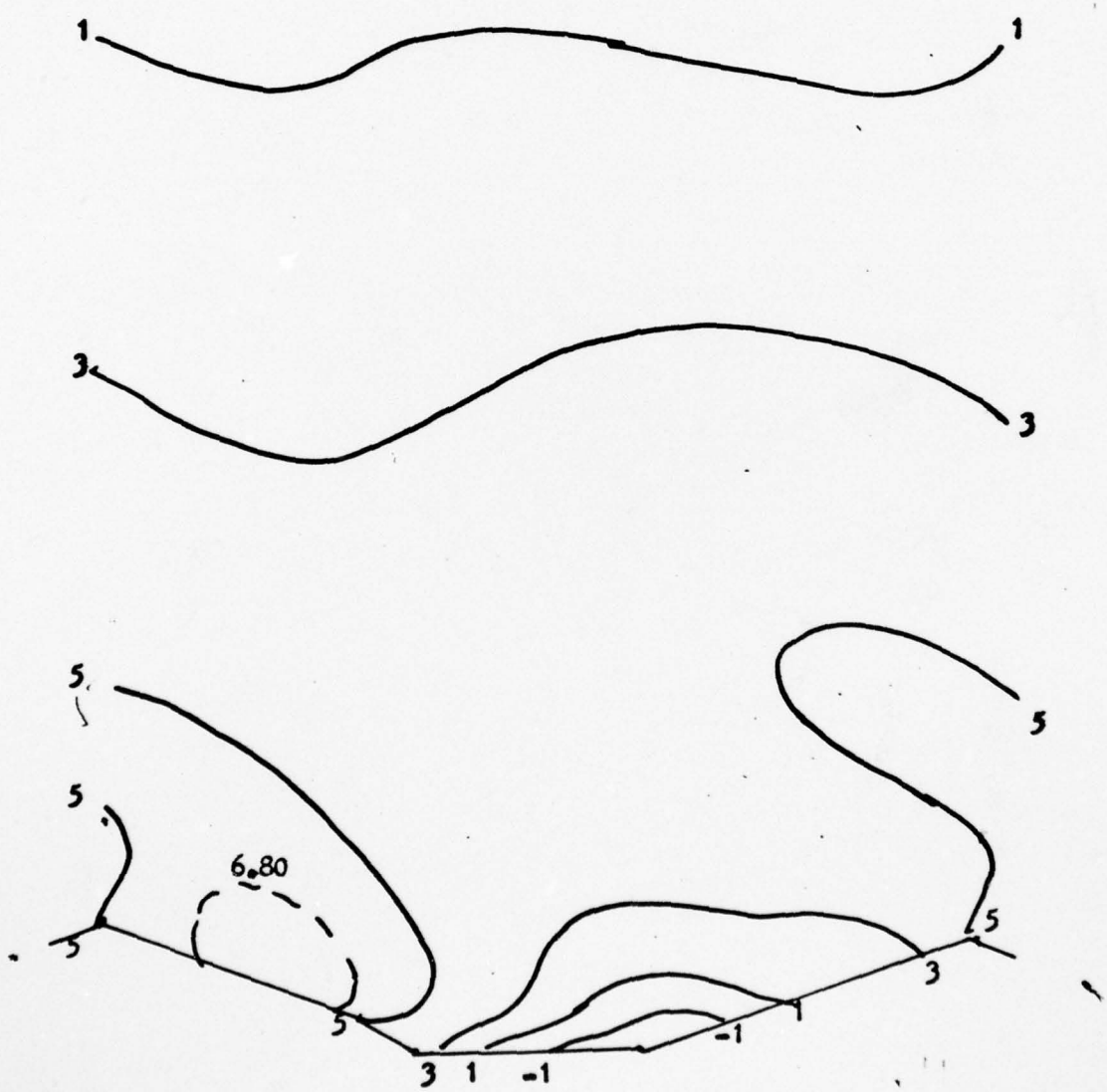

Fig.12. Isopleths of wind components and temperature deviations for Run #10 at J=7 for t=750 sec (a to d) a.u b.v c.w d.T

12a. u

12b. v

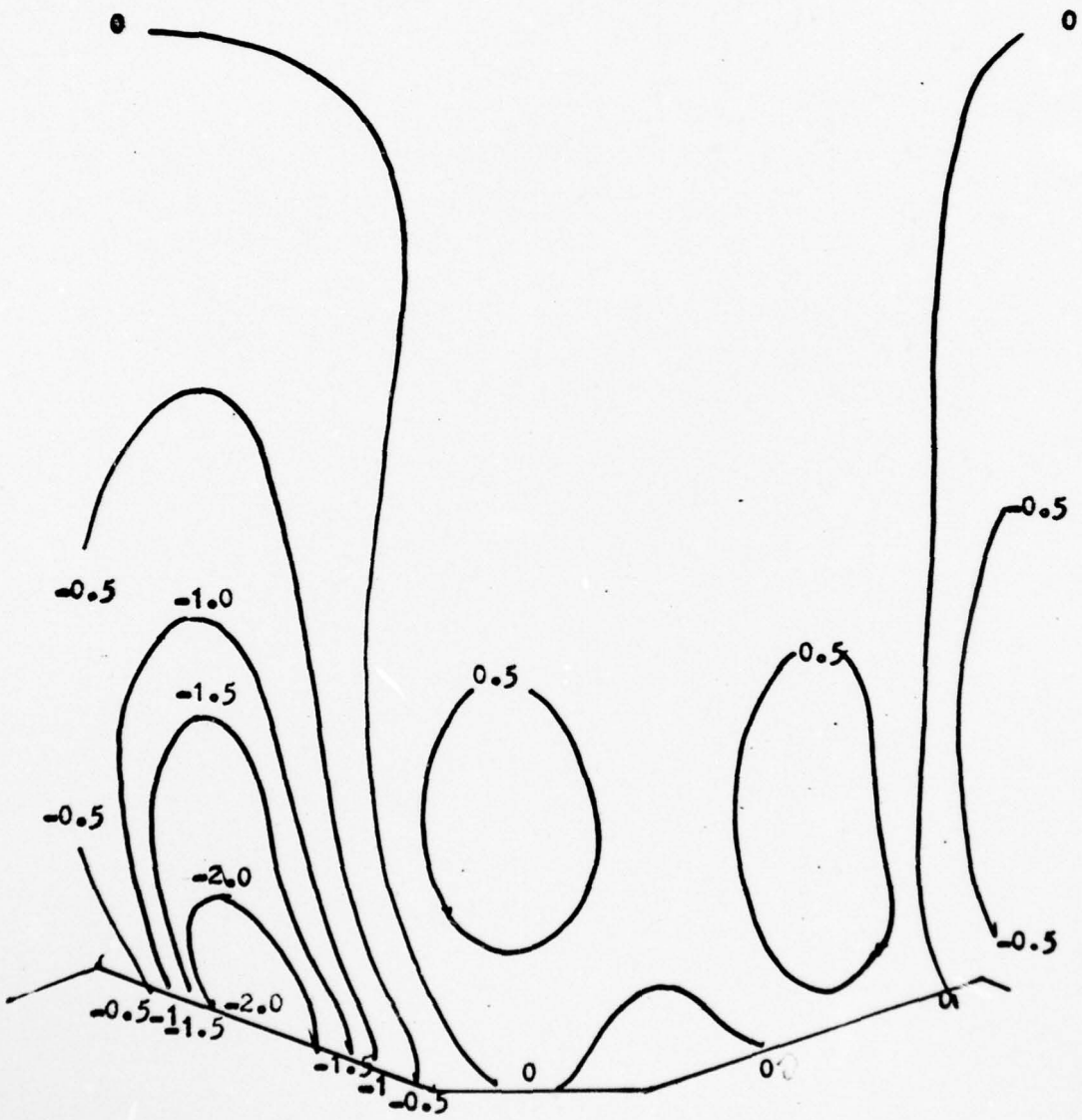

120. W

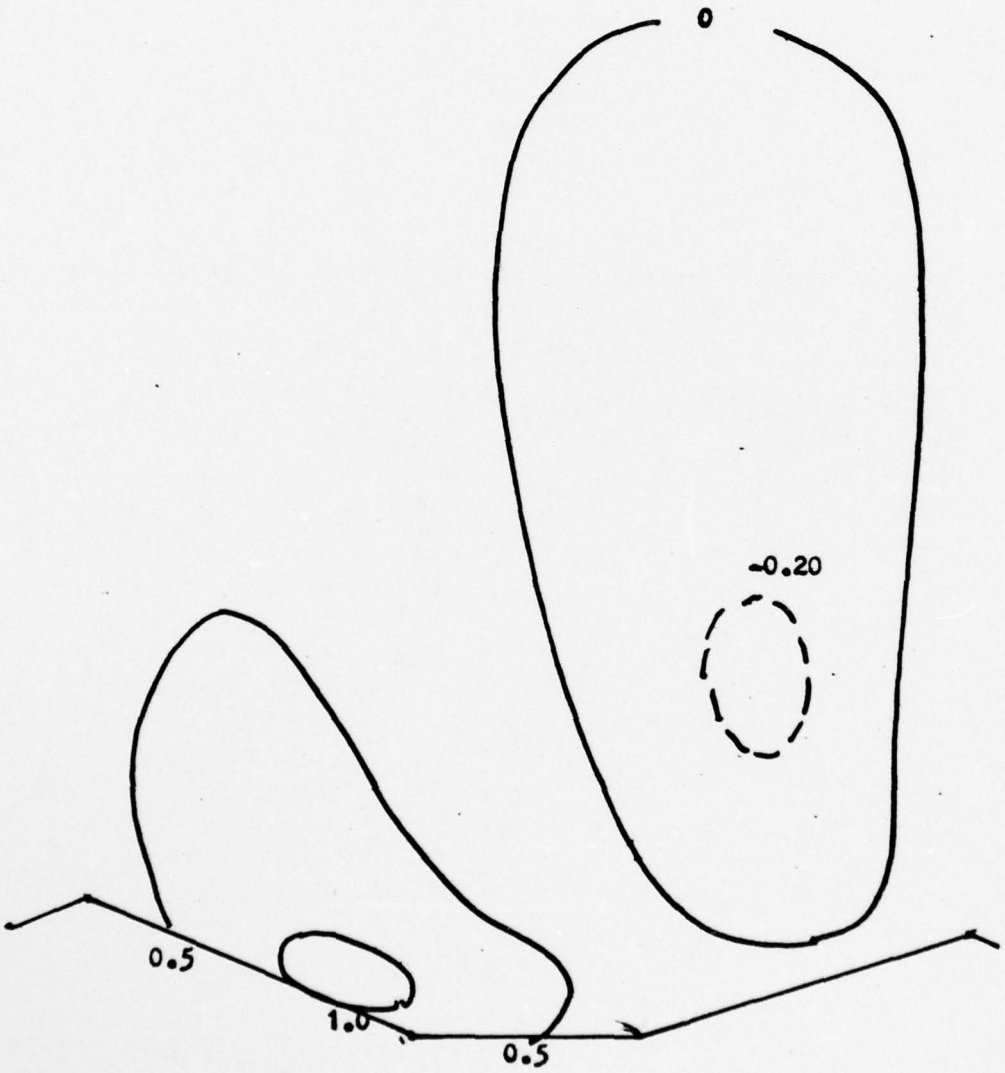

12d. T

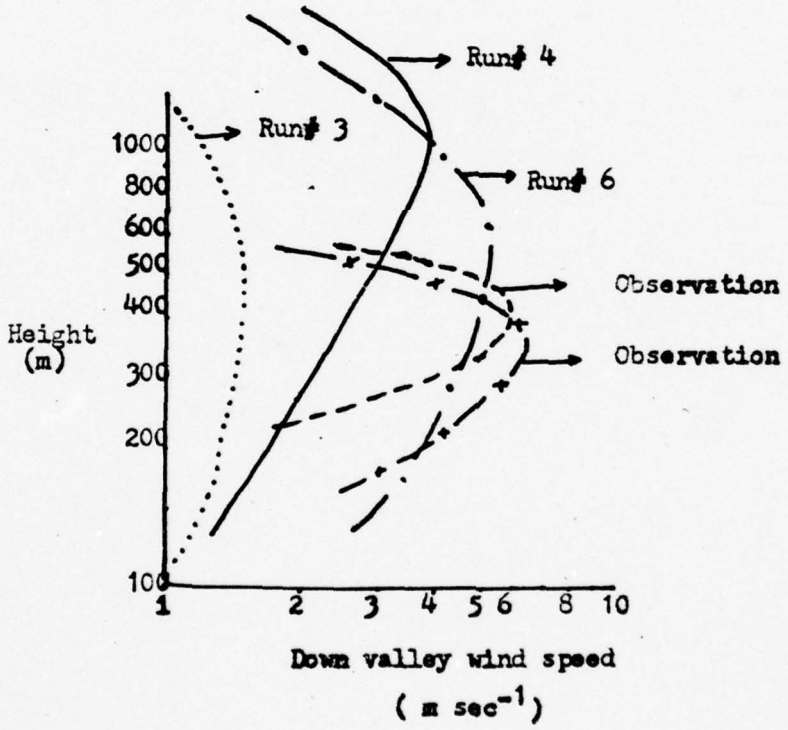

Fig.13. Comparison of computed down-valley wind profile with observational data.

Appendix A

A THEORETICAL STUDY OF GROUND SURFACE TEMPERATURE AND HEAT FLUX IN APPLICATION TO MOUNTAIN-VALLEY CIRCULATION

Wen Tang

Published in the Proceedings of the Joint Scientific Meeting on Mountain Meteorology and Biometeorology, AMS, SGBB, SSG, Interlaken, Switzerland, June 10-14, 1976

1. Introduction

The diurnal surface thermal condition has been shown to be an important controlling factor on daily circulation in the planetary boundary layer.

Recent investigations of mountain-valley circulation by Tang(1976), and by Tang and Peng (1974) with a numerical model, show that thermal boundary conditions have an essential influence on circulation in the boundary layer. The assumption on the thermal boundary condition for their investigation is a prescribed surface temperature or heat flux at the ground surface. Since the mountain-valley terrain consists of uneven surfaces such as slopes, ridges, and valleys, the amount of solar and long-wave radiation over these surfaces is different from that on a horizontal plane. Incorporation of a variable surface heat flux in the study would make it a very complex problem. A most realistic mountain-valley circulation model considering this temporally and spatially variable surface heat flux is yet to be developed. The purpose of this study is to derive an analytical expression of the ground surface temperature and heat flux, at each small time step, in terms of solar and long-wave radiation, geometrical factors of the terrain, and initial surface temperature. The result can be utilized for a numerical experiment of atmospheric motion and temperature over a simple mountain-valley terrain.

In two previous studies Ruh (1959, 1964) invesitgated the influence of a sloping surface on radiation. The present study develops a method for obtaining surface temperature by solving the equation of

1. Introduction

The diurnal surface thermal condition has been shown to be an important controlling factor on daily circulation in the planetary boundary layer.

Recent investigations of mountain-valley circulation by Tang(1976), and by Tang and Peng (1974) with a numerical model, show that thermal boundary conditions have an essential influence on circulation in the boundary layer. The assumption on the thermal boundary condition for their investigation is a prescribed surface temperature or heat flux at the ground surface. Since the mountain-valley terrain consists of uneven surfaces such as slopes, ridges, and valleys, the amount of solar and long-wave radiation over these surfaces is different from that on a horizontal plane. Incorporation of a variable surface heat flux in the study would make it a very complex problem. A most realistic mountain-valley circulation model considering this temporally and spatially variable surface heat flux is yet to be developed. The purpose of this study is to derive an analytical expression of the ground surface temperature and heat flux, at each small time step, in terms of solar and long-wave radiation, geometrical factors of the terrain, and initial surface temperature. The result can be utilized for a numerical experiment of atmospheric motion and temperature over a simple mountain-valley terrain.

In two previous studies Ruh (1959, 1964) invesitgated the influence of a sloping surface on radiation. The present study develops a method for obtaining surface temperature by solving the equation of

heat conduction of the soil and the energy balance equation at the ground, by including the terrain influence on radiation . The heat balance condition at the ground surface over a mountain-valley terrain at different locations across the valley is conceivably not the same. As a consequence the ground surface temperature will vary from place to place, at least in the daytime. The heat flux from the ground surface will interact with atmospheric motion and temperature to develop a very complicated dynamic system. Our ultimate goal is to solve this complete system numerically for mountain-valley circulation. However, our immediate interest is the formulation of the ground surface temperature of a typical valley terrain.

2. Solar radiation on the sloping surface

For an undulating mountain-valley terrain as shown in Fig. 1, the mountain ridge on the east side of a north-south valley will cast its shadow on the west side of the valley (Fig. 1). The solar radiation reached on the slope may be written as

$$S = S_o \cos i \quad , \tag{1}$$

where S_o = solar constant

i = the acute angle between the sun's rays and the normal to the slope $\vec{n}$,

Then $\cos i$ can be written as

$$\cos i = \cos\alpha \sin h + \sin\alpha \cos h \cos\psi \, , \tag{2}$$

where α = the angle of inclination of the slope

h = the elevation angle

$\psi = \psi_o - \psi_n$ ($\psi < 0$, if measured counter-clockwise from the south; $\psi > 0$, if measured clockwise from the south)

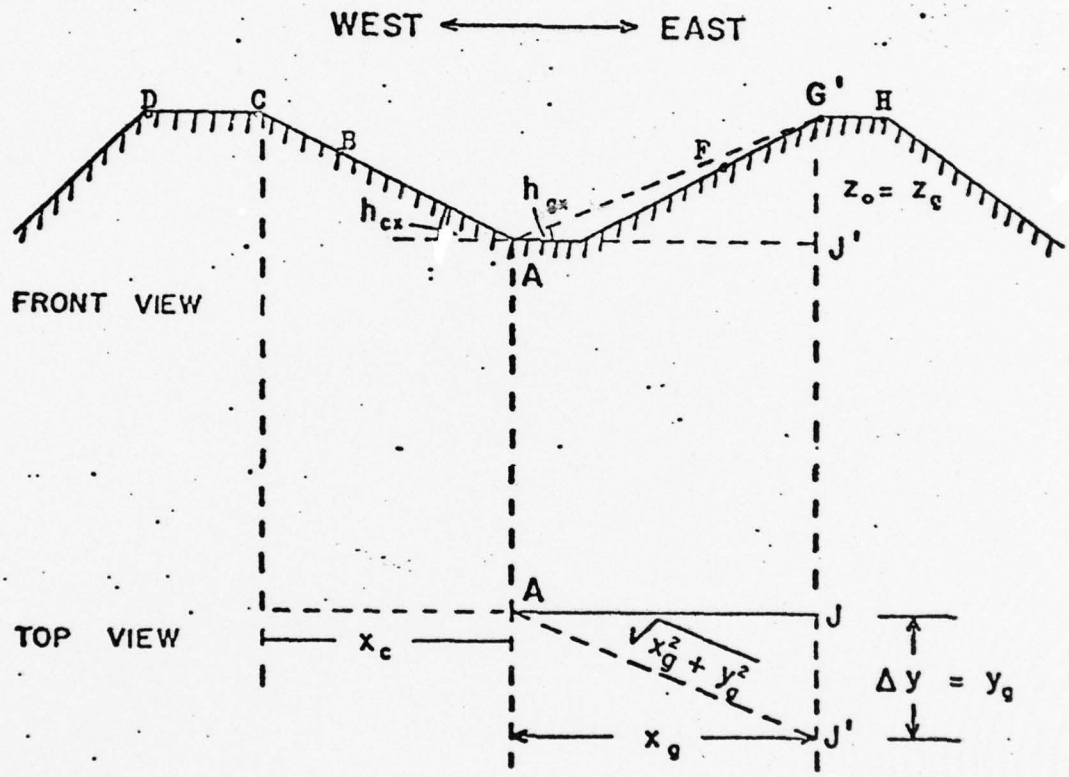

Fig. 1. A projective geometrical relationship between the sun's ray and the terrain.

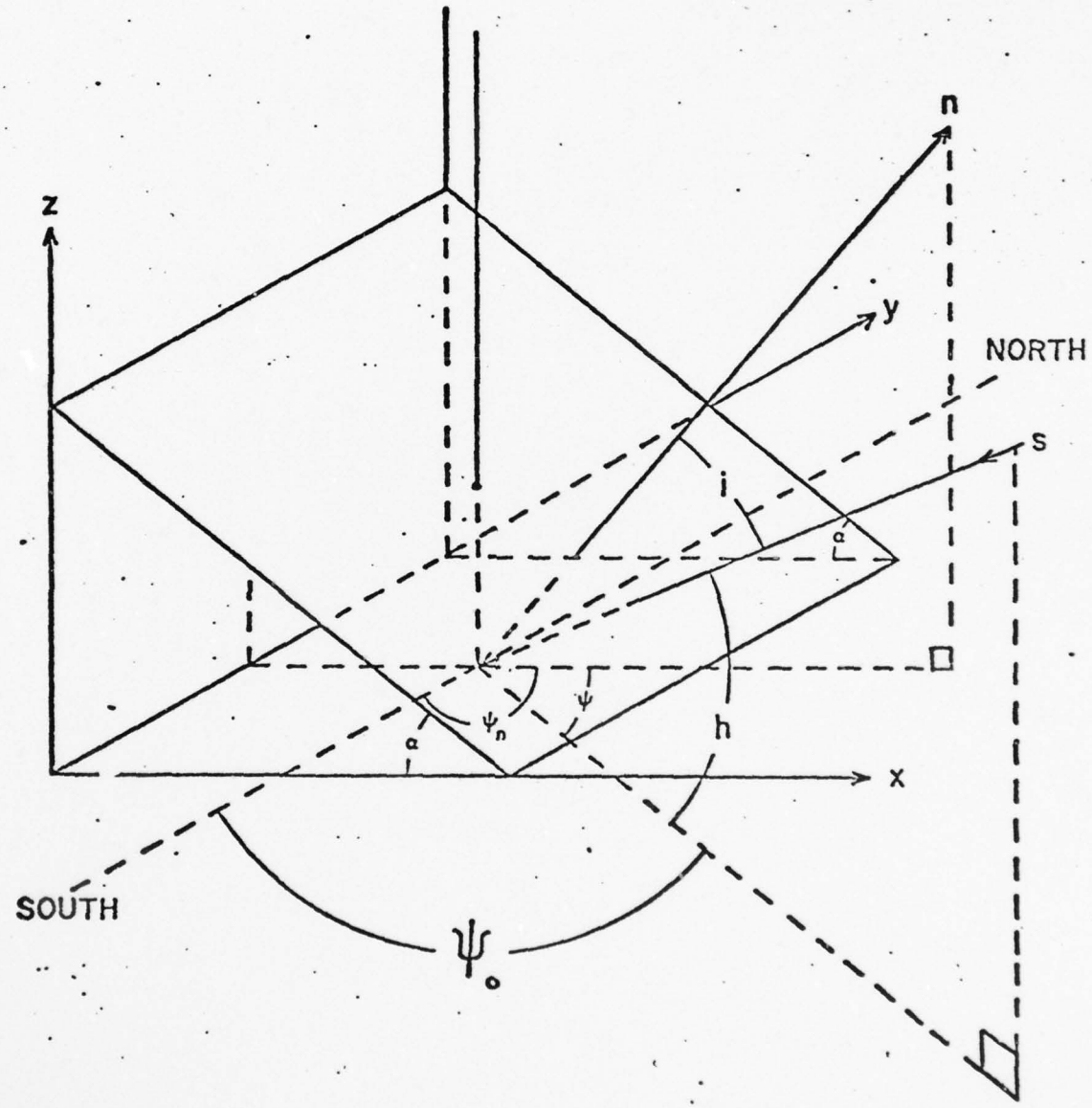

Fig. 2. . Solid geometry concerning the relationships among the orientation of a sloping surface, sun's ray, altitude and azimuth of the sun and the meridian.

AD-A051 221 ECOLOGICAL ENTERPRISES INC BEDFORD MA F/G 4/2
THEORETICAL STUDY OF THREE-DIMENSIONAL SLOPE AND VALLEY WIND SY--ETC(U)
DEC 77 W TANG, L PENG DAAG29-76-C-0007
UNCLASSIFIED NL

2 OF 2
AD
A051221

END
DATE
FILMED
4-78
DDC

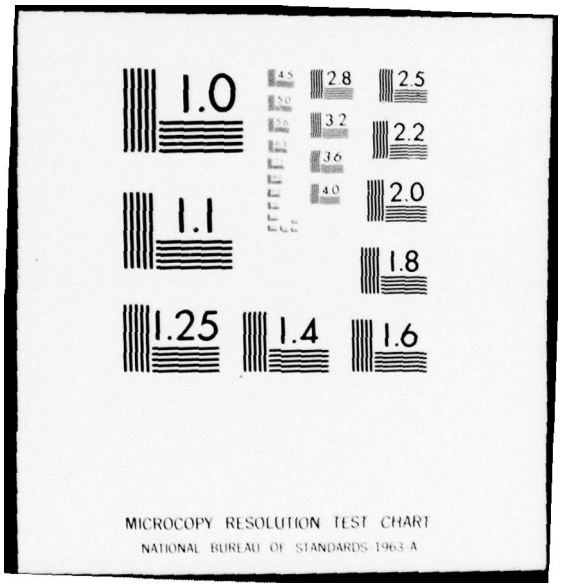
1.0
1.1
1.25
1.4
1.6
1.8
2.0
2.2
2.5
2.8
3.2
3.6
4.0
4.5
5.0
5.6
MICROCOPY RESOLUTION TEST CHART
NATIONAL BUREAU OF STANDARDS-1963-A

ψ_0 = azimuth of the sun

ψ_n = azimuth of the normal to the slope.

Using the laws of cosine and sine in spherical trignometry and the geometrical relationships of various angles shown in Fig. 2, one obtains the following set of equations (e.g., see Robinson, 1966)

$$\sin h = \sin\varphi \sin\delta + \cos\varphi \cos\delta \cos\omega \tag{3}$$

$$\cos h \sin\psi_0 = \cos\delta \sin\omega \tag{4}$$

$$\cos h \cos\varphi \cos\psi_0 = \sin\varphi \sin h - \sin\delta \tag{5}$$

where δ = latitude

φ = declination of the sun

ω = hour angle.

Substituting (3),(4), and (5) into (2), eliminating ψ_0, and rearranging yields the radiation flux on the slope.

$$S = S_0(J\sin\delta + K\cos\delta\cos\omega + \sin\psi_n \sin\alpha \cos\delta \sin\omega) \tag{6}$$

where
$$\begin{aligned} J &= \sin\varphi\cos\alpha - \cos\varphi\sin\alpha\cos\psi_n \\ K &= \cos\varphi\cos\alpha + \sin\varphi\sin\alpha\cos\psi_n \end{aligned} \tag{7}$$

For an east (or west) -facing slope, $\psi_n = \frac{-\pi}{2}$ $(\psi_n = \frac{\pi}{2})$

$$S_{e,w} = S_0(\sin\varphi\cos\alpha\sin\delta + \cos\varphi\cos\alpha\cos\delta\cos\omega + \sin\alpha\cos\delta\sin\omega) \tag{8}$$

For a horizontal surface, $\alpha = 0$

$$S_{e,w} = S = S_0(\sin\varphi\sin\delta + \cos\varphi\cos\delta\cos\omega) \tag{9}$$

This can be applied to the level surfaces on the ridge and valley floor. For a case on the valley floor, at point A in Fig. 1 for example, a

critical hour-angle ω_c corresponding to sunrise or sunset has to be determined.

Since

$$\cos \psi = \frac{x_g}{\sqrt{x_g^2 + y_g^2}} \tag{10}$$

and

$$\sin h_{gx} = \frac{z_g}{\sqrt{x_g^2 + z_g^2}} \tag{11}$$

then $$\sin h_g = \frac{z_g}{\sqrt{x_g^2 + y_g^2 + z_g^2}} = \frac{\cos \psi}{\sqrt{\cot^2 h_{gx} + \cos^2 \psi}} \tag{12}$$

For the present case, where the valley axis is in the north-south direction, $\psi_n = \frac{\pm\pi}{2}$.

Equation (12) then becomes

$$\sin h_g = \frac{\sin \psi_0}{\sqrt{\cot^2 h_{gx} + \sin^2 \psi_0}} \tag{13}$$

Since ψ_0 cannot be determined when the corresponding ω is not known, one cannot solve (13). Therefore we need another equation to determine the relationship between ω and ψ_0. This can be achieved by using the relationships (3), (4), and (5) to obtain

$$\sin^2 \psi_0 = \frac{\sin^2 \omega}{\sin^2 \omega + (\cos \varphi \tan \delta + \sin \varphi \cos \omega)^2} \tag{14}$$

The critical ω_c can be obtained by the 'cut and try' method with given φ and δ from

$$\frac{\dfrac{\sin^2\omega}{\sin^2\omega + (\cos\varphi\tan\delta + \sin\varphi\cos\omega)^2}}{\cot^2 h_{gx} + \dfrac{\sin^2\omega}{\sin^2\omega + (\cos\varphi\tan\delta + \sin\varphi\cos\omega)^2}} = \left[\sin\varphi\sin\delta + \cos\varphi\cos\delta\cos\omega\right]^2 \qquad (15)$$

Another method to determine ω_c is to simply set Eq. (8) to zero. However, the angle α has to be changed into the appropriate critical solar elevation angle for the point in question.

By this method the solar flux of all positions on the mountain-valley surface can be computed. If the physical surface of the mountain-valley terrain is symmetrical and periodic in space, the total energy received in 24 hours will be the same for both east and west slopes. However, the accumulated energy received at symmetrical positions on opposite slopes will be different at any given instant during the day. For practical purposes one may just compute the flux every half hour for some typical locations. For further computations, the data can be interpolated for any time interval and position needed. This flux will be used to determine the surface temperature and heat flux.

3. Long-wave radiation

The next most important item in the energy balance equation after solar radiation is the effective long-wave radiation flux. Because the mountain surface itself can screen away the IR radiation for a given azimuth ψ, and a given elevation angle h subtended by the mountain, the effective IR flux can be written as (Fuh, 1964):

$$I = \int_{-\pi}^{\pi} d\psi \int_{h(\psi)}^{\frac{\pi}{2}} (e_s - e_g) \cos l \cos h \, dh$$

$$+ \int_{-\pi}^{\pi} d\psi \int_{h_\alpha(\psi)}^{h(\psi)} (e_s - e_e) \cos l \cos h \, dh \quad , \qquad (16)$$

where e_s = IR radiation intensity on the slope at the point in question

e_g = IR radiation from the atmosphere

e_e = IR radiation from the opposite slope

$h_\alpha(\psi)$ = elevation angle produced by the slope surface (inclination α) itself in the direction .

In this study, ridge lines are assumed to be parallel as shown schematically in Figure 1, and $h(\psi)$ for the elevation angle of east and west slopes observed at Point A, h_G and h_C respectively, can be written as

$$h_G = \arcsin \left[\frac{\cos^2 \psi}{\cot^2(h_{gx}) + \cos^2 \psi} \right]^{\frac{1}{2}}$$

and

$$h_C = \arcsin \left[\frac{\cos^2 \psi}{\cot^2(h_{cx}) + \cos^2 \psi} \right]^{\frac{1}{2}}$$

The angle $h_\alpha(\psi)$ is the elevation angle due to the slope itself where the observation site stands.

If the IR radiation is isotropic within the integration limits and the valley is infinitely long, the integral in Equation (16) can be evaluated and becomes

$$I = \frac{\pi}{2}(e_m - e_g)S + \pi(e_m - e_s)\left(1 - \frac{1}{2}S\right)$$

where

$$S = \left((\cos(h_{gx}) + \cos(h_{cx}))\cdot\cos\alpha - (\sin(h_{gx}) - \sin(h_{cx})\cdot\sin\alpha \right)$$

When the black body temperatures are used, I at A is

$$I_A = \frac{1}{2}\left[I_H - \sigma(\beta_s T_s^4 - \beta_e T_e^4) \right] \left[(\cos h_{gx} + \cos h_{cx})\cdot \cos\alpha - (\sin h_{gx} - \sin h_{cx})\sin\alpha \right] + \sigma(\beta_s T_s^4 - \beta_e T_e^4) \quad (21)$$

where I_H = effective IR radiation flux (i.e. difference of IR radiation between mountain surfaces and atmosphere) on a horizontal surface

T_S = the absolute temperature of the surface at the point in question

T_e = the absolute temperature of the opposite slope

β_s , β_e = the emissivity of the earth's surface at the point in question, and of the opposite slope, respectively

h_{gx} , h_{cx} = elevation angle due to mountain ridges GH and CD respectively

σ = Stefan-Boltzmann constant.

Since $\alpha \leq 25$ as assumed in the present model and $h_{gx} \leq \alpha$, and $h_{cx} \leq \alpha$, it is evident that

$$\sin\alpha(\sin h_{gx} - \sin h_{cx}) \ll (\cos h_{gx} + \cos h_{cx})\cos\alpha .$$

Furthermore $T_s - T_e$ is generally small. The overall affective IR radiation may be approximated as

$$I_A \simeq \frac{1}{2} I_H (\cos h_{gx} + \cos h_{cx})\cos\alpha . \qquad (22)$$

However the quantity I_H , defined as the effective IR radiation on a horizontal surface, must be calculated iteratively. We may use an empirical formula for I_H developed by Brunt (1939), i.e.,

$$I_H = \sigma T_{SA}^4 (1 - a - b\sqrt{e}) , \qquad (23)$$

where $a = 0.44$

$b = 0.08$

e = surface vapor pressure in millibars

T_{SA} = the surface temperature at the point in question.

(In the present problem T_s is the temperature at the point A, which is used to calculate I_A at A). Finally we may write the effective IR radiative flux as

$$I = \frac{1}{2}\sigma T_s^4 (1 - a - b\sqrt{e})(\cos h_{gx} + \cos h_{cx})\cos\alpha, \qquad (24)$$

The value of I depends on the position on the mountain-valley surface and can be calculated for each point on the surface. The surface temp-

erature in the expression for I remains to be determined later by solving the heat conduction equation of the soil and a system of thermo-hydrodynamic equations of the atmosphere simultaneously.

4. Heat conduction equation of soil and the boundary conditions

The general equation of the mountain-valley surface may be written as

$$D = D(x)$$

Using z to indicate the height above the fixed level surface, and the height above the ground surface, we have

$$z = D(x) + \zeta$$

The heat conduction equation which governs the variation of the soil temperature may be written approximately as

$$\frac{\partial T_s}{\partial t} = K_s \frac{\partial^2 T_s}{\partial \zeta^2}$$

where $K_s = \lambda_s / c_s \rho_s$

λ_s = thermal diffusivity of the soil

ρ_s = density of the soil

c_s = specific heat of the soil

The boundary condition at the ground surface, after neglecting scattering, precipitation and evaporation, and assuming the normal temperature gradient to be about the same as the vertical temperature gradient, will be approximately

$$S - I + \lambda \frac{\partial T}{\partial z} - \lambda_s \frac{\partial T_s}{\partial \zeta} = 0 , \qquad (25)$$

where S = solar radiation reached on the slope

I = long-wave exchange between the slope and the environment

λ_s = thermal diffusivity of the soil

λ = eddy conductivity of the air (assumed constant in the layer 1.4m above ground, and may vary with time)

T , T_s = temperatures of the air and soil respectively.

For the boundary condition at $\zeta = -\infty$, T_s is finite.

5. Solution of surface temperature

The differential equation of the heat conduction of the soil may be written in finite difference form for time differential. Assume

$$T_s = T_0 + Bz + T_s'(\zeta, x, t) , \tag{26}$$

where B = prescribed for $z>0$,

and $B = 0$ for $z<0$.

We designate the elevation of the valley floor as $z=0$. Substituting T_s into the finite difference equations of heat conduction of soil leads to

$$\frac{T_s'^{t+\Delta t} - T_s'^{t}}{\Delta t \cdot \lambda_s / c_s \rho_s} = \frac{\partial^2 T_s'^{t+\Delta t}}{\partial \zeta^2} \tag{27}$$

in which z is replaced by ζ near the surface. The solution of this equation, obtained by varying the parameters and assuming that $T_s'^{t}$ is a known function, and can be written as

$$T_s'^{t+\Delta t}(x, \zeta, t) = A(x) e^{\gamma\zeta} + B' e^{-\gamma\zeta} + \frac{1}{\gamma} \int_{-\infty}^{\zeta} \sinh \gamma(\zeta - \zeta') (-\gamma^2 T_s'^{t}) d\zeta' \tag{28}$$

where $\gamma = \frac{1}{\sqrt{\Delta t \cdot \lambda_s / c_s \rho_s}}$. Applying the boundary conditions at $z \longrightarrow -\infty$ leads to $B' = 0$. Next the coefficient $A(x)$ should be determined from the energy balance equation at $\zeta = 0$ with analytical solutions of S

and I at each grid point.

Assuming the condition of the soil temperature at the air-soil interface to be continuous, we have the detailed expression of the energy balance equation as

$$\left(\lambda_s \frac{\partial T_s}{\partial z}\right)^{t+\Delta t} = \lambda \frac{T^{t+\Delta t} - T_s^{t+\Delta t}}{\Delta z} + S_0 \Big\{ (\sin\varphi\cos\alpha - \cos\varphi\sin\alpha\cos\psi_n) \cdot \sin\delta + (\cos\varphi\cos\alpha + \sin\varphi\sin\alpha\cos\psi_n) \cdot \cos\delta\cos\omega + \sin\psi_n \sin\alpha\cos\delta\sin\omega \Big\}^{t+\Delta t} - \frac{1}{2}\sigma (T_s^{t+\Delta t})^4 (1 - a - b\sqrt{e}) \cdot (\cos h_{gx} + \cos h_{cx}) \cos\alpha \tag{29}$$

Substituting $T_s = T_o + Bz + T_s'(x,z,t)$, into (29) and rearranging leads to

$$\left\{\lambda_s \frac{\partial T_s'}{\partial \zeta} + \left[\frac{\lambda}{\Delta z} + 2\sigma T_o^3 (1 - a - b\sqrt{e})(\cos h_{gx} + \cos h_{cx})\cos\alpha\right] T_s'\right\}^{t+\Delta t} = F(x, \psi_n, \omega)^{t+\Delta t} \tag{30}$$

where

$$F(x,\psi_n,\omega) = -\lambda_s B + \frac{\lambda}{\Delta z} T^{t+\Delta t} - \frac{\lambda}{\Delta z}(T_o + Bz(x)) + S_o \Big\{ (\sin\varphi\cos\alpha - \cos\varphi\sin\alpha\cos\psi_n)\sin\delta + (\cos\varphi\cos\alpha + \sin\varphi\sin\alpha\cos\psi_n)\cos\sigma\cos\omega$$

$$+ \sin\psi_n \sin\alpha \cos\delta \sin\omega \Big\}^{t+\Delta t}$$

$$-\frac{\sigma}{2}\left\{T_0^4 + 4T_0^3 Bz\right\}(1-a-b\sqrt{e})(\cos h_{gx} + \cos h_{cx})\cos\alpha \,. \qquad (31)$$

The soil heat flux at the ground surface ($\zeta = 0$) can be obtained from (28) as

$$\lambda_s \frac{\partial T_s'}{\partial \zeta}\Big|_{\zeta=0}^{t+\Delta t} = \lambda_s A(x)\gamma + \frac{\lambda_s}{2}\int_{-\infty}^{0}\left[e^{-\gamma\zeta'} + e^{\gamma\zeta'}\right](-\gamma^2 T_s'^{\,t})\,d\zeta' \,. \qquad (32)$$

After substituting $\lambda_s \frac{\partial T_s'}{\partial \zeta}\Big|_{\zeta=0}^{t+\Delta t}$ into the energy balance equation at $\zeta = 0$ and solving for A(x), we have

$$A(x) = \frac{1}{\gamma\lambda_s + \left[\frac{\lambda}{\Delta z} + 2\sigma T_0^3 (1-a-b\sqrt{e})(\cos h_{gx} + \cos h_{cx})\cos\alpha\right]}$$

$$\cdot \left\{\gamma^2\lambda_s \int_{-\infty}^{0} \cosh\gamma\zeta' \cdot T_s'\,d\zeta - \gamma\left[\frac{\lambda}{\Delta z} + 2\sigma T_0^3(1-a-b\sqrt{e})\right.\right.$$

$$\left.\cdot (\cos h_{gx} + \cos h_{cx})\cos\alpha\right] \int_{-\infty}^{0} \sinh\gamma\zeta' \cdot T_s'^{\,t}\,d\zeta'$$

$$\left. + F^{t+\Delta t}\right\} . \qquad (33)$$

For a given location x and time t, A is constant and $T_s'^{\,t+\Delta t}(x, \zeta, t)$ is determined. With known $T_s'^{\,t}$, $T_s'^{\,t+\Delta t}$ can be calculated if the temperature of the air above the surface is known. Set

$$L = \frac{\lambda}{\Delta z} + \left[2\sigma T_0^3 (1-a-b\sqrt{e})(\cos h_{gx} + \cos h_{cx})\cos\alpha\right].$$

Then $T_s'^{t+\Delta t}$ may be written as

$$T_s'^{t+\Delta t}(\zeta) = \frac{F^{t+\Delta t} e^{\gamma\zeta}}{\lambda_s\gamma + L} + \frac{\gamma}{2}\left(\frac{\lambda_s\gamma - L}{\lambda_s\gamma + L}\right)\int_{-\infty}^{0} e^{\gamma(\zeta+\zeta')} T_s'^{t}\, d\zeta' +$$

$$+ \frac{\gamma}{2}\int_{\zeta}^{0} e^{\gamma(\zeta-\zeta')} T_s'^{t}\, d\zeta' + \frac{\gamma}{2}\int_{-\infty}^{\zeta} e^{-\gamma(\zeta-\zeta')} T_s'^{t}\, d\zeta'. \qquad (34)$$

At ground, $\zeta = 0$. The three integral terms in Eq. (34) are combined to become

$$\frac{\gamma^2\lambda_s}{\lambda_s\gamma + L}\int_{-\infty}^{0} (e^{\gamma\zeta'}) T_s'^{t}\, d\zeta'$$

From observations of soil temperature variation with depth T_s' may be assumed without too much error as

$$T_s' = G\, e^{l\zeta'} \cos(ft + l\zeta').$$

Then

$$\int_{-\infty}^{0} e^{\gamma\zeta'} T_s'\, d\zeta = \frac{G}{(\gamma + l)^2 + l^2}\left\{(\gamma + l)\cos ft + l \sin ft\right\} \qquad (35)$$

For integration, the time interval t= 30 minutes, $K_s \cong .75 \times 10^{-3}$ cm^{2}sec^{-1}, and $\gamma \cong 0.86$ cm^{-1}. Diurnal variation in soil temperature at a depth of 50 cm is nearly zero at O'Neill, Nebraska, Aug. 31, 1953, based on data obtained by Lettau and Davidson (1957). It follows that $l \leq \frac{1}{50}$. This means that l is negligible in comparison to γ. Neglecting l all together from (34) yields an error less than 3%. For meso-scale calculations this error is acceptable. Then $T_s'^{t+\Delta t}$ may be simply written as

$$T_s,^{t+\Delta t}\Big|_{\zeta=0} = \frac{F^{t+\Delta t}}{\lambda_s\gamma + L} + \frac{\lambda_s\gamma}{\lambda_s\gamma + L} \cdot (T_s,^{t})_{\zeta=0} \qquad (36)$$

Finally we have

$$T_s\Big|_{\zeta=0}^{t+\Delta t} = T_0 + Bz + \frac{F^{t+\Delta t}}{\lambda_s\gamma + L} + \frac{\lambda_s\gamma}{\lambda_s\gamma + L} \cdot (T_s,^{t})_{\zeta=0}. \qquad (37)$$

Eq. (36) should be solved simultaneously with the set of finite difference equations governing the air temperature and motion in the boundary layer. The solution can be obtained if the air temperature at a height Δz above the surface at time $t + \Delta t$, and the ground surface temperature at time t, are known. An initial rough but realistic estimate of air temperature $T^{t+\Delta t}$ may be made for the first computation of $T_s{}^{t+\Delta t}$. With the flux at time $t + \Delta t$ one can compute the atmospheric temperature $T^{t+2\Delta t}$ from the set of governing differential equations in the atmosphere. Continue this computation iteratively to obtain $T_s{}^{t+n\Delta t}$, where n is an integer one wishes to assume. This approximated method was developed mainly for the purpose of mountain-valley circulation studies. It can also be applied to studies of micrometeorological problems as long as the geometry of the terrain is simple. In the present model the point of interest, the effective IR radiation on the surface I_H, is not directly calculated, but rather is replaced by an empirical formula. So long as the surface geometry is simple, a simple anlytical solution can be derived.

5. Results and Discussion

Equation (36) is used to compute ground temperature for three different positions in a valley located 5 miles north of Manchester Center, Vermont. They are Point A on the valley floor, Point B on the west slope, and Point F on the east slope. The heights of Points B and F are about 440m and 420m above Point A respectively. The ridge lines are 548m above the valley floor and are 7.8km apart. Point A is approximately 2km horizontal distance from the west ridge. The average slope at Point F is rather gentle, being 6.3°. The slope on the west side varies from 12.5° on the lower half to 18.8° on the upper half where Point B is.

Other physical parameters used in the computation are as follows:

$\lambda = 0.239$ cal $cm^{-1}sec^{-1}deg^{-1}$	$a = 0.44$
λ = also varies as a function of time(see Table 1)	$b = 0.08$
$\lambda_s = 0.001$	$e = 10$
$t = 1800$ sec	$z = 140$ cm
$c_s \rho_s = 0.4$ cal $cm^{-3}deg^{-1}$	$\delta = 20°$
albedo = 0.15	$\varphi = 43.16°$

Table 1. Assumed variation of λ with time over the course of a day.

hour (EST)	0	2	4	6	8	10	12	14	16	18	20	22	24
λ (cal cm^{-1} $deg^{-1}sec^{-1}$)	.05	.05	.06	.10	.24	.28	.30	.30	.20	.12	.08	.05	.05

The sunrise and sunset hours for Points A, B, and F computed from this model are (0515, 1752 E.S.T.), (0445, 1735 E.S.T.), and (0515, 1911 E.S.T.) respectively.

The air temperatures at the three points are recorded by thermographs located 1.4m above the gound. The data of August 7, 1957 taken from Davidson and Rao (1958) are used in the computation and are shown in Figure 3 by dashed lines.

Since there is no observed ground temperature T_s at each site, a reasonable initial T_s or T_s' value has to be given for input. This value is determined with a trial run using an appropriate T_s or T_s' until the result converges to a constant and its rate of change is about the same or slightly larger than that of air temperature at midnight for a given set of assumed values for parameters. For daily use, T_s can be observed and there is no need for such trial runs.

Based on the physical configuration of the terrain and input air temperatures for each point, the corresponding computed ground temperatures and upward heat fluxes under three different assumptions of λ are shown in Figures 3 and 4 respectively. In Figure 3 the computed ground temperatures for cases of constant λ, variable λ, and doubled value of the variable λ are denoted by light, heavy, and dash-dotted curves. The observed air temperatures are denoted by dashed curves. In Figure 4 the computed upward heat fluxes for constant λ, smaller variable λ, and larger variable λ cases are denoted by dashed, solid, and dash-dotted curves respectively.

The computed sunrise and sunset hours shown earlier are correct because two different formulas mentioned earlier give the same computed results. Besides the computed sunrise hour at Point B is the earliest, and the computed sunset hour at Point F is the latest, among the three sites. All of these results are in close agreement with values from other sources.

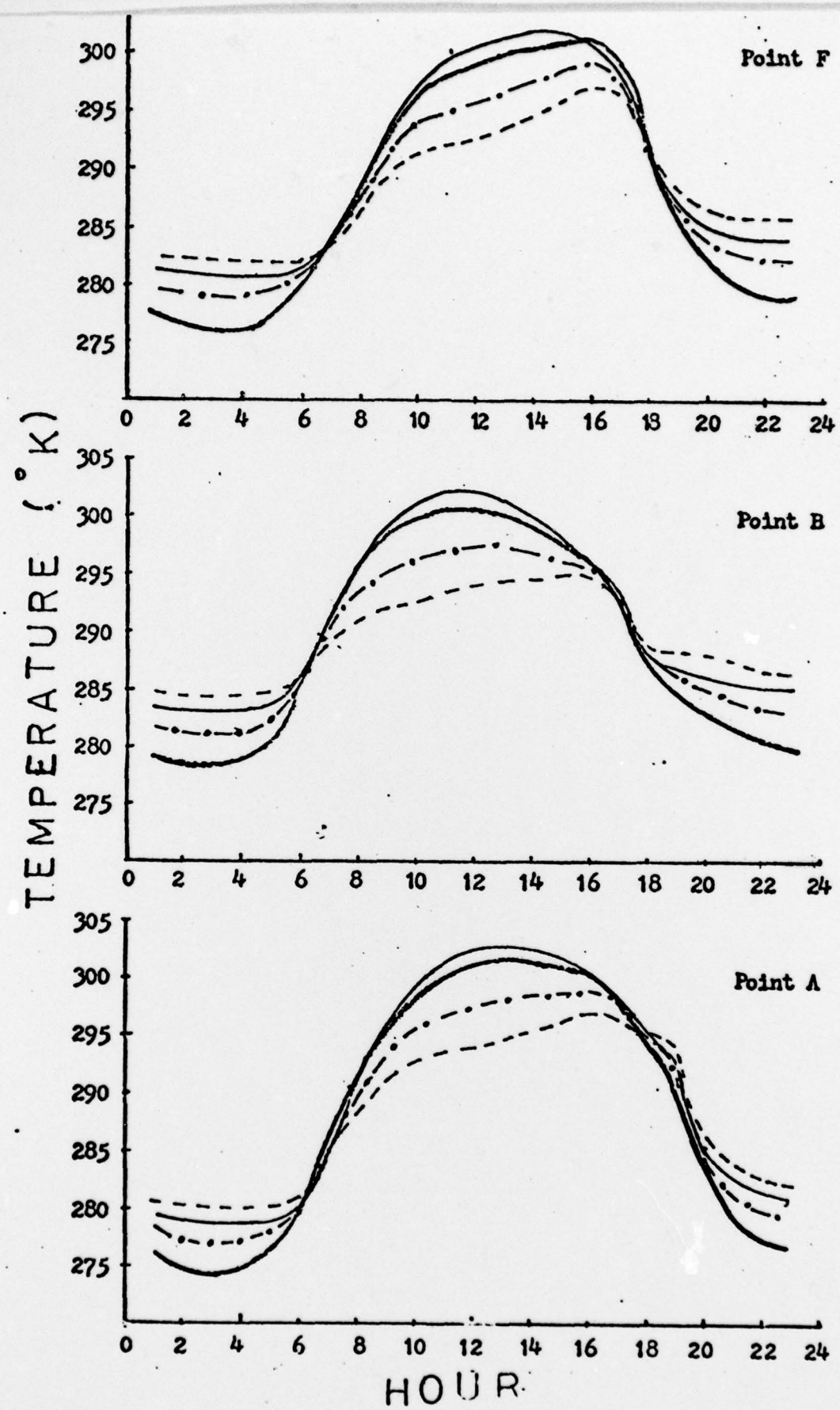

Figure 3. Observed diurnal air temperature (dashed curve), and computed diurnal ground temperature for variable λ (heavy solid curve), for constant λ (light solid curve), and for doubled variable λ (dash-dotted curve), for Point A on the valley floor, Point B on the west slope, and and Point F on the east slope of the valley.

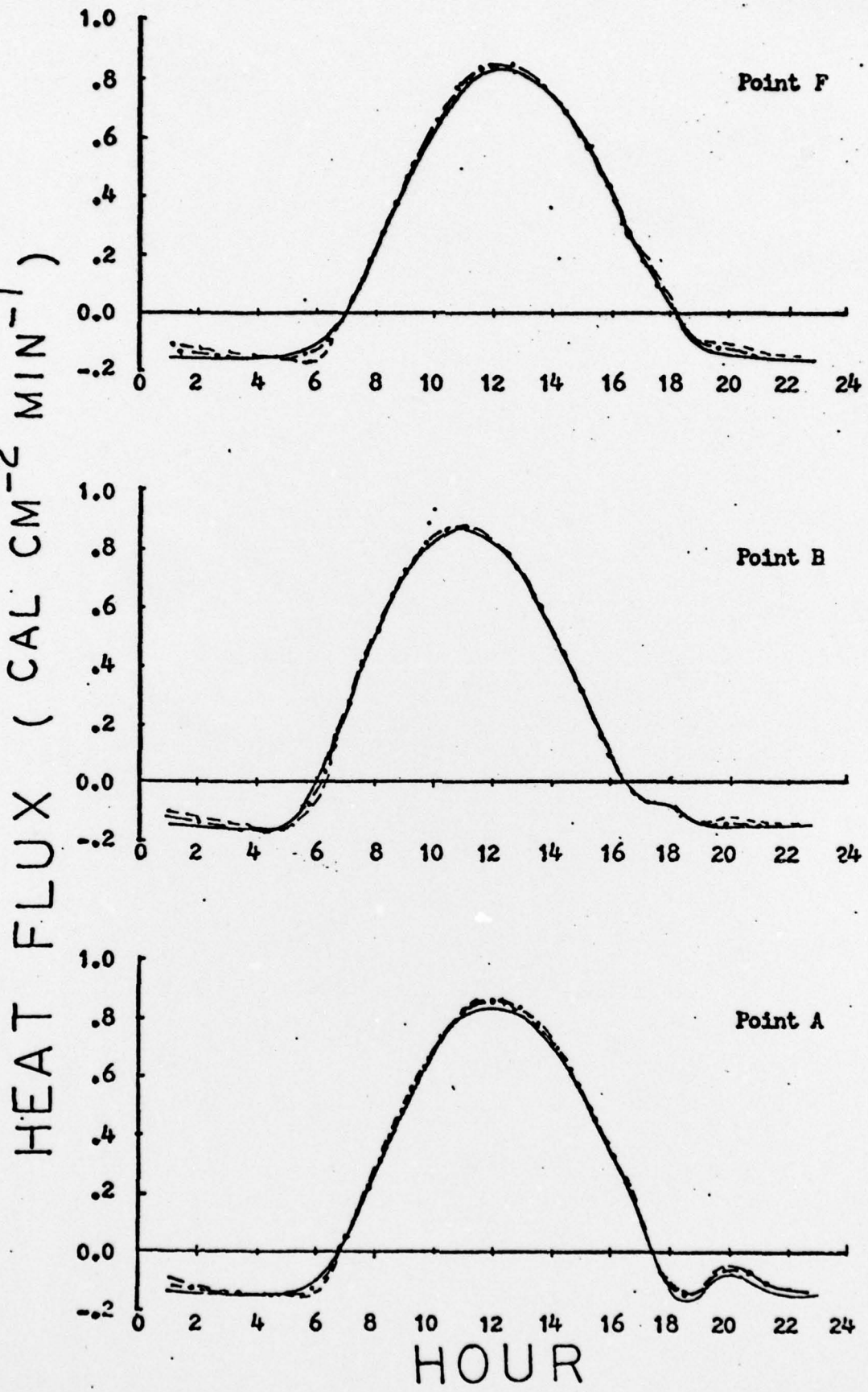

Figure 4.. Computed diurnal upward heat flux for constant λ (solid curve), variable λ (dashed curve), and doubled variable λ (dash-dotted curve) for Points A, B, and F.

Examination shows that the computed ground temperature reaches the level of air temperature at each site about half an hour after sunrise. Then both air and ground temperatures start to rise. The times before attaining maximum T_s of the individual site occur first on the west slope, then on the valley floor, and finally on the east slope in Figure 3. This is as expected because of the present topographic configuration. T_s starts to drop generally in the afternoon but drops precipitously after sunset for Point A and just before sunset for Points B and F. The phenomenon at Points B and F can probably be attributed to the large drop in air temperature, and to turbulence taking away heat from the ground and reducing ground temperature much faster. Another interesting phenomonon apparent from Figure 3 is that the daily range of ground temperature is largest at the site in the valley, being a few degrees greater than at the sites on the slopes. The differences in the ranges of ground temperature are in agreement with those of air temperature. This phenomonon appears in many valleys.

The results of the heat flux computations in Figure 4 have almost the same shape and magnitude for the three different cases of λ. Although the ground temperatures T_s for different λ's are different at a particular site, the changes in heat flux are slight. The reason is that the product of the smaller λ with the large vertical temperature gradient (between the air temperature at 1.4m level and ground temperature) is nearly the same as the product of the larger λ with the smaller vertical gradient. The system adjusts itself so that the change in flux is gradual. The trend in the order of occurence of maximum heat flux follows that of the order of occurence of maximum temperature at the three sites. The total heat flux which diffused due to eddy processes was greatest at Point F. This is believed to be because it has the longest period of sunshine.

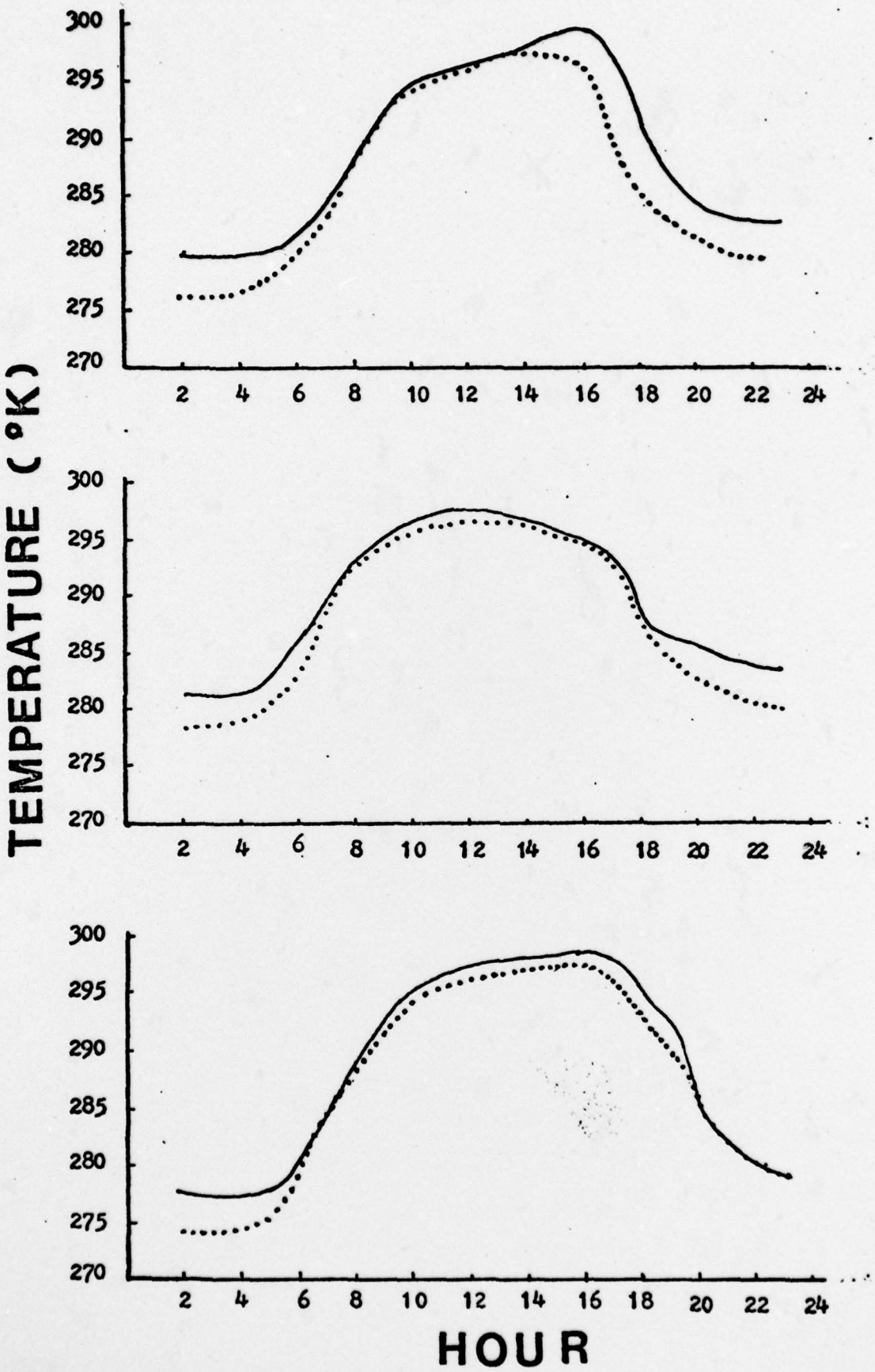

Figure 5. Computed temperatures for variable vapor pressure, e, (solid curve) and for zero vapor pressure (dashed curve).

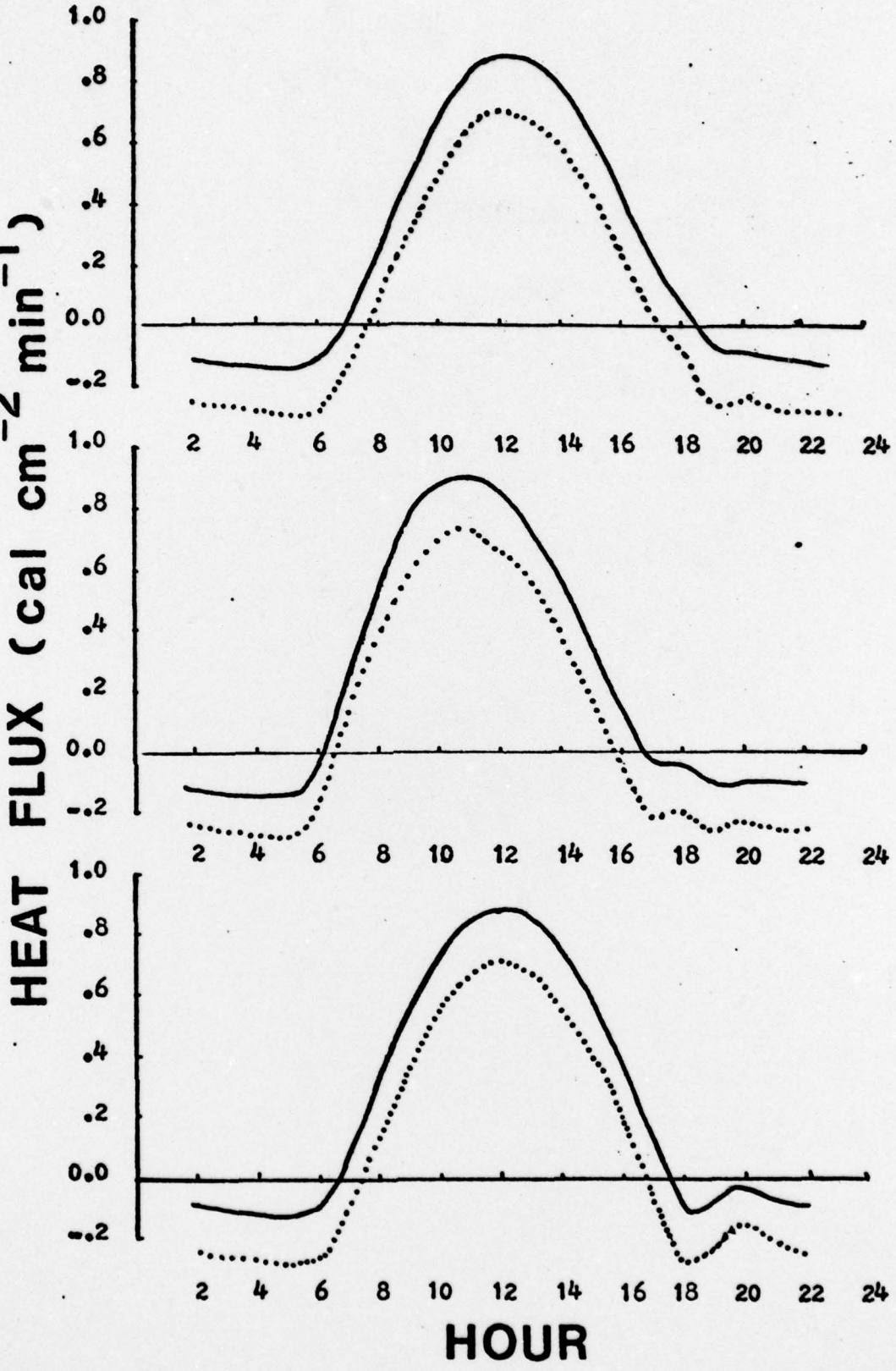

Figure 6. Computed upward heat flux for variable vapor pressure, e, (solid curve) and for zero vapor pressure (dashed curve).

The computed maximum upward heat flux at all three sites is around 0.9 cal $cm^{-2}min^{-1}$, which has the same order of magnitude as the turbulent heat flux for different height ranges for free convection over flat terrain observed by Taylor and Swinbank independently (see Priestley, 1959).

Computations for temperature and upward heat flux are also made with two different assumptions of vapor pressure. The solid curves denote the case for variable vapor pressure which is based on observations made elsewhere for terrain with vegetation. The dashed curves denote the case for zero vapor pressure. It is seen that dry atmosphere yields lower temperatures for both day and nighttime because of decreased long-wave radiation from the atmosphere and thus more heat loss to space. Indeed this is a purely idealistic case. The solid curve may be considered a case of high vapor pressure. Other conditions being equal, the variation of T and heat flux due to change of vapor pressure may be bounded by these two curves. For normal conditions, the curves should be closer to the solid curves for both temperature and heat flux.

In view of the computed results whown in Figure 3, the eddy diffusivity of heat, λ , is important to the determination of ground temperature. In this study prescribed values are used. However λ should be determined from the circulation model and solved from the goverming set of hydro-thermodynamic equations in the atmospheric boundary layer. Air temperature is also a very important factor in determining ground temperature. Obtaining air temperature by solving the heat equation of air, which includes eddy diffusion and long-wave radiation terms for air, would be very useful.

In conclusion the computed results are very encouraging. Further

improvement can be made for application to mountain-valley terrain. The purpose of this study is to study 3-dimensional meso-scale circulations in typical uneven topography. An attempt is being made to apply this idea to mountain-valley terrain. Results are still some time to come.

REFERENCES

Brunt, D., 1939: Physical and Dynamical Meteorology. Second Edition, New York, Cambridge University Press, p. 428.

Davidson, B. and P.K. Rao, 1958: Preliminary Report on Valley Wind Studies in Vermont, 1957. Final Report under Contract No. AF19(604)1971.

Fuh, B.P., 1959: The influence of the slope on the sunniness. Scientia Sinica, 8, pp. 700-726.

_____, 1964: The determination of the components of radiation balances in an undulating country. ACTA Meteorological Sinica, 34, pp. 62-73. (in Chinese)

Lettau, H.H. and B. Davidson, 1957: Exploring the Atmosphere's First Mile. Vol. I and II, Oxford, Pergamon Press.

Priestley, C.H.B., 1959: Turbulent Transfer in the Lower Atmosphere. Chicago, The University of Chicago Press, 130 pp.

Robinson, N., 1966: Solar Radiation. New York, Elsevier Publishing Co., p.347.

Tang, W. and L. Peng, 1974: Mountain-Valley Circulation and Dispersion of Vehicular Exhaust Gases from a Valley Highway. Preprint Volume, Symposium on Atmospheric Diffusion and Air Pollution, Santa Barbara, California, 9-13 Sept., 1974. Amer. Meteor. Soc.

Tang, W., 1976: Theoretical Study of Cross-Valley Wind Circulation. Arch. Met. Geoph. Biokl., Ser. A, 25, 1-18.